Investigation of thruster performance in reduced under-thruster clearance during station-keeping operation

M.Sc. Marine Technology

Nicola Bovo

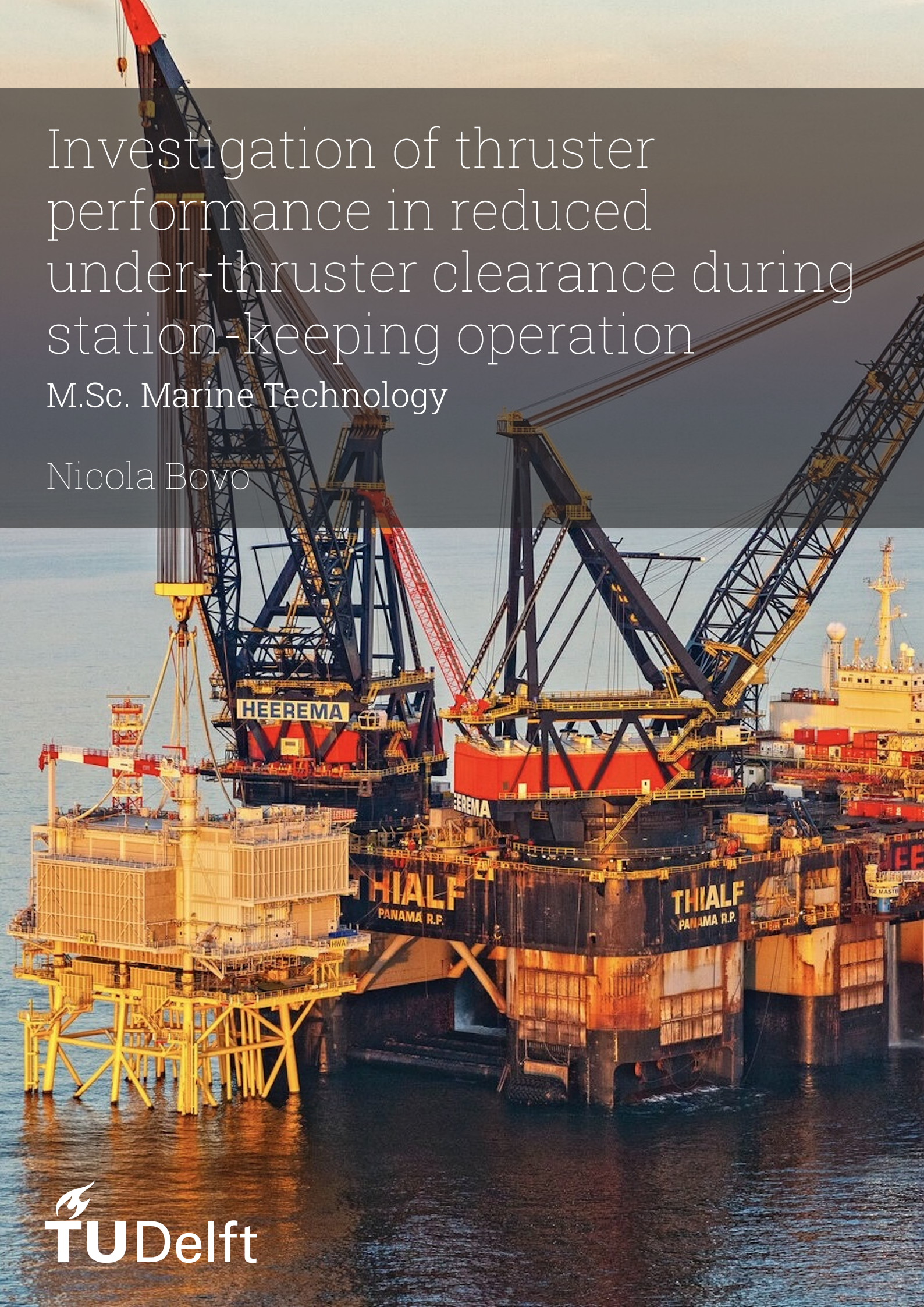

TU Delft

This page is intentionally left blank.

Thesis for the degree of MSc in Marine Technology in the specialization of Ship Hydromechanics

Investigation of thruster performance in reduced under-thruster clearance during station-keeping operation

by

Nicola Bovo

Performed at

Heerema Marine Contractors

This thesis (MT.24/25.001.M) is classified as confidential in accordance with the general conditions for projects by the TU Delft

September 25, 2024

Company supervisor:	
Responsible supervisor:	Ir. Maarten Burger
Daily supervisors:	Ir. Rinke Feenstra, Ir. Radboud van Dijk
Thesis exam committee:	Dr. Daniele Fiscaletti
Chair/Responsible Professor:	Dr.ir. Henk de Koning Gans
Staff Member:	Dr.ir. Peter Wellens
Staff Member:	Ir. Radboud van Dijk
Company Member:	
Author Details:	5619157
Studynumber:	

TU Delft

MARINE CONTRACTORS

Preface

This report presents my Master's thesis in Marine Technology at TU Delft. My move from Italy to the Netherlands was driven by my passion for the offshore sector, and TU Delft, along with the Netherlands' strong offshore industry, provided the perfect environment to deepen my knowledge.

During my studies, I gained a better understanding of offshore vessels and developed a keen interest in their operation, especially focusing on dynamic positioning systems. I also explored the basics of hydrodynamics as they apply to these vessels and their operations. This thesis combines my interest in the offshore industry with the knowledge I have gained in marine engineering and hydrodynamics.

During my research, I was an intern at Heerema Marine Contractors, a leading company in offshore heavy lifting. This hands-on experience allowed me to apply what I learned in the classroom to real-world problems and understand the industry's working environment.

I would like to express my gratitude to my supervisor at TU Delft, Daniele Fiscaletti, for his guidance and feedback. I also want to acknowledge the support from Rinke Feenstra and Radboud van Dijk, along with the entire Marine Engineering department at Heerema Marine Contractors, where I dedicated most of my time to working on this thesis. Special thanks go to the CFD experts of Heerema Engineering Solutions, Gino Parisella and Alessio Pistidda, who played a fundamental role in the development and execution of this thesis.

Lastly, I want to thank my family and my friends for their support and encouragement throughout this journey.

Nicola Bovo
Delft, September 2024

Abstract

The capability to maintain position in different operational scenarios is crucial for every offshore vessel, including semisubmersible vessels, which are traditionally designed to operate in deep water conditions. With the transition to new sources of energy production, such as wind turbines, the necessity for these vessels to operate in shallower waters is increasing. This aspect necessitates identifying the impact of such conditions on the vessel's capacity to maintain its position. This thesis focuses on identifying the governing factor in the reduction of thruster efficiency and, therefore, evaluating the thrust delivered by the thruster to the semisubmersible vessel when operating near the seabed. Specifically, it is relevant to identify which parameters, or combinations, induce an additional reduction in the effective thrust propellers deliver to the vessel in reduced clearance beneath the thruster, thereby affecting the vessel station-keeping capability.

The primary goal of this work is to estimate the reduction in the delivered thrust when a thruster operates in proximity to the seabed. Therefore, it is crucial to identify the sources of thrust reduction for a semisubmersible vessel based on the available literature and previous tests on similar vessels. Specifically, the interactions between hull, current, and thrusters have been identified as the most impacting effects in reducing thruster efficiency. Therefore, it was possible to estimate the impact of each of these mentioned types of thruster interactions both with analytical solutions and the suggested formulation from the register class (e.g., *ABS* [2]). The results indicate that the interaction between the thruster outflow and the hull, combined with the impact of the current on this condition, is strongly modified when compared with deep-water conditions.

Approximately 50 computational-fluid-dynamics (CFD) steady-state simulations have been performed to investigate the current effect and the vessel's geometrical characteristics under different current speed with reduced under-thruster clearance. These simulations were conducted across three different water depths at a single vessel draft, combined with four distinct beam-side current speeds. The primary focus is on evaluating the flow development beneath the hull and comparing it with the deep water scenario. The analysis revealed that the proximity of the seabed partly influences the flow deviation. Contrarily, the flow velocity, and consequently, the frictional resistance, predominantly affects the thruster's performance. A significant finding is that the thruster's delivered thrust could decrease by up to 53%, with respect to open water conditions, when operating in a current of 1 knot with 6 meters of under-thruster clearance. These results confirm the hypothesis regarding the impact of shallow water conditions on delivered thrust. The obtained data highlights the importance of accounting for additional thrust loss in situations of reduced under-thruster clearance, as this aspect was not previously considered for dynamic positioning operations.

The investigated topic covers a broader scope than the presented results. However, this thesis marks the starting point for future research. It emphasizes the significance of studying the impact on thruster performance under reduced under-thrust clearance conditions and provides the thrust reduction obtained for the specific case of beam-side current condition and the thruster operating in the direction of the downstream floater. Furthermore, the obtained uncertainty indicates that the used CFD approach (steady-state) needs a more comprehensive analysis involving time-consuming numerical solutions to address the vortex shedding phenomena, especially for high current values.

Contents

List of Figures

List of Tables

Nomenclature

Abbreviations

Name	Definition
ABS	American Bureau of Shipping
AD	Actuator Disk
CFD	Computational fluid Dynamic
DP	Dynamic Positioning
FPP	Fixed pitch propeller
HMC	Heerema Marine Contractors
ITTC	International towing tank conference
LDV	Laser-Doppler System
MRF	Moving Reference Frame
NS	Navier-Stokes
OSV	Offshore Supply Vessel
PIV	Particle Imagery Velocity
SI	Sliding Interface
SSCV	Semi-Submersible Crane Vessel

Symbols

Symbol	Definition	Unit
V_s	inflow velocity on the propeller	[m/s]
n	propeller rotational speed	[rpm]
J	advance ratio	[-]
K_t	thrust coefficient	[-]
n_{MAX}	maximum propeller rotational speed	[rpm]
T_{OW}	open water thrust	[kN]
t	thrust reduction ratio T/T_{OW}	[-]
t_{hull}	thrust reduction ratio due to thruster-hull interaction	[-]
t_p	thrust reduction ratio due to downstream floater blockage effect	[-]
t_f	thrust reduction ratio due to frictional resistance	[-]
t_c	thrust reduction ratio due to Coandă effect	[-]
$t_{current}$	thrust reduction ratio due to thruster-current interaction	[-]
L_p	floaters distance	[m]
X_f	floater width	[m]
X_d	thruster distance form the downstream round bilge of the floater	[m]
C_{TH}	thruster-hull interaction coefficient related to the thruster and the hull	[m]
$C_{TH,unit}$	thruster-hull interaction coefficient related to the thruster (inflow velocity investigation)	[m]

1

Introduction

1.1. Overview of the offshore industry

Ensuring that a vessel remains in position is a crucial task for different types of vessels, especially for Semi-Submersible Crane Vessels (SSCV) such as Heerema Marine Contractors (HMC) vessels (see Figure 1.1), which are provided with dynamic position system to accomplish this result. The growing size of bottom-fixed offshore wind turbine installations has led to the requirement for specialized vessels to operate in shallow water areas, resulting in the deployment of dynamically positioned vessels in regions such as the North Sea. In these regions, operations related to the oil & gas industry, including offshore installation or removal activities, also often demand vessels to operate under similar conditions. In such areas, vessels are required to operate with a reduced underwater clearance below their propellers, which does not represent their design operating conditions. This development has raised concerns about how this condition could affect a vessel's ability to maintain its position, especially during commercial operations, including heavy lifting activities. It is of interest to investigate how the performance of the thrusters is affected in this working condition.

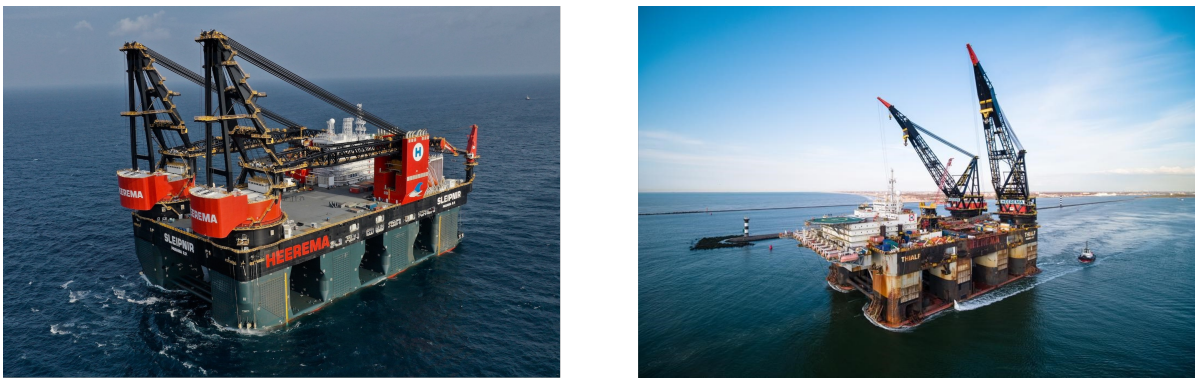

Figure 1.1: SSCV Sleipnir (left) and SSCV Thialf (right) at shallow draft.

The impact of shallow water becomes significant when considering vessels with a large draft. They could reach a low under-keel clearance in water depths that would not be considered shallow for other vessel types. Indeed, the low clearance below the keel and thrusters might influence the vessel's operability. This is notably the case for SSCVs, which are involved in the installation of topsides and jackets. Therefore, acquiring a deeper understanding of the hydrodynamic effects associated with low clearance under the thrusters is essential. This paper aims to explore the hydrodynamic aspects to improve existing knowledge on the impact of shallow water on dynamic positioning capabilities.

A typical example of the shallow water/shallow draft condition related to a semisubmersible vessel is illustrated in Figure 1.2. SSCVs usually operate at a high draft, which leads to a smaller under-thruster clearance, even in water depths that are not considered shallow for Offshore Supply Vessels (OSV). Therefore, the possibility of reaching a reduced under-thruster clearance for SSCVs is higher than for the rest of the offshore fleet, hence the importance of further investigating this scenario.

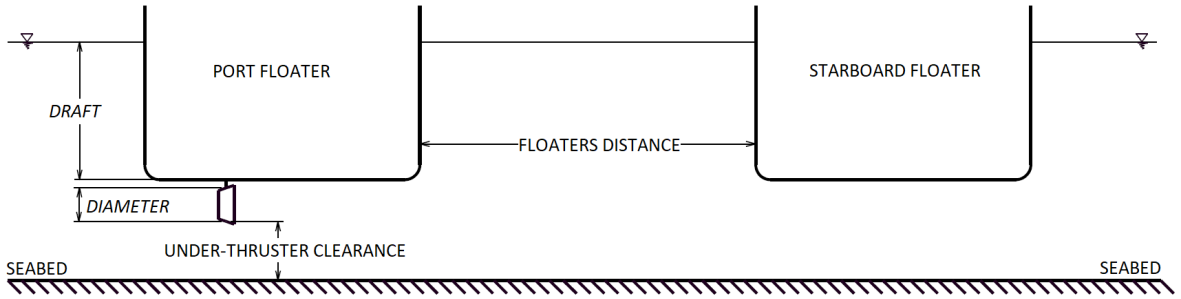

Figure 1.2: Front view of semisubmersible vessel in shallow water/shallow draft scenario.

1.2. Dynamic positioning systems in offshore operations

The primary focus of this thesis is to identify how the hydrodynamic behaviour of the flow around and beneath a semi-submersible vessel changes with a low clearance under the thrusters. The specific emphasis is on investigating how the interactions between incoming flow, thrusters, and hull are influenced by introducing an additional constraint represented by seabed proximity.

Evaluation of these interactions is well recognised in industry [24], and numerous studies have been conducted to estimate how such interactions result in a reduction of thrust compared to its performance in open water. Despite many improvements made in this area, including incorporating interaction assessments in the classification society guidelines [2], there is limited research on shallow water environments. Exploring shallow water depths is of interest to the maritime industry, as this subject is not fully understood yet, as noted in the DNV GL Dynamic Positioning philosophy guideline [16]. Further research has been conducted, particularly on the reliability of positioning systems by IMCA [23].

It is essential to quantify and predict the effect of these interactions to effectively incorporate possible losses into thrust allocation systems, as they are closely related to the stationkeeping performances of the vessel. In particular, these interactions have been examined in the context of deep water, and the prevailing approach in a typical DP system involves defining forbidden zones where the effectiveness of the thruster is considered null [48]. In contrast, thrusters are assumed to have constant efficiency in all directions except the forbidden zones. Despite this, interactions such as thruster-hull and thruster-thruster interactions can deteriorate the performance of the thrusters, depending on various parameters such as thruster direction, external factors like current, and the relative position of thrusters. [40].

DP current is the conventional method to evaluate the disturbances affecting the vessel. The concept of DP current can be visualized through Equation.1.1.

$$DP\ current = Thruster\ force - Wind\ Load \tag{1.1}$$

The calculation of the DP current involves evaluating the force acting on the vessel, which cannot be directly measured. The thrust magnitude and direction can be derived from the thruster performance specification and directly measured, as well as the wind measurement. Therefore, the external forces included in the DP current consist of current and wave load, external forces acting on the vessel (e.g. external loads during operations), thruster interactions, and more generally, all non-model phenomena[28].

While a prediction can be made for wave and current load based on the forecast, thruster interactions are often assumed to result in constant thrust reduction. However, this parameter generally does not include thruster-seabed interaction, which could lead to a higher calculated DP current in shallow water environments. It is relevant to understand the effects of shallow water conditions on the DP current within this context.

As a side note, it is essential to emphasise that the main focus of the research is not the scouring process caused by the thruster wash. Instead, the focus is on the thruster's efficiency when operating in proximity to the seabed. However, by assessing the thruster's efficiency, the outflow velocity characteristics (magnitude and direction) are derived, which are also crucial in predicting scouring.

1.3. Characteristics of the case study offshore vessel

The problem analysis starts with the description which is the case study vessel of a semi-submersible crane vessel used by HMC. It consists of two pontoons connected to the main deck via four columns. Key characteristics are described in Table 1.1.

Length:	206 [m]
Width:	88.4 [m]
Draft:	11.9 - 31.6 [m]

Table 1.1: Thialf characteristics

It is equipped with a DP3 system comprising three horizontal azimuth thrusters located below each pontoon (see Figure 1.3).

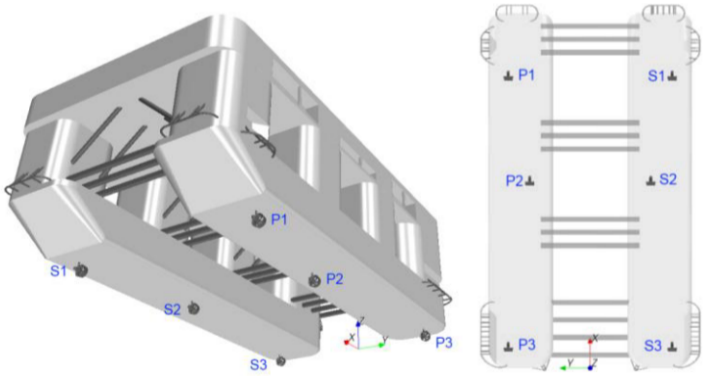

Name	Description
P1	PortSide Front
P2	PortSide Center
P3	PortSide Aft
S1	StarBoard Front
S2	StarBoard Center
S3	StarBoard Aft

Figure 1.3: Visual representation of the Thialf thruster position (*Ottens et al.* [44])

The propellers are of the FPP type (fixed pitch propeller), meaning that thrust is adjusted by changing the rotational speed. They are orientated horizontally, with no specified tilt angle for the thruster. This feature is especially significant in terms of the impact of the Coandă effect on thruster wash [30].

1.4. Thesis motivation

The present project pertains to the performance of a semisubmersible vessel operating in shallow waters, such as the North Sea, where thrusters operate in close proximity to the seabed. The decision to investigate this issue occurred when the vessel's crew observed an unusual increase in the power needed by the thrusters to maintain their position. As a result, the primary aim of the project was to uncover the causes behind this behaviour of the DP (dynamic positioning) system.

Field tests were conducted in the North Sea in 2023 as part of the project. These tests aimed to assess and quantify the interactions occurring beneath the hull and determine their impact on thruster performance. The objective was to evaluate two potential sources of thrust loss.

- The interaction between the thruster and the hull;
- The interaction between thrusters.

Multiple tests were conducted on the vessel to investigate the effect of these interactions in low under-keel-clearance conditions, particularly in relation to the thrusters' performance. This section describes the thesis's focus and the conclusions drawn from the tests, especially the differences in the obtained thrust in the two scenarios.

- Upstream thrusters delivering thrust at 90° (sideways).
- Downstream thrusters delivering thrust at 90° (sideways).

In both tests, the thrust has been applied manually based on the information displayed in the DP system. However, it should be mentioned that the system calculates the provided thrust based on the [rpm], therefore no differentiation has been applied between the upstream and downstream thrusters. Indeed, the system does not take into account the variable thrust loss due to the position of the thruster. It rather assumes a constant thrust reduction factor regardless of the thruster direction and position (in this case, the thruster forbidden zones were not taken into account for the test purposes).

Figure 1.4 provides a schematic representation of the approach used. The main goal of the tests is to evaluate the difference in the interaction of thruster outflow with the downstream pontoon (left) compared with thruster operation below a single hull (right).

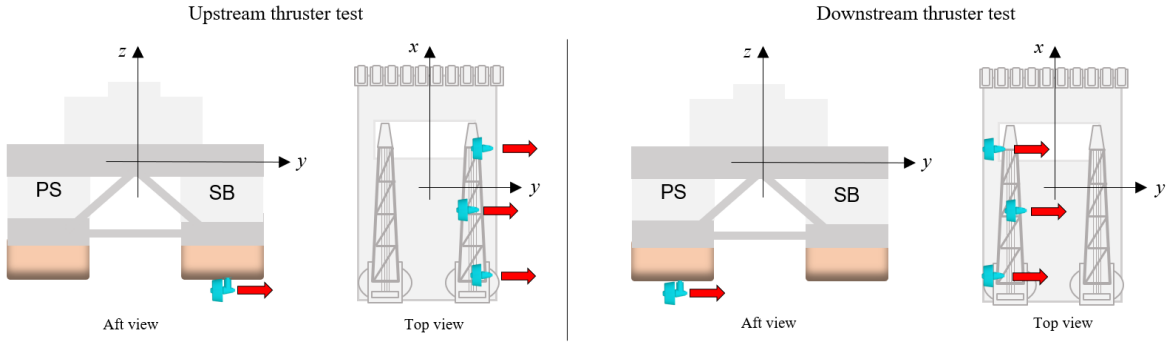

Figure 1.4: Schematic representation of the tests performed to investigate the effect of interaction between thruster and hull.

Four repetitions of the mentioned tests have been done within two different days. It is relevant to mention that the defined conditions have been tested consecutively. Therefore, minor changes are expected between the upstream DNA and the consecutive downstream tests. Despite this aspect, providing a clear overview of the uncertainties in such a scenario is interesting. This aspect will be further developed in the next section.

The collected information consists of the following:

- Thruster rotational speed [rpm];
- Thruster azimuth angle [°];
- Vessel Heading [°];
- Vessel Speed [m/s] in East and North direction from GPS measurement;
- Wind speed [m/s] and direction [°]

In addition, weather forecasts are available. They provide information about current (speed and direction) and waves (H_s and direction) even though the data is available every 3 hours.
However, it should be noted that the tidal current prediction, which is the only current component acknowledged for the area, is available every 10 minutes.

These data will be used to evaluate the vessel speed on the water (V_w), which is then applied to the following formula as a correlation of force and speed.

$$F_y = C_{d,y} \cdot V_{w,y}^2 \tag{1.2}$$

where:

- F_y consists of the y-axis component of the force thrusters deliver. Specifically, given the $[rpm]$ and orientation of the thrusters, it is possible to obtain the direction and magnitude of the delivered speed. However, these data are obtained considering no forward speed and the open water (OW) condition.
- $C_{d,y}$ is the loading coefficient, which includes all external forces acting on the vessel (current, wind, waves, etc.).
- $V_{w,y}$ represents the velocity on water towards the y-direction. This parameter has been obtained by combining the GPS velocity with the current speed according to the following formulation.

$$V_{w,y} = V_{GPS,y} + V_{current,y} \tag{1.3}$$

All the mentioned directions are based on the vessel-based coordinate system as shown in Figure 1.4.

Given the complete set of available information, the primary goal was to evaluate the magnitude of the interactions that take place between the hulls, therefore using the downstream thruster as the base case. However, it is important to highlight that the downstream tests are subject to interactions due to the deviation and modification of both upstream and downstream thruster flow. This information cannot be derived from the measured data. Moreover, the tests were conducted in shallow water/shallow draft conditions where thruster clearances were limited at an average value of 10 [m]. Therefore, the useful information that could be derived from these tests consists of an approximation of the thrust difference between upstream and downstream thrusters due to interactions.

In the evaluation of these differences, the following procedure has been used:

1. Data from downstream tests are post-processed to evaluate the secondary trace of the delivered thrust as measured by the DP system. This is obtained as a function of the rotational speed of the propeller (n);
2. Velocity on the water in the y-direction ($V_{w,y}$) during the downstream test is obtained (Equation 1.3). This velocity is used to obtain the load coefficient $C_{d,y-downstream}$ through equation 1.2;
3. Similarly to the first step, the velocity in water along the y-axis is evaluated for the upstream thruster test. This information can be multiplied by the previously obtained coefficient $C_{d,y-downstream}$ to further calculate the expected requested thrust (F_y);
4. The last step consists of comparing the force obtained at step 3 with the thrust derived delivered in the upstream tests. Indeed, F_y measured at step 3 considered the load coefficient $C_{d,y}$ equal for upstream and downstream cases. However, the predicted force in step 3 is expected to be lower than the delivered force from the upstream thruster due to additional interaction between the hulls.

The difference between the expected force using $C_{d,y-downstream}$ and the one obtained using the calculated $C_{d,y-downstream}$ represents the difference in terms on additional loads that act on the vessel between downstream and upstream cases.

To obtain reliable results, it is relevant to consider only the periods of time during tests when equilibrium is reached. Thus, not only is the thrust from the system constant, but also the speed of the water along the y-axis. Constant velocity implies equilibrium of forces and, therefore, no acceleration of the vessel. Considering this goal, three out of four tests resulted in sufficiently constant water speed, specifically the first three. Therefore, only these tests have been taken into account to derive conclusions. Results are plotted in Figure 1.5, where percentages are calculated as follows.

$$V_{ratio} = \frac{V_{w,y_{mean,upstream}} - V_{w,y_{mean,downstream}}}{V_{w,y_{mean,upstream}}} \tag{1.4}$$

$$T_{ratio} = \frac{T_{up} - C_{d,y-downstream} \cdot Vw, y_{mean,upstream}}{C_{d,y-downstream} \cdot Vw, y_{mean,upstream}} \tag{1.5}$$

As presented in Figure 1.5, the difference between upstream and downstream delivered thrust ranges from 10% to 15%. This suggests an initial conclusion that a consistent portion of thrust may be lost due to the interaction between the thruster outflow and the hull, particularly the downstream pontoon. However, it is essential to assess the uncertainties associated with these tests, rendering these results tentative.

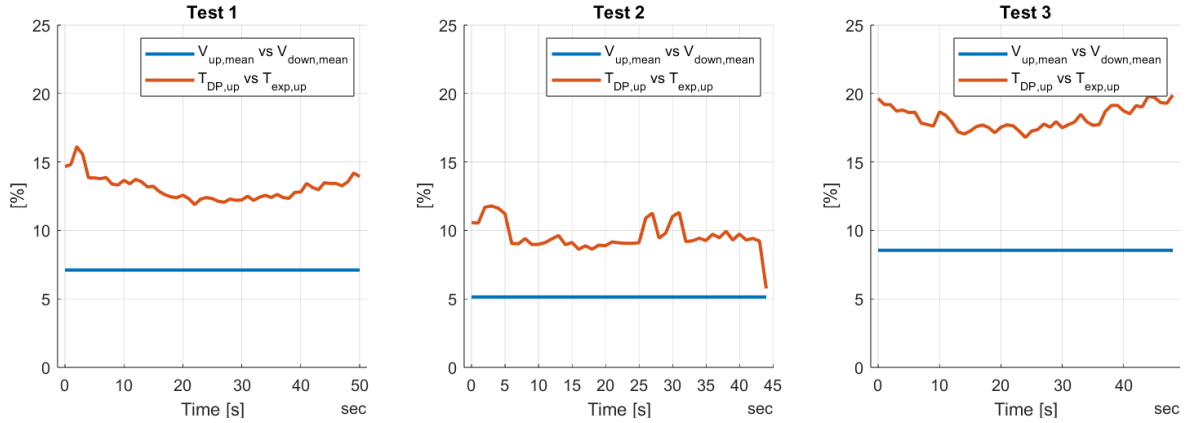

Figure 1.5: Percentage difference of: mean velocity on the water along the y-axis on the upstream and downstream thruster (blue line). Delivered thrust during upstream tests measured from [rpm] and direction compared with the expected thrust assuming that $C_{d,y-downstream} = C_{d,y-upstream}$ (red line)

.

To accurately evaluate the magnitude of these interactions, it would be advisable to isolate the load components caused by waves, wind, and current based on a more precise evaluation, as the present tests have been subject to different uncertainties:

- External forces measurements;
  - Wind;
  - Waves;
  - Current.
- Delivered thrust compared to the values obtained by the system.

Despite the uncertainties associated with these tests, the obtained results provide confidence in understanding the interaction between the thruster and the hull and between the thrusters themselves. These data, along with observations of the vessel's behaviour, motivate the research investigations presented in the current thesis.

1.5. Statement of the research problem

The interactions that occur when a thruster is operating beneath a vessel are multiple: thruster-hull, thruster-current, and thruster-thruster interaction are examples of them, and their effects may cause a reduction of the effective thrust. These interaction effects result from pressure and friction forces on the vessel hull, combined with a change in thruster inflow velocity, caused by current and the wake flow from nearby thrusters [12].

When looking at dynamically positioned vessels, especially twin-floater semisubmersible vessels, more elements of thrust loss are introduced. For instance, the impinging of the jet produced by the thruster on the downstream hull (blockage effect) does not exist for monohulls. Another aspect that plays a role in a vessel's DP capability is the interaction of the thruster with the seabed.

Despite the presence of the seabed potentially leading to changes in flow behaviour and, thus, a different effective thrust, this aspect has not been largely developed and examined in the literature.

Thruster interactions have been primarily investigated in a technical report by *Lehn* [36]. It provides a straightforward formulation to offer a clear picture of how the thruster-generated force can be affected by interactions and external loads:

$$\vec{F_I} = (\vec{F} - \vec{F_C}) - \vec{T} \tag{1.6}$$

where:

- F_I is the interaction force
- F is the total force registered with the working thruster and given external loads
- F_C is the total environmental force
- T is the total available thrust (registered from the DP system)

This research aims to improve the understanding of the relationship between thruster jet stream, hull and seabed during dynamic positioning operations in shallow waters with limited clearance below the thruster (*under-thruster-clearance*). This clearance is the distance between the propeller blade tip and the seabed. An under-thruster clearance of 6 meters is a reference value for initial calculations.

Before delving into the problem, it is important to clearly understand the various types of interaction that occur on a dynamically positioned vessel, not only in shallow waters but also in deep water conditions. Both ITTC [24] and ABS [2] provide a comprehensive list of interaction effects, particularly focusing on semisubmersible vessels:

- **Thruster-Thruster interaction**: When a thruster operates behind another thruster, it receives a positive inflow velocity. This effect leads to a decrease in the delivered thrust.

- **Thruster-Hull interaction**: This consists of the interaction between the thruster outflow and the hull. The effects include frictional losses, the flow deviation due to the Coandă effect, and the blockage effect (caused by the impact of the thruster outflow with the opposite pontoon). This effect could become particularly relevant in the presence of another hull behind the flow, as is the case for a semisubmersible vessel.

- **Thruster-Current interaction**: When a current is present, it could lead to changes in the effective thrust direction. This aspect is particularly relevant when the high environmental current could lead to significant inefficiencies [52]. Furthermore, the presence of the current leads to a positive inflow velocity on the thruster, resulting in thrust reduction.

- **Thruster-Wave interaction**: Two main effects are related to the interaction between the thruster and the waves:
  - Degradation due to oscillating flow caused by waves;
  - Ventilation.

In addition to the interactions mentioned above, the proximity between the thrusters and the seabed could influence the assessment of thruster efficiency, as the additional constraints imposed by the reduced under-thruster clearance could result in variations in the known interactions. Therefore, a comprehensive evaluation of its impact is the subject of the current study.

Furthermore, a common characteristic among dynamically positioned vessels is the presence of multiple thrusters at different hull locations. As confirmed by *Shatto et al.* [50], to achieve lower fuel consumption, it is preferable to use more thrusters at a relatively low load rather than fewer thrusters at a higher load. Therefore, evaluating to what extent the aforementioned interactions affect station-keeping performance, leading to an increase in the requested power, is a relevant aspect.

This research direction is also based on first-hand experience provided by the crew on board the vessel. Direct feedback from the crew indicates that when operating in shallow water areas, the DP system detects a DP current that does not align with the forecast current and wave conditions, leading to relatively increased power demand on the thrusters. Consequently, this prompts the need for further investigation into this. First-hand experience highlights the need to increase the loads on the thruster to maintain position.

In conclusion, the present thesis aims to investigate the thruster interaction phenomena from both a theoretical and practical standpoint. The main goal is firstly to establish the appropriate theoretical frameworks to physically explain the physics of the problem and later develop a numerical methodology to estimate the impact of seabed proximity on the effectively delivered thrust. The driving scope of the entire thesis is therefore summarized in the research question:

"What is the impact of reduced under-thruster clearance on the efficiency of the thruster in DP operations?"

Subquestions have also been defined to establish more precise research directions.

- How does beam-side current, in combination with reduced under-thruster clearance, impact thruster efficiency?
- What is the impact of the geometrical characteristics of the hull (floaters distance) and the position of the thruster on the performance of the vessel when operating in beam-side current and reduced under-thruster conditions, with comparison to the deep water case?

1.6. Report structure and organization

The present report is structured in four major blocks: literature review, thruster interactions analytical estimation, CFD methodology and results, and conclusions.
It begins with describing thruster outflow characteristics in open-water scenarios and below the ship's hull (Chapter 2). Additionally, theoretical and experimental accounts of the Coandă effect will be presented, as it constitutes a fundamental phenomenon in jet stream development. Each type of interaction will be examined, with a focus on findings from previous studies to gain an understanding of their operational mechanisms, including estimations of potential thrust loss related to these factors.

After conducting a comprehensive literature review, analytical calculations were carried out in Chapter 3 to provide an initial estimation of the impact that each type of interaction has on the thrust delivered to the vessel. These calculations constitute the basis of the next step.

The last step of the process, and the most relevant one to obtain useful results, involves Computational Fluid Dynamics (CFD) simulations which have been developed for this specific purpose. In particular, the description of theoretical aspects related to the CFD approach will be provided, as well as its limitations in Chapter 4. In the next chapter (Chapter 5), the results obtained from the performed results are presented and post-processed with a particular focus on the practical impact of the measured thrust reduction.

The last chapter (6) identifies the obtained outcomes as well as the future work needed to improve the present work and which future investigation could follow the findings of this thesis.

2

Literature research

The literature review chapter consists of the premises of the present work. It is particularly relevant to provide a detailed description of both the physical and practical aspects of the interactions affecting semisubmersible crane vessels (SSCV). Highlighting the already available knowledge in this regard aims to provide the framework for defining the follow-up work. The structure is set up to first introduce a fundamental effect that involves a jet stream in proximity to a boundary, as the hull and seabed represent. Subsequently, a description of each interaction effect is presented to highlight which of them is more relevant to the scope of the present work.

2.1. The Coandă effect and its relevance to offshore operations

The Coandă effect is defined by ITTC as one of the sources of trust loss, and it is included in the group of thruster-hull interaction. As the main goal of this project is to estimate the thruster interactions through a numerical approach (Computational Fluid Dynamic), a theoretical analysis of the Coandă effect is required to provide the reader with a clear understanding of this phenomenon. In particular, this chapter aims to describe how this effect plays a fundamental role in assessing the interactions between the hull and the thruster outflow.

An effective definition of the Coandă effect in marine environments is given by *Lehn (1985)* [35] as the tendency of jets and propeller outflow to deflect towards surrounding surfaces. This behaviour is of primary interest and may lead to significant thrust losses; therefore, it is important to provide an overview of the mathematical and practical description of the phenomenon. According to the brief description provided by Lehn, some further steps can be done as also mentioned in the *Faltinsen* [19] theory about the Cŏanda effect. Indeed, if a boundary is present in the nearby of the jet stream, the velocity will be at the maximum between the jet and the boundary, which therefore leads to low pressure according to Bernoulli's law. The final outcome consists of the flow being diverted towards the surface due to the present force.

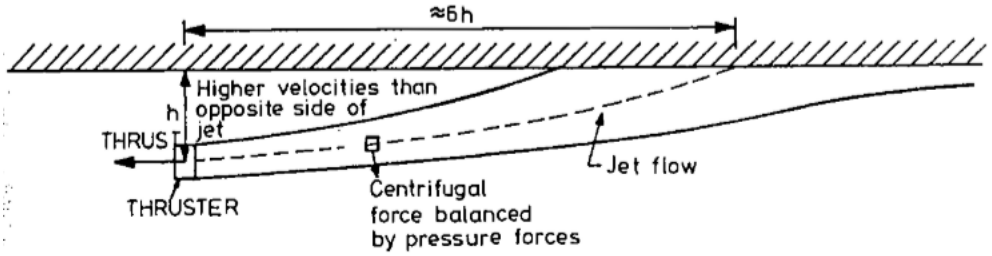

Figure 2.1: Representation of the deflection of propeller slips stream due to Coandă effect by *Faltinsen* [19]

.

The experimental results remain a valuable approach to defining the phenomena. This has also been stated by *Lehn* [35], *Nienhuis* [43], and *Fjørtoft* [20], which extensively covered a series of model tests to provide specific information on the Coandă effect and how the flow deviation impacts the different types of interaction, leading to additional thrust losses. This effect will be extensively described in the hull interaction section 2.3.

The study by *Nienhuis* [43] constitutes a pioneering work on thruster-hull interaction. In this study, the effects of thruster-hull interaction are assessed. Specifically, the author quantified the flow deflection obtained from varying the relative position between the thruster and round bilge. As presented in Figure 2.2, these results are useful to better understand how the velocity profile of a thruster below the hull is affected by the presence of the hull. The impact of thruster position on the Coandă effect can be seen from the velocity distribution for three different thruster positions provided by *Nienhuis (1983)* [43].

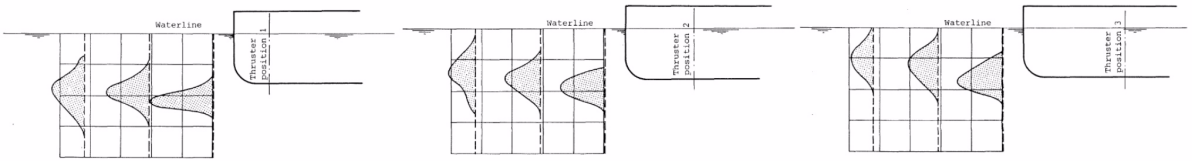

Figure 2.2: Vertical deflection of the maximum longitudinal velocity caused by the Coandă effect depending on thruster position below the hull (*Nienhuis*)[43]

Not only the thruster position, as shown in Figure 2.2, but also the shape of the hull above the thruster affects the shape of the thruster outflow. Specifically, the radius of the round bilge of the pontoon. In fact, a larger deviation is experienced in the flow developed under a barge with a large round bilge radius. Furthermore, the flow velocity also affects the flow deviation, as stated by *Fjørtfoft* [20]. This phenomenon can be attributed to the "deterioration" of the flow field, resulting in a decrease in velocity. Consequently, the centripetal force (V^2/R) required to maintain the attached flow decreases. Therefore, a higher thrust will generate higher flow velocity, therefore the mitigation of the flow deviation.

The described Coandă effect is strongly related to the presence of a surface in proximity of the jet. This effect could be mitigated with a tilted thruster, which consists of a non-horizontal thruster, leading to an outflow direction that is not parallel to the bottom of the hull. This aspect has been investigated in different publications including *Jürgens et al.* [30] and *Bulten et al.* [7]. Figure 2.3 represents the difference between these two types of thrusters in terms of flow direction.

Figure 2.3: Velocity distribution as a function of the tilt angle of the propeller axis by *Jürgens et al.* [30]: horizontal (left) and tilted thruster (right). For the horizontal propeller (0°) the flow is more diverted to the opposite pontoon than the tilted one (8°).

After briefly describing the Coandă effect, it becomes evident that this phenomenon manifests whenever a fluid jet interacts with a nearby surface. Therefore, in the context of a thruster operating near a vessel hull, the outflow can deviate towards other surfaces, such as the downstream floater in the case of a semisubmersible vessel. This deviation contributes to additional losses in terms of the effective thrust delivered to the vessel. The Coandă effect remains a dominant element in another effect known as the blockage effect. Here, the thruster outflow impinges on the downstream floater, further complicating the flow dynamics and reducing effective thrust.

Furthermore, introducing a second constraint to the jet, represented by the seabed, introduces another Coandă effect due to the presence of this additional boundary. For simplification, the seabed can be compared to a flat wall, influencing how the jet from the thruster behaves as it interacts with this boundary. Studies, such as one conducted by *Johnston et al.* in 2012 [29], have specifically investigated how the seabed influences the development of propeller wash and its impact on vessel dynamics.

The experimental setup involved measuring the velocity profile at different radial positions in the thruster jet stream at different distances from the propeller location. These results were achieved through model tests and velocity measurements using PIV. An under-thruster-clearance-over-diameter ratio of 1.26 has been considered, and measurements are provided at the centerline location as well as $r/R_p = 2.5$ (Radial position r, over propeller radius R_p). It was observed that as the radial distance increased, the measured axial velocity was significantly higher compared to the unconfined condition. This difference was found to increase further away from the propeller position.

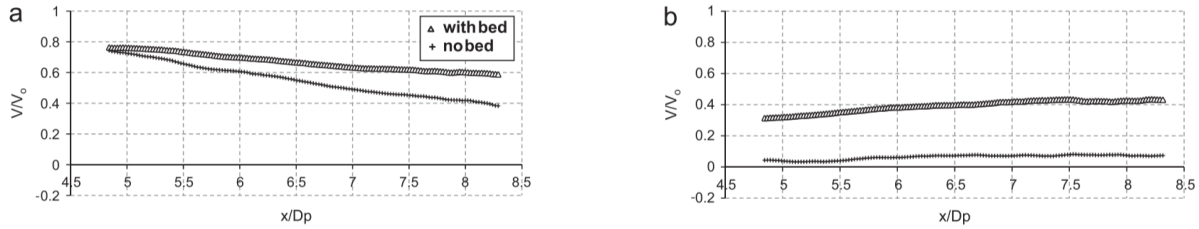

Figure 2.4: Longitudinal velocity profiles at centerline (a) of the jet stream and at $r/R_p = 2.5$ (b) of the propeller jet-stream with and without seabed by *Johnston et al.* [29]

In confined conditions, as shown in Figure 2.4, the axial velocity is consistently higher than in the deep water case. Hence, a boundary in an expanding propeller jet causes the jet to expand more rapidly towards the boundary and to impact the boundary earlier than expected under deep circumstances. [29]. Indeed, expansion angles have consistently been found to be higher. This implies that the jet stream deflect towards the seabed with higher angle than deep water[53].

Further investigation of the deviation of the propelled jet stream due to the presence of the seabed has been carried out by *Wei et al.* [53]. Specifically, they investigated different clearance conditions, and here the cases of $Z_b = 2D_p$ and $Z_b = D_p$ (Z_b = clearance, D_p = propeller diameter) will be reported.

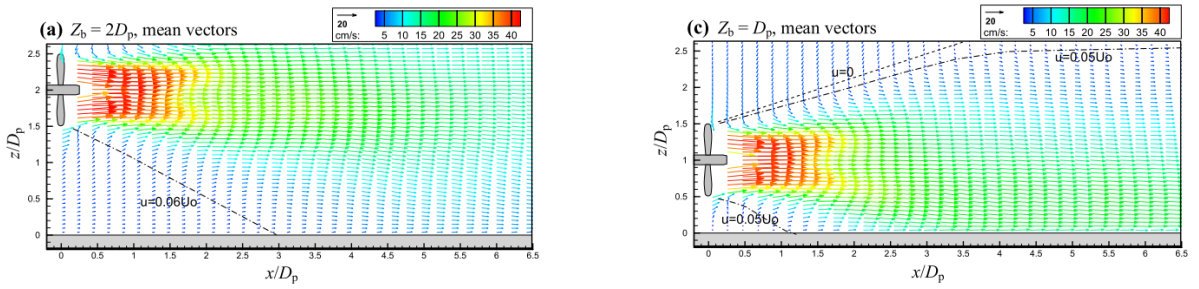

Figure 2.5: Vector plots and streamlines of mean velocity field with clearance of $Z_b = 2D_p$ (left) and $Z_b = D_p$ (right) by *Wei et al.* [53].

Due to the relatively elevated clearance at $Z_b = 2D_p$, as shown in Figure 2.5, the impingement point is located further downstream compared to configurations with lower clearances. This suggests that a significant portion of the jet energy has dissipated before reaching the bed. Consequently, the jet exhibits characteristics similar to those of an unconfined jet, and its overall shape undergoes minimal deformation.

For the case of a reduced clearance ($Z_b = D_p$), the flow is diverted, and the symmetrical, unconfined jet model is no longer applicable. This deviation occurs as a result of Coandă effects induced by the boundary, which influence the flow dynamics. This is shown in Figure 2.5. It is, therefore, proven that the effect of the seabed could influence the propeller jet stream direction.

Further investigations with reference to the practical case of a semisubmersible vessel in station-keeping conditions will be pursued and described in the next chapters.

2.2. Definition of thruster flow interactions in DP vessels

The next step is to describe the dynamics of a jet stream operating beneath the hull from both a theoretical and experimental perspective. By explaining what the Coandă effect consists of, we can then move forward in the analysis of the thruster's interaction.

In defining the problem of interest, a brief presentation of the effects leading to a reduction in the effective thrust has been provided. Therefore, it is primarily important to focus on each of them in more detail. This section aims to provide a clear indication to the reader about the state-of-the-art literature on these effects and to highlight which steps need to be followed in the present work to expand the actual knowledge about this topic. Initially, a more general description of these effects is listed below as suggested by *Arditti et al.* [3]:

- Phenomena related to the outflow of the thruster($\eta_{outflow}$):
  - thruster - hull interactions;
- Phenomena related to the inflow of the thruster (η_{inflow}):
  - thruster - thruster interactions;
  - thruster - current interactions;
  - thruster - wave interactions.

which leads to the following efficiency definition:

$$\eta_{total} = \eta_{outflow} \cdot \eta_{inflow} \tag{2.1}$$

2.3. Interaction between thrusters and vessel hull

The interaction between the hull and the thruster jet stream in the context of a semisubmersible vessel can be categorised into two different components which consist of:

- Interactions between the thruster jet stream and the hull above the thruster. This consists of both the deflection of the flow towards the hull due to the Coandă effect and the friction on the hull surface leading to a degradation of the thrust.
- Interaction between the jet stream and the opposite pontoon, therefore, the blockage effect is also influenced by the Coandă effect. Indeed, the impingement of the thruster wash leads to a pressure distribution which then results in a force opposed to the thrust.

2.3.1. Effects of the hull bottom on thruster jet stream

The Coandă effect is of main interest when analyzing the interaction between the thruster jet stream and the hull. A general description has already been provided in Section 2.1. However, the characteristics provided in the literature will be presented and analyzed in more detail in this chapter. Specifically, the goal of the next sections is to provide the necessary background to understand how the hull geometry and operational characteristics affect the thruster outflow beneath the hull. It is important to introduce this phenomenon extensively to further interpret the results obtained from the CFD simulations.

Thruster position & Round bilge radius

The effect of the thruster position both in terms of distance from the hull and distance from the round bilge of the hull is presented in the following lines. These parameters indeed affect the attachment length and therefore the velocity profile. As presented in Chapter 2.1, not only the length of attachment but also the deviation of the flow depends on the mentioned distances.

Lehn [35], *Nienhuis* [43] and *Fjørtoft* [20] widely investigated this phenomenon through model tests, but also further measurements, both with CFD and PIV measure, have been carried out by *Cozijn et al*. As presented by *Cozijn et al.* [8], the presence of a hull above the thruster causes the propeller jet to lose the typical rounded shape as in open water, which assumes a flattened shape in correspondence with the floater as shown in Figure 2.6 compared to Figure 2.7.

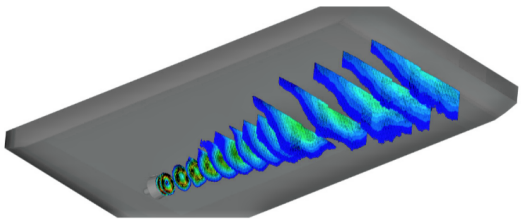

Figure 2.6: PIV results for vertical thruster under a plate. Cozijn - Wake flow behind azimuth thruster - Fig. 12

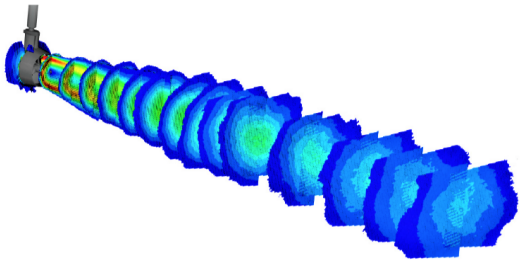

Figure 2.7: PIV results for vertical thruster in Open water. Cozijn - Wake flow behind azimuth thruster - Fig. 11

Furthermore, the resulting velocity field is higher in proximity to the floater compared to the results obtained for open water [8] due to the restriction of the flow caused by the hull above it. The mentioned effect has also been observed by *Nienhuis* [43], which, however, found that only a minor increase has been registered in terms of maximum velocity. The results obtained by *Nienhuis* are reported in Figure 2.8. The reported measurement has been performed with a nozzle type 36 and no current. Furthermore, only one propeller speed has been considered. Similar results to those already presented were derived by *Cozijn* in 2012 [11].

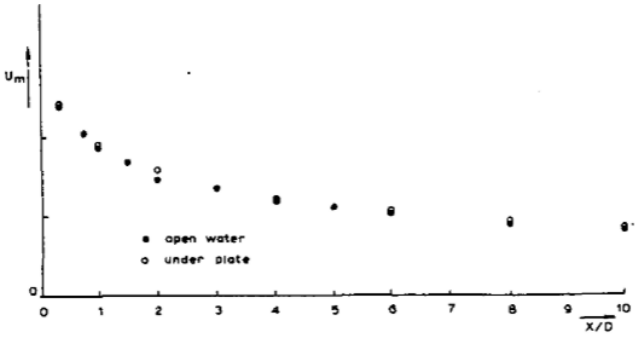

Figure 2.8: Magnitude and location of maximum axial velocity in the behind condition in open water and under a plate by *Nienhuis* [43]

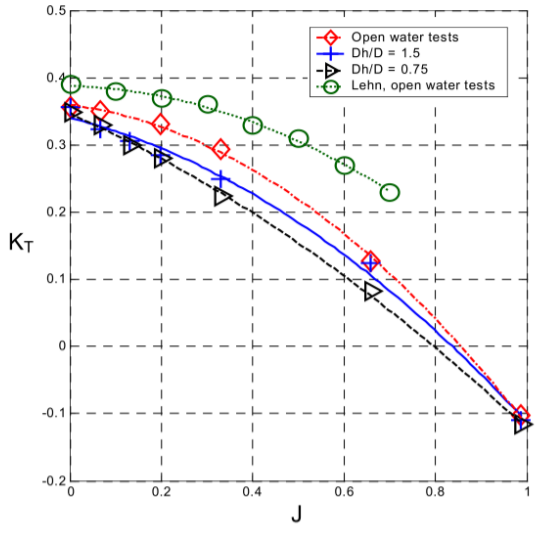

Figure 2.9: Thrust coefficient vs advance ratio at different distances form the hull of the thruster (vertical position) by *Ekstrom et al.* [18]

The flow development, hence the delivered thrust, is influenced by the presence of the hull above it. With regard to this aspect, a more detailed description of the thruster's vertical and horizontal position impact, as well as the effect of the radius of the round bilge on the thrust, is provided. These aspects have already been briefly discussed in Chapter 2.1.

Regarding the vertical position of the thruster *Fjørtoft* [20] states that by increasing the vertical distance between the thruster and the hull, the thrust loss is reduced. Regarding this aspect, experimental values are provided by *Ekstrom et al.* [18]. They are shown in Figure 2.9, and it should be noted that for a higher distance between the propeller axis and the hull, a higher K_T is recorded, leading to a higher thrust delivered for a fixed value of the advance ratio J.

Regarding the horizontal position of the user, decreasing the horizontal distance between the thruster and the model side will generally reduce the thrust loss. More investigations have been carried out other than *Ninenhuis* (Figure 2.2). *Cozijn et al.* [8] specifically investigated the effect of different distances combined with different bilge radii, proving that the effect of a larger distance between the thruster position and the hull leads to an enhanced deviation due to the Coandă effect. The setup used is shown in Figure 2.10.

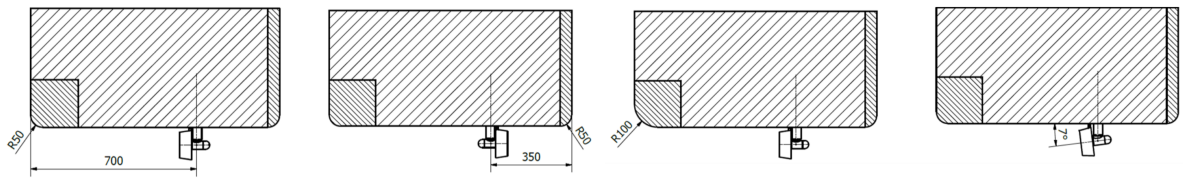

Figure 2.10: Barge configuration for investigation of thruster position effect in thruster-hull interactions (*Cozijn et al.* [8])

In fact, the radius of the bilge has a relevant effect on the deviation of the jet stream. Specifically, the larger the radius, the higher the deviation due to the Coandă effect [43, 8, 11, 20]. This statement is confirmed and visualised in Fig. 2.11.

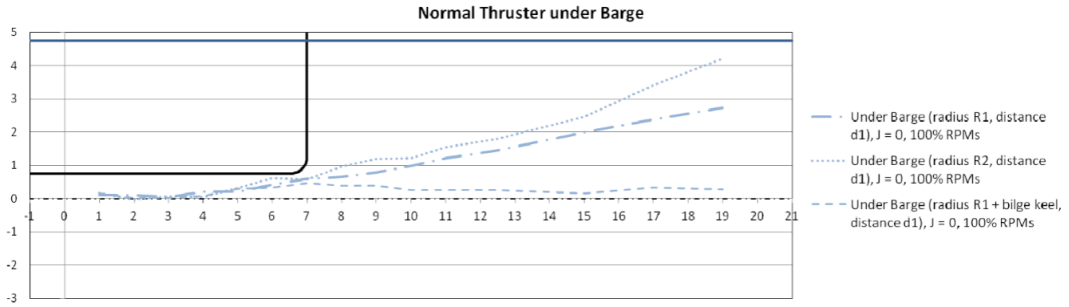

Figure 2.11: Thruster wake Under Barge (radius R1 / radius R2 / radius R1 + bilge keel) by *Cozijn et al.* [11]

The presented description is to be expected since, for a larger distance from the side, the velocity in the jet cross section at the bilge drops. Consequently, the flow will remain attached to the bilge for a longer time because the centripetal force (suction force) required for a given deflection will be smaller, as proven by *Lehn* [35] and confirmed by *Fjørtoft* [20]. The Coandă effect is enhanced when the thruster is positioned far from the round bilge. Furthermore, as the required flow acceleration increases with V^2/R, an increase in the bilge radius leads to the same tendency [43]. Therefore, a higher thrust will mitigate the flow deviation.

CFD investigation of the effect of round bilge and thruster position beneath the hull has been carried out by *Maciel et al.* [39], whose results are presented in Figure 2.12. The obtained scenarios are in accordance with the previously introduced conclusions. Nevertheless, a more precise axial velocity distribution is available through CFD simulations.

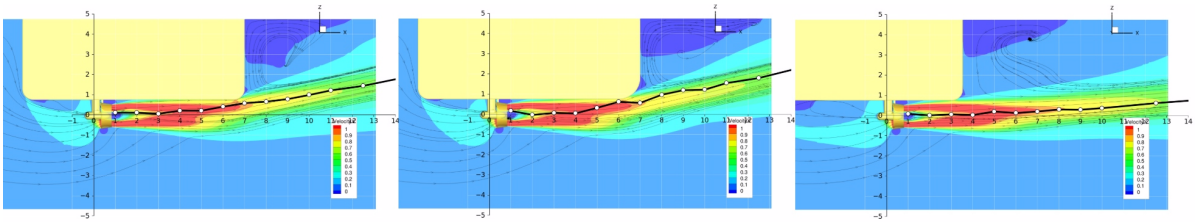

Figure 2.12: CFD x-velocity flow field (V_x) under a barge in different condition: base case (right), increased round bilge radius (centre) and close to the side (*Maciel et al.* [39])

However, it should be pointed out that when the thruster is very close to the round bilge, the angle of attack between the jet stream and the bulge structure could be more favourable and induce a more evident Coandă effect. Specifically, this is the case when the thruster wash does not attach to the flat part of the bottom but is rather attracted by the round bilge, leading to higher deflection of the flow [20].

American Bureau of Shipping [2] suggests to take into account a thrust deduction factor $t_c = 0.97$ (this represents the remaining available thrust) due to the Coandă effect. Therefore, the thrust is considered to be reduced by 3% due to the deviation of the thruster wash. However, it should be mentioned that the proposed value is an average thrust loss measured in previous studies and does not take into account any influence from the distance between the thruster and the floater, round bilge radius, and water depth. Therefore, it can be concluded that the proposed value should be taken with care, and a more in-depth analysis is required.

2.3.2. Impact of blockage effects on thruster performance

Blockage effect consists of the propeller jet stream impinging on the opposite pontoon leading to a reduction of the thrust output of the thruster. This effect first depends on the distance between the pontoon and the azimuth angle of the thruster [2]. Furthermore, *Cozijn et al.* [12] defined the blockage effect as the main source of thruster-hull interaction. Extensive investigation has been carried out with both model tests [9, 8, 12] and CFD simulations [44, 45, 9, 33, 32]. This effect is strictly related to the pressure developed on the opposite pontoon, which depends on the magnitude and direction of the velocity field generated by the thruster.

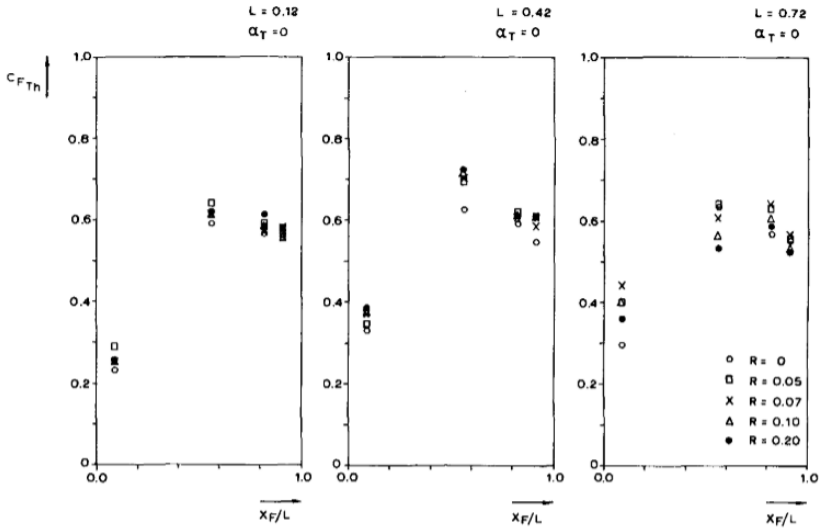

Figure 2.13: Transverse floater force as influenced floater position X_F, bilge radius R and thruster position L. In the x-axis, the distance between floaters is normalized over the thruster distance from the pontoon side, on the y-axis the force coefficients $C_{F_{Th}}$ represent the measured force on the floater as a percentage of the thrust of the thruster. (*Nienhuis*)[43])

Multiple experimental investigations have been carried out on the effect of the distance between the floaters, the radius of the bilge and the position of the thruster as the governing parameters by *Nienhuis* [43]. Figure 2.13 reports the thrust force coefficient as a function of the bilge radius (R) and the floater position X_F normalised with the thrust position l. Three different thruster positions have been considered. It resulted that both the distance between the floaters and the position of the thruster primarily plays a role in the reduction of thrust.

However, these results should be considered as a first reference and more detailed investigations are needed. This was also confirmed by Cozijn et al. [9]. A different nozzle geometry is indeed identified as a possible difference in the results obtained for the flow development and, therefore, in the blockage effect evaluation.

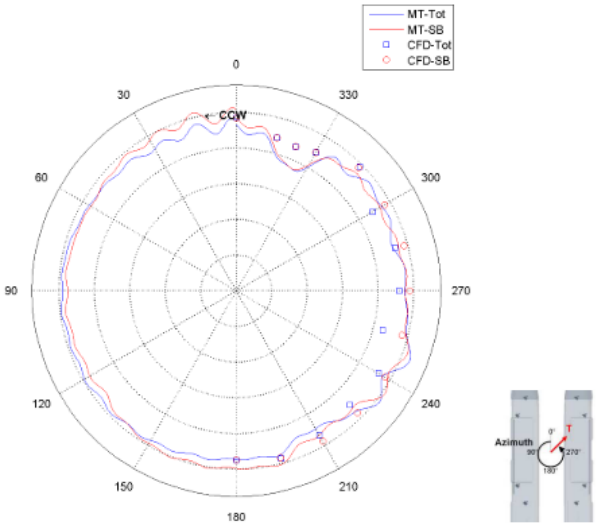

Figure 2.14: Single thruster-hull efficiency comparison between model test (MT) and CFD by *Ottens et al.* [46]. *Tot* means the total force on the vessel, *SB* means the force measured only on the starboard thruster to evaluate the thruster-hull interaction

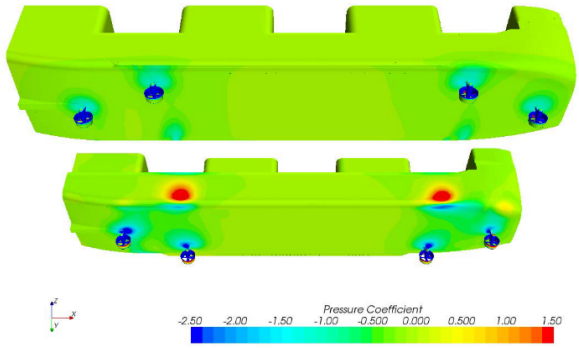

Figure 2.15: Visualization of the impingement of the thruster on the opposite floater, azimuth at 270. (*Ottens et al.* [46])

Further studies have also been carried out by *Ottens et al.* [46] using CFD to gain more insight into the dependence of the blockage effect with reference to thruster orientation. Specifically, the azimuth angles are fixed for the range of $[180 : 15 : 360]$, and one propeller speed $[rpm]$ has been investigated. Figure 2.14 visually represents the thrust deduction measured when the thruster is pointing towards the opposite pontoon. As shown, a pressure peak is present on the thruster wash direction on the surface of the opposite pontoon, which corresponds with the thrust deduction minimum on the thruster efficiency plot (Figure 2.14).

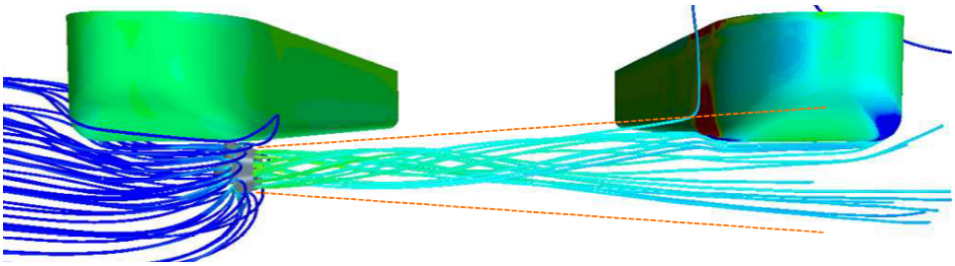

Figure 2.16: Streamlines for semisubmersible vessel with horizontal thruster at bollard pull condition with sideways operation. (*Bulten et al* [7])

The reduction of available thrust due to thruster-hull interactions has also been identified by *Bulten et al.* [7] as a major contributor to the decrease in thrust performance with the recorded thrust reduction factor up to 0.5. A relevant contribution to the research purpose of this thesis is the visualisation of the thruster-generated flow streamlines, which describe the impingement of the thrust wash on the opposite pontoon, (Figure 2.16), leading to considerable thrust loss.

Another proof of the relevant impact that the blockage effect has on the thruster efficiency is provided by *Jürgens et al.* [30]. This study focuses primarily on the difference between vertical and tilted thrusters. However, it provides good information about the problem. The result of this study is that the horizontal force produced by a tilted thruster could be 50 % higher than a horizontal one. This happens due to the blockage effect, which occurs on the opposite pontoon to the one where the thruster is located. Such a blockage is mitigated when the thruster is tilted. Graphical representation is provided in Figure 2.17.

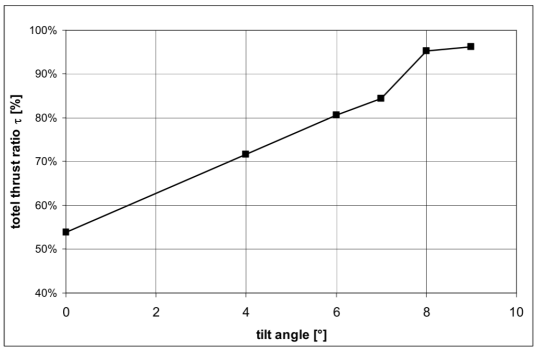

Figure 2.17: Total thrust ratio as the function of the tilt angle (*Jürgens et al.* [30]).

The total thrust ratio τ is defined as follows.

$$\tau = \frac{F_h}{T_h} \tag{2.2}$$

where:

- F_h: resulting horizontal force on the model;
- T_h: horizontal thrust of the open water thruster.

Therefore, assuming that the case with the maximum tilting angle has almost no interactions with the opposite pontoon, it can be derived that the magnitude of the blockage effect on the opposite pontoon should definitely be taken into account as a major player of thrust loss. While this is accounted for in the DP system for deep water, no information is available about shallow water, either from the deviation of the flow or the magnitude of this effect due to the higher inflow velocity, which is also a relevant parameter for thruster-thruster interactions.

ABS Guideline for Dynamic Positioning Systems [2] provides a formulation for the estimation of thrust reduction ratio (t_p) due to pontoon blockage as a function of the length (L_p) of the downstream centerline distance between two pontoons in meters. However, it should be noted that the proposed formulation relates to the deep water case.

$$t_p = 0.8 \cdot \left(\frac{L_p}{55}\right) \tag{2.3}$$

The thruster-hull interaction has also been investigated by CFD [22] for a specific model test equipped with a tilted propeller gearbox. This solution is meant to mitigate the blockage effect of the downstream pontoon and represents a solution to reduce the thrust-hull interactions [30]. Alternatively, the use of a bilge keel could provide a significant reduction in the interaction between the thruster and the hull [11], as the resulting thruster jet stream is not diverted to the opposite pontoon due to the Coandă effect, leading to lower thrust losses (see Figure 2.18). However, the bilge keel also introduced additional frictional losses.

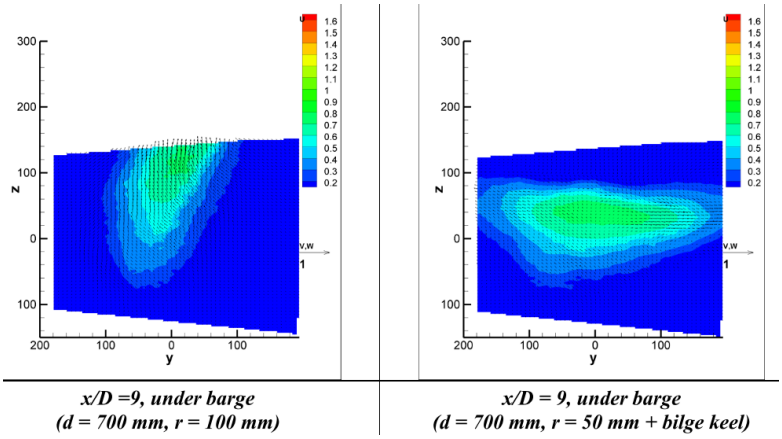

Figure 2.18: Comparison of velocity profile of thruster outflow at distance $x/D = 9$ between round bilge (left) and round bilge + bilge keel (right) by *Cozijn et al.* [11].

2.4. Interaction between thrusters and sea current

Thruster-current interaction can be considered a separate interaction that influences the thruster-hull interaction and thruster-thruster interactions. This is due to the fact that:

- Thruster jet stream are diverted, leading to different pressure fields in the next structures (blockage);
- The current produces different inflow velocities in the propeller compared to open water conditions [24].

As stated by *Cozijn et al.* [13], a DP vessel will experience a velocity inflow (V_{rel}) on the thruster due to current, leading to a reduction of the delivered thrust (T) if the propeller rotational speed (n) is fixed. This reduction is illustrated in Figure 2.19, where increasing the advance ratio J the thrust coefficient curve K_T(blue line) reduces with current direction with positive (AZIM = 0) inflow velocity.

$$J = \frac{V_{rel}}{nD} \qquad K_T = \frac{T}{\rho_{water} \cdot n^2 \cdot D^4} \tag{2.4}$$

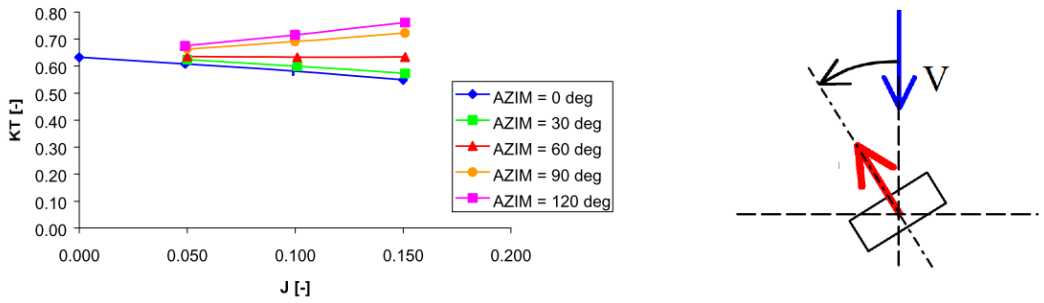

Figure 2.19: $K_T - J$ curve for a thruster in fixed current speed condition and variable azimuth angle (*AZIM*). At AZIM = 0° thrust decreases (positive inflow), at AZIM between 60° and 120° thrust increase (inflow aligned with thrust) (*Van Dijk et al* [52])

Further investigation, with greater attention to the flow in the region near the propeller, has been carried out by *Zhang et al.* [55]. This study is mostly related to the definition of the inflow and outflow of a ducted propeller. Therefore, some tests have been carried out to compare the behaviour of the heavily loaded propeller ($J = 0$, bollard pull condition) with a less loaded thruster ($J = 0.6$). The latter condition could be considered the worst situation, as the advance ratio J remains around 0 during normal DP operations. However, some details about the outflow can be derived.

Specifically, right after the nozzle, the high-speed flow pattern becomes unstable, leading to a bell-shaped velocity distribution. However, what is notable is that for higher advance ratios (J), the two peaks in the velocity distribution last longer, leading to higher velocity peaks at further distances compared to the bollard pull condition.

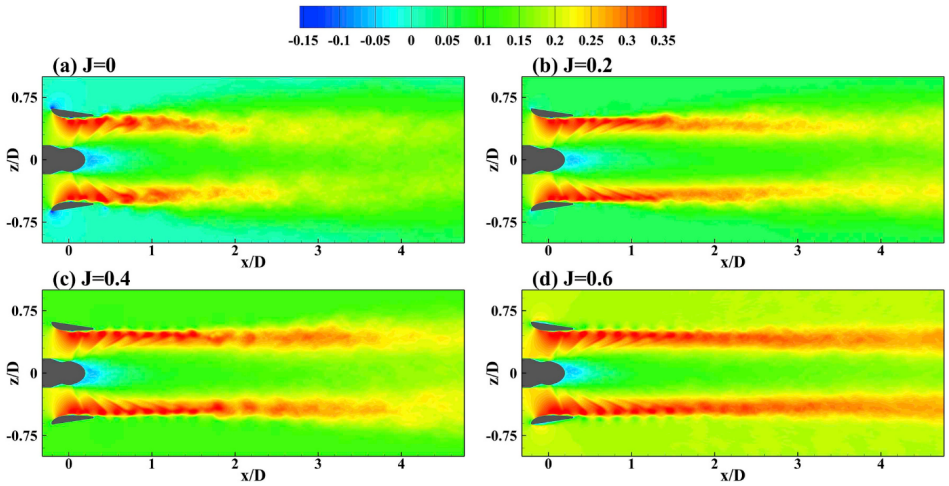

Figure 2.20: Phase-averaged stream wise velocity field in the plane at four advance coefficients *Zhang et al.*. The streamwise velocity is normalized by $U_{ref} = n\pi D$ (blade tip velocity). [55]

From a broader perspective, including the presence of the hull, PIV measurements improved the understanding of which effect current could have on thruster-hull interaction and, in particular, on the blockage effect. Specifically, *Cozijn et al.* investigated the effect of current (advance ratio $J = 0.2$) on a semisubmersible vessel, which resulted in an increase of the Coandă effect for horizontal thrusters, therefore more severe thrust-hull interaction.

Ottens et al. [46, 45] ran Computational Fluid Dynamics (CFD) simulations on the effects of current on a Semi-Submersible Crane Vessel (SSCV). Through these simulations, [46] aimed to establish a benchmark for CFD calculations concerning thruster interactions both with and without current.

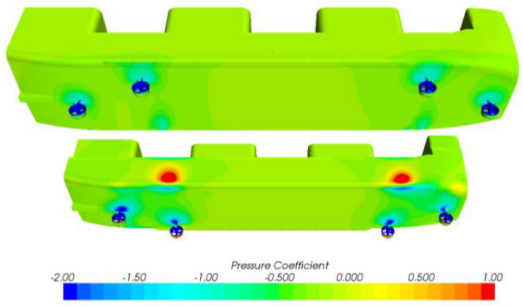

Figure 2.21: Visualization of the impingement of the wakes on the downstream pontoon without current, azimuth 270°s (*Ottens et al.* [45]).

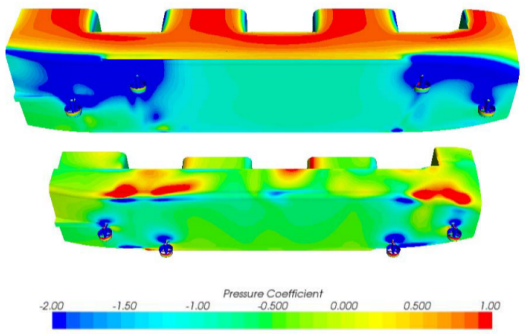

Figure 2.22: Visualization of the impingement of the wakes on the downstream pontoon in beam current of 2 knots, azimuth 270° (*Ottens et al.* [45]).

The subsequent research [45] focused on utilizing CFD to establish a benchmark for a semisubmersible vessel. Therefore, results will be presented to investigate the effect of current in deep water, which, however, leads to the importance of investigating the problem in shallow water when, due to blockage, the current load increases [32].

The result provided in Figure 2.21 and 2.22 shows a titled nozzle solution, which is introduced to mitigate the effect of thruster-hull interaction [30]. Despite that, the impingement of the thruster jet on the opposite pontoon and the effect of the current result in a more spread-out pressure distribution on the pontoon downstream of the one on which the thruster is installed. When the current velocity is increased, it results in a reduction in the impingement effect (at the same propeller rotation rate) due to the lower relative velocity in the wake [45].

To quantify the thruster-current interaction, a straightforward approach can be used to calculate the thrust loss, as suggested by *Van Dijk et al.* [52]. Specifically, the direct performance interaction due to an inflow velocity different from zero can be treated using the open-water propeller diagram and, therefore, by changing the advance ratio J). However, this provides a simplified approach by assuming that the inflow is uniform over the entire thruster area. In this calculation, the relative angle between the current and thruster can be evaluated using the relative angle and basic trigonometry. However, as mentioned by (*Koop et al.* [31]), this assumption could not always be considered valid, as the boundary layer of the seabed affects the tangential velocity distribution, leading to different velocity inflow.

2.5. Interaction between multiple thrusters operating simultaneously

Thruster-thruster interaction consists of the interference which happens between two or more thrusters operating simultaneously. It is caused by two primary reasons [52]:

- Blockage due to the impingement of thruster wash on another thruster;
- Efficiency loss due to modification of an in-behind thruster suction flow caused by the thruster upstream.

The visual representation of what thruster-thruster interaction consists in is provided in Figure 2.23.

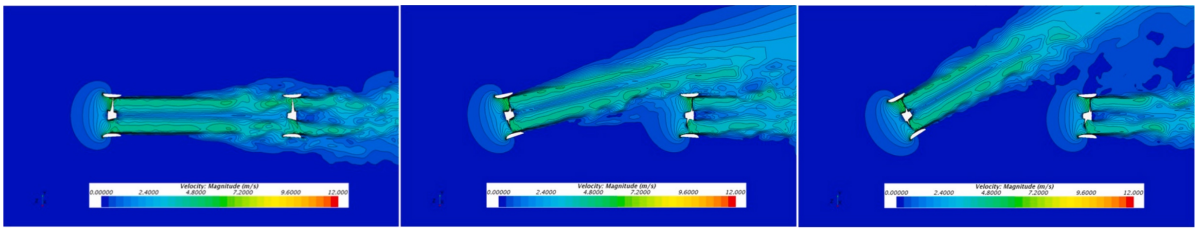

Figure 2.23: Velocity distribution of thruster outflow/inflow velocity as function of azimuth angle (*Zhou et al.* [56])

Lehn [35] provided the first investigation on the magnitude of the thruster-thruster interaction, describing the in-tandem condition (one thruster operating behind the other) as the most critical scenario. Specifically, the tests referred to the interaction in open water conditions and a thruster distance of 5 diameters of the propeller. In this scenario, a loss of around 50% compared to bollard pull thrust is measured for the downstream thruster. However, no thrust reduction is registered when the forward thruster is turned by 15°, and a distance of 6 propeller diameters is in place between the thrusters. The closer the thrusters are, the higher the angle required to maintain 100% thrust in the thruster behind.

Following and more extensive tests have been performed by *Nienhuis* [43], who investigated the differences in the thruster-thruster interaction when a plate is placed on top of the thruster. The specific reduction in thrust and torque in the rear thruster has been evaluated based on the distance between the thruster. A similar test has been developed with reference to the effect of the angle.

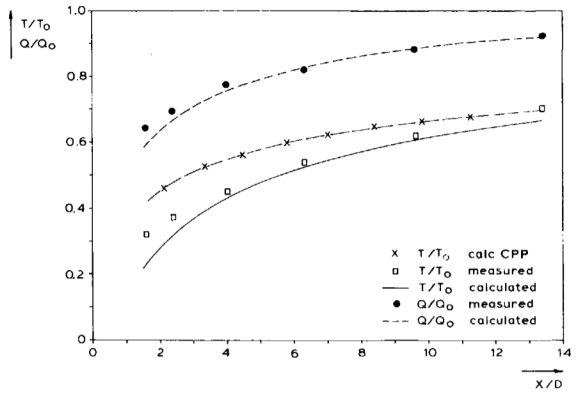

Figure 2.24: Thruster-thruster interaction in open water depending on the distance between thruster by *Nienhuis* [43]

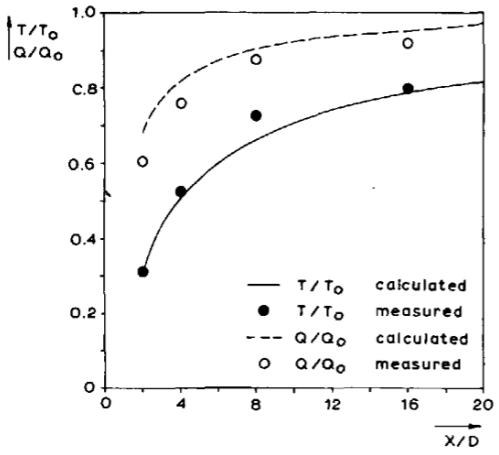

Figure 2.25: Thruster-thruster interaction under a plate depending on the distance between thruster by *Nienhuis* [43]

As can be seen in Figures 2.24 and 2.25, the interaction in open water continues over greater distances between the thrusters due to the enhanced spreading of the jet when it is in proximity to a flat plate. Furthermore, when two thrusters operate in line (0° in Figure 2.26 and Figure 2.27), the maximum thrust reduction is experienced. As obtained by *Lehn* [35] closer thrusters requires a higher azimuth angle of the thruster in front to obtain 100% thrust of the in-behind thruster (Figure 2.26 and Figure 2.27).

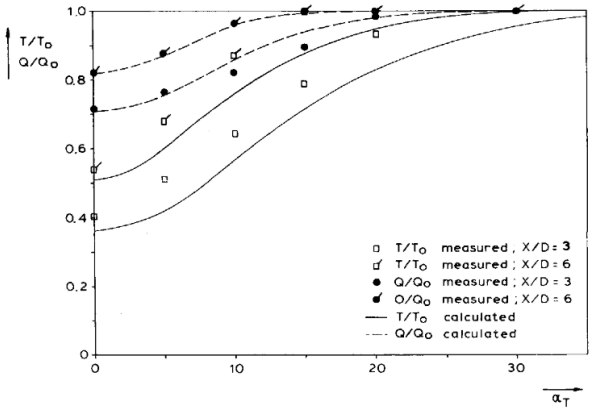

Figure 2.26: Thruster-thruster interaction open water depending on azimuth angle of the forward thruster by *Nienhuis* [43]

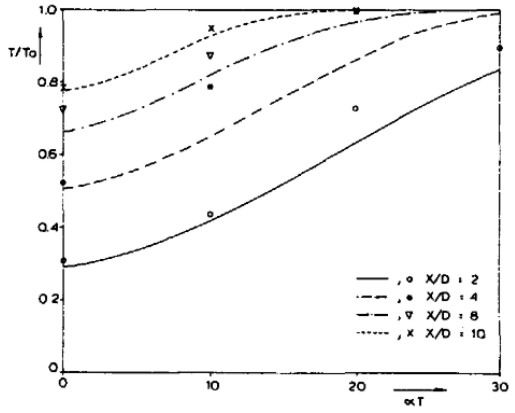

Figure 2.27: Thruster-thruster interaction under a plate depending on on azimuth angle of the forward thruster by *Nienhuis* [43]

More recently *Ekstrom et al.* [18, 6] continued the investigation on thruster-thruster interaction for a monohull vessel with two thrusters operating in proximity of each other. However, these investigations relate to the thruster-thruster interaction in current conditions, therefore a more in-depth description is reported in Section 2.4.

Based on the work produced by *Nienhuis* [43] and *Lehn* [35], *Dang et al.* [14] derived an empirical formula to asses the thrust deduction factor (t) of two thrusters under a plate which depends on the distance between the thrusters. A second formula is provided to obtain the thrust deduction factor (t_ϕ) depending on the azimuth angle (ϕ) of the forward thruster at fixed distance.

$$t = \frac{T}{T_{OW}} = 1 - 0.75^{(x/D)^{2/3}} \qquad t_\phi = t + (1-t) \cdot \frac{\phi^3}{130/t^3 + \phi^3} \tag{2.5}$$

where t is the thrust deduction ratio at zero steering angle.

The equations provided are general and not specific for the semisubmersible vessel in the object; therefore, further investigation of their applicability has been conducted by *Ottens et al.* [44]. Full-scale CFD simulations have been carried out, and full-scale tests have been performed to assess and test different thruster configurations.

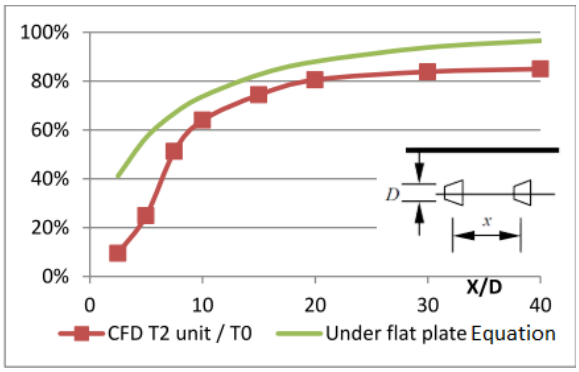

Figure 2.28: Thrust reduction of downstream thruster. Two thrusters in-tandem condition under a flat plate changing the distance between the thrusters. First thruster at azimuth angle 0°. Comparison between CFD and Eq.2.5 (*Ottens et al.* [44])

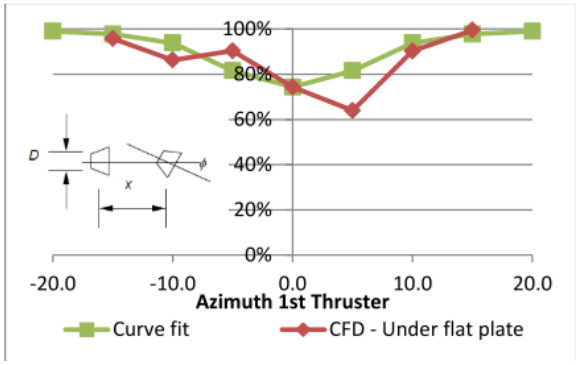

Figure 2.29: Thrust reduction of downstream floater. Two thrusters in-tandem condition under a flat plate changing azimuth angles of upstream thruster. Thruster distance of $x/D = 15$. Comparison between CFD and Eq.2.5 (*Ottens et al.* [44])

Figures 2.28 and 2.29 shows the interaction losses on the downstream thrusters on a semisubmersible vessel. It is evident that the considered case evaluated through CFD shows greater reduction in thrust compared to *Dang et al.* [14] equations. However, the trend of thruster-thruster interaction remains consistent across both series. A better agreement between prediction and CFD results is obtained for the investigation of different azimuth angles.

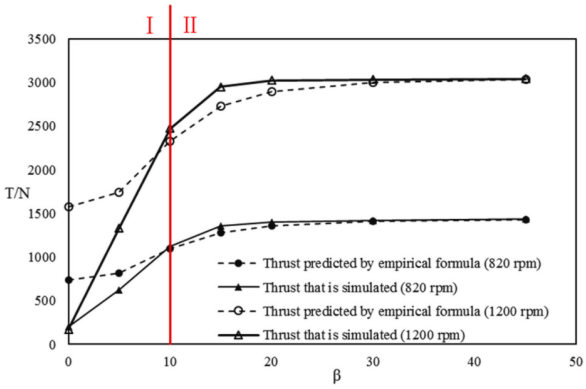

Figure 2.30: Comparison of thrust values in the downstream thruster obtained by the simulation and empirical formula. *Y-axis* provide the measured thrust on the downstream (in-behind) thruster, and *x-axis* represents the azimuth angle of the upstream (forward) thruster (β). Zone I: Disagreement between ABS estimation and numerical simulation results. Zone II: Azimuth angles in which results are in accordance with the ABS estimation.(*Zhou et al.* [56])

In addition, verification of the provided equation for the estimation of thrust loss due to thruster-thruster interaction has been performed in the study on ROVs (Remotely Operated Vehicles) by *Zhou et al.* [56], who tested two different propeller speeds and compared them to the estimates. The results show that the predictions reported by *ABS* [2] (Eq.2.5) are suitable to estimate the decrease in thrust of the propeller behind when the azimuth angle of the forward thruster is equal to or more than 10° (zone II), as shown in Figure 2.30.

Arditti et al. suggests an effective method to quantify the thruster current/thruster-thruster interaction, with specific reference to the inflow and outflow velocity. The outflow interaction has already been described in a previous chapter, whereas the inflow interaction is described as similar to the thruster-current interaction. Indeed, the different inflow velocities affect the delivered thrust and torque of of the downstream thruster. In particular, *Arditti et al.* [4] evaluates the inflow velocity at the entrance of the thruster and incorporates it into the current effect. By defining this information, it is possible to obtain the thrust reduction with respect to the bollard pull delivered thrust due to thruster-thruster and thruster-current interaction.

This method is based on the assumptions that:

1. the flow is conserved;
2. the induced velocity and the current are summed without any interaction;
3. the current is uniform and constant.

These assumptions allows to implement the described method in a thrust allocation algorithm. However, this topic goes beyond the scope of the current project.

2.6. Impact of wave interactions on thruster performance

The thruster wave interaction is another effect that could and should be taken into account when looking at the thruster interaction effects. Two main effects are addressed as thruster wave interaction:

- Inflow velocity variation, due to the orbital motions of waves;
- Ventilation

Regarding the inflow velocity variation, as stated by *Van Dijk et al.* [52], for deeply submerged thrusters, these oscillating flows may cause degradation, but due to the anti-symmetric relation between K_T and J, the mean degradation is small. In fact, variation in inflow velocity due to orbital motions of waves leads to variations in thrust and torque. Further investigation was carried out by *Cozijn et al.* [10] through model tests that involved the evaluation of an isolated thruster and a thruster under the hull. Despite unsteady flow conditions registered losses up to 10% in open water condition, for thrusters under the hull, losses between 1% and 4% have been registered, Therefore, compared to other interaction estimates available in the literature, thruster-wave interaction is comparatively lower.

Ventilation phenomena are defined as the occurrence of a partially emerging thruster. This is caused by the ship's vertical motion in waves (Figure 2.31). In contrast with what is measured for the inflow velocity variations, this is a relevant problem for DP vessels, which are usually operated close to the $J = 0$ condition, therefore with low inflow velocity on the thruster [38]. However, it is fundamental to mention that ventilation occurs when thrusters operates in proximity to the free surface.

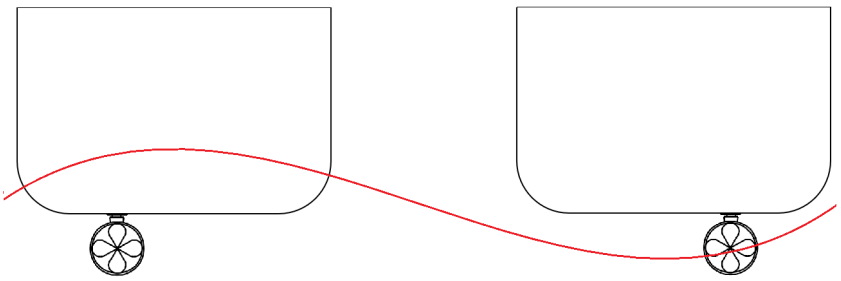

Figure 2.31: Aft view of a semisubmersible vessel. Ventilation occurs on the right thruster as it emerges form the water due to waves amplitude

Phillips et al. [47] conducted an in-depth analysis to investigate the effect of the immersion ratio on the average load of a thruster. As measured in multiple tests at the model scale, ventilation is a relevant issue when the thruster is located in close proximity to the free surface and under particularly harsh weather conditions. This was observed in the study by *Albers et al.* [1], where the ventilation of the thruster (specifically the bow thruster) resulted in a consistent thrust loss. Operational heave RAO motion plays a crucial role in assessing thruster ventilation. Further evaluation will be, therefore, carried out.

Further investigation of the effect of ventilation on ducted propellers in calm water condition, was carried out by *Phillips et al.* [47]. They derived that the ventilation takes place up to a depth over propeller radius ratio of the propeller (h/R) of 2.4. They also stated that 'with increasing immersion ($1 \leq h/R \leq 2.4$), both blade thrust and torque, as well as total and duct thrust, continue to increase.' Due to the high operational draft for the Thialf vessel, ventilation could be marked as irrelevant in the case study. However, more in-depth analysis, including vessel motion and a range of waves, will be carried out with the available tools within the company.

2.7. Effects of seabed proximity on thruster operation

Interaction with the seabed is a significant area of interest for scour assessment. However, the focus of this thesis does not involve evaluating the scouring effects of thrusters. Instead, it centers on examining the hydrodynamic aspects of thruster performance in shallow water. The seabed is therefore considered as a flat plate without moving particles. Currently, there is a lack of literature on the influence of low clearance beneath thrusters. Indeed, the seabed impact is investigated by referencing previous studies on sailing ships, maneuvering tests, and typical flow conditions resembling channel flow.

Relevant information on the effect of operating a thruster in shallow condition is provided by *Mucha et al.* [41]. The insights of this study are particularly relevant to identify the essence of the problem. In their research, a benchmark has been set to analyse the effect of shallow water using PIV measurements. They assessed both the resistance and the requested power to obtain a certain velocity for different values of under-keel clearance (*ukc*). Under-keel clearance (*ukc*) is defined as the distance between the even keel condition and the seabed as shown in Figure 2.32. The primary finding of this research reveals an increase in the required thrust when a ship navigates in shallow water, prompting the question: 'What is the effect of shallow water on a vessel operating in bollard pull conditions, such as a dynamically positioned vessel?'

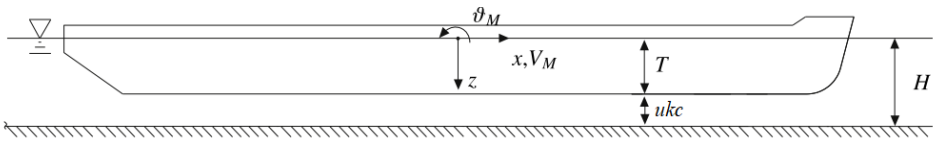

Figure 2.32: Coordinate system for resistance and propulsion tests (*Mucha et al.* [41]).

With reference to the introduced parameter *ukc*, it should be mentioned that a low clearance between hull and the seabed might also happen in deep water as this variable depends not only on the water depth but also on the vessel draft. However, for the case of the actual projects, shallow water will be considered (water depth between 20 and 30 meters).

As shown in Figure 2.33b, measured resistance for vessel speed of $V_M = 0.97[m/s]$ in shallow water ($H/T = 1.2$) is double than deep water ($H/T = \infty$). Consistent with the differences found in the resistance evaluation (Figure 2.33b), delivered power also noticeably increases as illustrated in 2.33a . Consequently, this emphasises the need to quantify and define a benchmark not only for sailing ships but also for vessels operating in shallow water during DP operations.

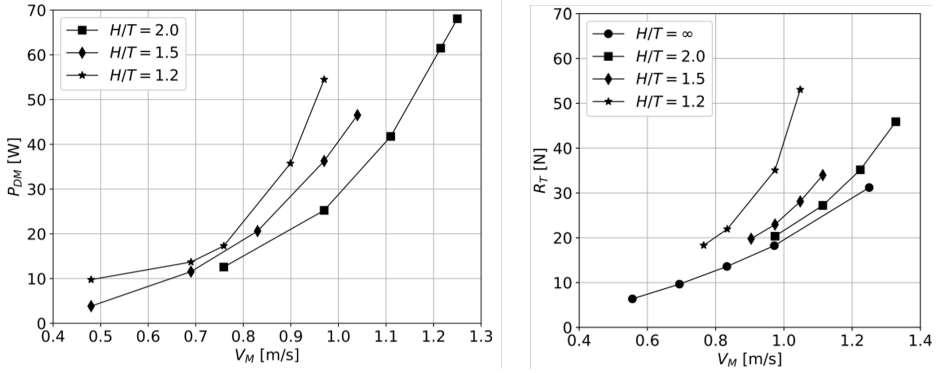

Figure 2.33: *a):* Delivered power over forward speed (V_M) at different water depths (H over draft (T) ratio for an inland vessel by *Mucha et al.* [41]. *b):* Resistance test results over forward speed at different water depths for an inland vessel by *Mucha et al.* [41]

Similarly, *Tello Ruiz et al.* [51] conducted a series of model tests mainly focused on evaluating thruster interactions under bollard pull and transit velocity conditions to gain a better understanding of the effects of shallow water. Specifically, the model is equipped with two contra-rotating Z drives.

Although the study was conducted on an inland vessel with a different hull shape and thruster configuration, some relevant insights can still be derived. Comparison between two *ukc* (35% and 150% of draft) revealed that the condition of shallow water increases the already known interaction effects observed in deep water. The general trend suggests that with higher *ukc*, the available thrust increases. However, it is also important to mention that when one thruster outflow impacts another thruster, the effect of shallow water becomes less relevant since the dominant component in the velocity inflow, and hence the delivered thrust, is provided by the flow file generated by the thruster as explained in Section 2.5.

The only available limited research on the effect of a small under-thruster clearance (shallow water condition) under the thruster in bollard pull conditions is provided by *Li et al.* [37]. Their study focuses on investigating how shallow water could affect thruster performance in open water, as well as under hull conditions. The reference system is provided in Figure 2.34.

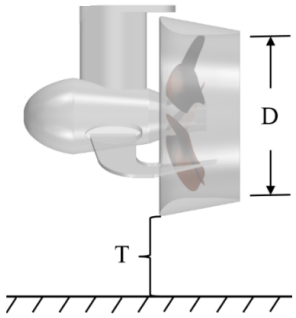

Figure 2.34: Parameters definition by *Li et al.* [37]: T is the distance between nozzle lowest point; D is the propeller diameter

The thrust provided has been derived from increasing to a stable value until an under-thruster clearance over diameter ratio of around 1 (Figure 2.35). This means that while the clearance is greater than 1 propeller diameter, no impact on thruster efficiency is recorded under open water conditions. However, for lower clearances, an increase in the inflow velocity and its direction is registered.

Similarly, the same trend in thruster performance reduction is observed for thrusters operating behind the hull; however, a lower thrust is registered due to the different inflow velocity caused by the presence of the hull. Specifically, in the bollard pull condition and with a thruster clearance (T) of 1 diameter, the measured axial inflow velocity is 7.27% higher than the operating water condition.

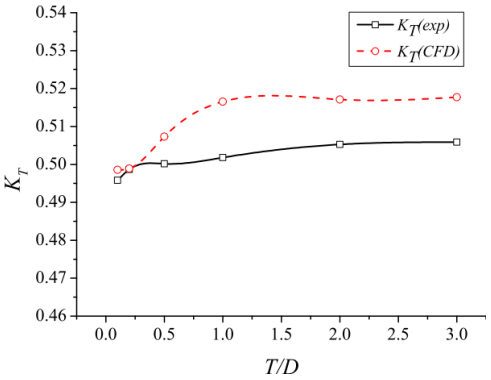

Figure 2.35: Azimuth thruster open water bollard performance at different thruster clearance T by *Li et al.* [37]

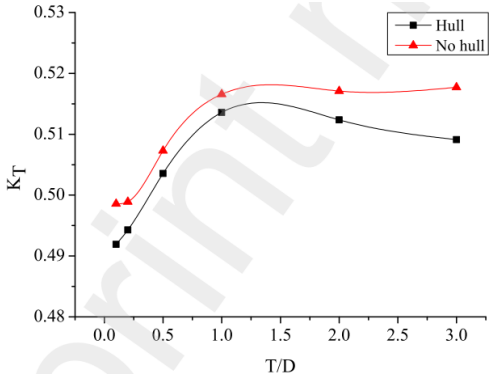

Figure 2.36: Azimuth thruster in-behind hull performance vs open water at different thruster clearance T by *Li et al.* [37]

However, the tests have been carried out on a model scale, with a conventional hull, no current involved, and no presence of a second pontoon. Therefore, the effect of thruster-hull, thruster-current, and thruster-thruster interactions has not been investigated. Despite these aspects, the provided literature shows how the flow field around and behind the hull is the key factor in investigating thruster interaction effects.

Flow behaviour below hull

Beyond the general case of flow impacting a bluff body, limited resources are available for investigating marine-related scenarios involving shallow water flow beneath the hull. In this context, a particularly relevant study is provided by *Gourlay* [21] who used the under keel clearance (*ukc*) and water depth as primary inputs to approach the problem of defining the flow between hull and seabed. Specifically, this research focuses on a large vessel having a large flat bottom, such as a bulk carrier or a tanker, which partially resembles the case of a semisubmersible vessel. The ship is fixed in the considered frame of reference , and water streams past it.

As shown in Figure 2.37 in deep water conditions, the boundary layer gradually develops beneath the hull. However, when the seabed is closer than the boundary layer height, a modification in the flow is expected. In particular, the no-slip condition on the sea floor means that, in the ship-fixed frame of reference, the flow is required to move at exactly the speed of the free stream on the sea floor. [21]. Therefore, the boundary layer does not develop as a free one but is rather constrained by the presence of the seabed. Therefore, the provided representation (Figure 2.37) set the ship as a reference frame while the seabed is moving at the velocity of the free stream.

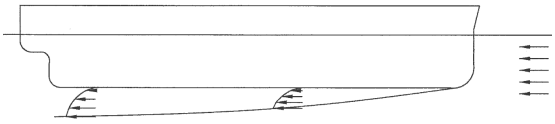

Figure 2.37: Free boundary layer beneath a vessel at moderate or large under-keel clearance. (*Gourlay* [21])

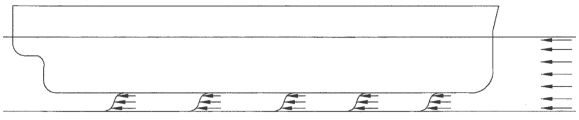

Figure 2.38: Suggested model for flow beneath a ship at small under-keel clearance. (*Gourlay* [21])

Specifically, the flow underneath the ship is mainly dominated by the no-slip boundary conditions on the hull and seabed. Similarly to a pipe flow, the boundary layer grows and then converges into a fully developed flow. However, the lower pressure gradient below the hull might lead to a quicker full development than the archetypal flow in a pipe. When the flow reaches full development, a nearly constant velocity pattern is established beneath the flat bottom of the ship because of continuity principles. This uniformity differs from a free boundary layer that extends toward the stern and is expected when there is minimal under-keel clearance [21].

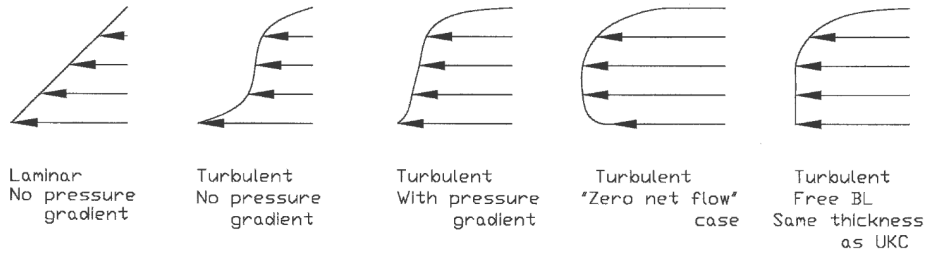

Figure 2.39: Comparison of mean velocity profiles for Couette flow between two plates by *Gourlay* [21]

The findings of *Gourlay* [21] suggest that the flow pattern is comparable to the Couette flow with a pressure gradient. This pressure gradient is the result of the significant difference in pressure between the incoming and outgoing flows, which is influenced by the pressure gradient induced by the propeller. The flow is influenced by the longitudinal pressure gradient, causing the velocity profile to fall between an anti-symmetric distribution and a distribution with zero net flow [21]. A reminder of different Couette flows is provided in Figure 2.39.

2.8. Conclusions from the literature review

This literature review has explored thruster interactions below the hull for a semisubmersible vessel, emphasizing both deep-water and shallow-water conditions. The limited knowledge of shallow water effects, particularly during bollard pull or current conditions, highlights a research gap. While model tests and numerical simulations are proven to be useful tools, full-scale numerical simulations have been noticed to offer a more comprehensive approach for the dual purpose of calculating the forces acting on the vessel and visualizing the flow development. The study will therefore use an existing full-scale CFD model to examine how water depth affects interactions, focusing on:

- Thruster-hull interaction;
- Thruster-current interaction
- Thruster-thruster interaction

Other factors, like thruster-wave interaction and ventilation, have less impact on thrust reduction. However, due to limited literature, further investigation is needed to exclude them from the scope. The goal is to identify the most significant interactions affecting thrust in shallow water, using high thruster load conditions and data analysis from various projects to predict increased thruster load trends for semisubmersible vessels.

3

Estimation of interaction effects

In this chapter, the follow-up developments from the literature are investigated. In particular, a simplified approach is used, which relies on basic methodology and formulations provided by regulatory institutions (*ABS* [2]) to obtain the first estimation of which types of interactions play a major role in conditions of low clearance under the thruster. Specifically, the methodology used to estimate the reduction in delivered thrust is introduced first, and the different types of interactions are analyzed.

3.1. Methodology for interaction estimation and Open Water diagram

As suggested by Fjørtoft [20], the representation of thrust performance could be expressed by the calculation of the thrust deduction factor t, which is defined as the ratio between the thrust in open water condition at 0 [m/s] inflow velocity (bollard pull condition) and the actual provided thrust in the prescribed condition. In the following calculation, the thrust deduction factor will be taken into account for all calculations.

$$t = \frac{T}{T_{OW}} \tag{3.1}$$

where T is the thrust in the prescribed condition derived from the open water diagram and T_{OW} is the bollard pull delivered thrust. The open water diagram is not available for the specific case of interest, but thruster performance is available at different thruster rotational speeds. From this information, the open water curve was obtained.

Based on the experience provided by the vessel's crew during DP operations, an increase in thrust loss has been observed for higher load cases. Therefore two thruster conditions have been taken into account for further calculations. In particular:

- 50% of the maximum rotational speed (n_{MAX}).
- 75% of the maximum rotational speed (n_{MAX}).

In the obtained open water diagram the parameter consists of the advanced ratio defined as J:

$$J = \frac{V_s}{nD} \tag{3.2}$$

and the thrust coefficient, represented as K_t,that is dimensionless representation of thrust as a function of J.

$$K_t = \frac{T}{\rho n D} \tag{3.3}$$

Through the definition of the advance ratio (J) depending on the inflow velocity (V_s), it is possible to obtain, through the open water diagram, the corresponding Kt. Therefore, the delivered thrust (T) can be compared with the open water thrust (T_{OW}). The following procedure has been followed:

1. From the velocity V_s, the advance ratio J is determined, trough Equation 3.2;
2. The thrust coefficient K_t is obtained for each loading condition using Equation 3.3 and for a velocity range between 0 and 12 knots;
3. The K_t curve is then plotted and a 4^{th} order polynomial is defined as approximation of the curve;
4. The polynomial coefficient for each loading condition is obtained, therefore a general approximation of the curve is obtained using the mean value among the four loading conditions.
5. The K_t curve is derived.

This approach allows for the creation of an Excel file that can be adapted to multiple vessels by changing the specific open water diagram provided.

3.2. Estimating effects of Thruster-Current interactions

The evaluation of thruster-current interaction has been carried out through the analysis of the thrust deduction factor t. Specifically, having set a fixed rotational velocity of the propeller ([rpm]), different inflow velocities have been used as a reference to evaluate the effect of the current on the delivered thrust. Furthermore, different thruster positions have been considered as illustrated in Figure 3.1 and Table 3.1.

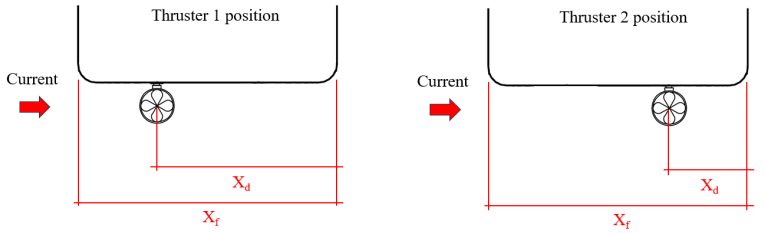

Figure 3.1: Aft view of an SSCV with thruster position (X_d) and floater width (X_f) details. Both thrusters are below the same pontoon at two different distances.

Table 3.1: Thruster positions (X_d) with reference to floater width (X_f).Both thrusters are below the same pontoon at two different distances.

	X_d/X_f
Thruster 1	0.7
Thruster 2	0.36

All the following calculations approach the problem from the inflow velocity V_s point of view. Therefore, the goal of the following procedures relies on obtaining the inflow velocity at the thruster location and comparing the provided thrust with positive inflow velocity with that one obtained in the open water condition at J=0 (Equation 3.4)his calculation was performed using the open-water diagram of the thruster, as described previously.

$$t = \frac{T}{T_{OW}} \tag{3.4}$$

The estimation of the expected velocity profile at the thruster location is crucial for assessing the current thruster interaction. This estimation is based on the following assumptions:

- The seabed consists of a flat plate and the bottom of the hull. Roughness is, therefore, assumed to be zero on every surface.
- Turbulent flow is considered in evaluating the boundary layer profile and the velocity development. However, vorticity and, therefore, eddy viscosity are not taken into account to fully resolve the equations of motion (Navier-Stokes), which are intended to be performed through CFD simulation.
- The thruster is considered to be placed in a fully developed flow with the assumption of the area between the hull bottom and seabed as a channel flow.
- The flow is assumed to be 2D; therefore, no transversal velocity along the x-axis is considered.
- The effect of current is investigated only at the thruster below the upstream pontoon (with reference to the current direction).

Two different scenarios have been considered: deep and shallow water. For deep water, the average velocity at thruster inflow is the current velocity. Shallow water condition has been identified at a clearance of 6 meters below the thruster.

The average velocity at the thruster location beneath the hull is evaluated using the continuity equation for a 2D flow of an incompressible flow. Specifically, the elementary continuity equation for hydrodynamics is obtained (Equation 3.5).

$$v_1 \cdot h_1 = v_2 \cdot h_2 \tag{3.5}$$

This equation applied to a clearance below the thruster of 6 meters, leads to a mean velocity at the thruster location of $2.3 \cdot V_c$, where V_c is the current velocity in open seas. Therefore, this is estimated to be the mean velocity of the uniform flow at the mentioned location.

To achieve a more accurate determination of the average velocity profile, it is necessary to consider the presence of the boundary layer. Given that the current stage of the investigation is still in the approximation phase, the estimation of the boundary layer in this context has been carried out utilising the velocity distribution and the definition of the thickness of the boundary layer associated with a plate in a unidirectional flow [5]. Boundary layer thickness is calculated as in Equation 3.6.

$$\frac{\delta}{y} = 0.37 \left(\frac{\nu}{V_s y} \right)^{1/5} = \frac{0.37}{Re_x^{1/5}}; \qquad \frac{\langle u \rangle}{V_s} = \left(\frac{z}{\delta(y)} \right)^{1/7} \tag{3.6}$$

where symbols are defined as follows:

- y is the transversal coordinate;
- $\langle u \rangle$ consists of the average velocity in the turbulent boundary layer;
- z is the vertical coordinate;
- $\delta(y)$ is the height of the boundary layer.

The seabed's presence has already been considered through the mean velocity calculation. However, to establish the approximate flow profile between the hull and the seabed, it is relevant to estimate the fully established length, which consists of the length after which the velocity has a parabolic distribution. This is obtained assuming that the parabolic profile is obtained when the height of the boundary layer $\delta(z)$ reaches half the distance between the two constraints (h).

$$\frac{h}{y} = \frac{0.37}{Re_x^{1/5}} \tag{3.7}$$

A value of 1048 meters is obtained for the specific case of interest. This highlights that the velocity profile is not fully developed within the defined approximation space. Therefore, the parabolic velocity profile is not reached. This result is used to assess the estimated inflow velocity profile at the thruster location, which has been calculated, accounting for the turbulent boundary layer, as shown in Figure 3.2.

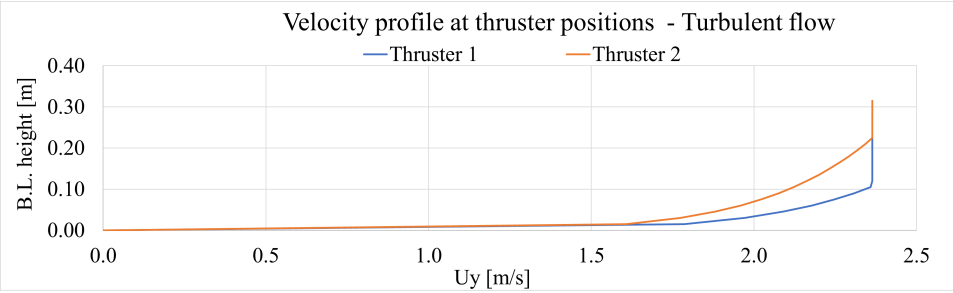

Figure 3.2: Boundary layer height estimation at different flow velocities (U_y).

As shown in Figure 3.3, the boundary layer extends up to a distance of 0.25 meters from the bottom hull for the Thruster 2 position. Therefore, it can be derived that the mean flow velocity for both thrusters is equal to the mean turbulent flow V_s, which consists of the current speed.

The thrust reduction factor due to thruster current interaction ($t_{current}$) has been analytically calculated according to the described procedure (Equation 3.5). In the worst case combination of 2 knots current speed and 50% of n_{MAX} thruster setting, a a thrust deduction factor $t_c = 0.64$ has been obtained through analytical calculations based on bi-dimensional flow approximations.

The procedure has also been performed for deep water, where a thrust deduction factor $t = 0.84$ has been calculated, with a relative difference of approximately 31% between deep water and 6 meters under-thruster clearance scenario. The deep water case also aligns with the ABS [2] guideline for the estimation of thruster-current interaction (Equation 3.8), as shown in Figure 3.3.

$$t_{current} = 1 - \left(\frac{400}{PA}\right)^2 \cdot 0.11 \cdot V_c \tag{3.8}$$

where PA is the propeller disk area load $[kW/m^2]$.

The obtained results are illustrated in Table 3.2.

Table 3.2: Thrust deduction factors at three inflow velocities and two water depths (6 meters and deep Water). Comparison with the *ABS*[2] guidelines.

	6 meters (Analytic)		**100 meters (Analytic)**		**ABS**	
	$50\%rpm_{MAX}$	$75\%rpm_{MAX}$	$50\%rpm_{MAX}$	$75\%rpm_{MAX}$	$50\%rpm_{MAX}$	$75\%rpm_{MAX}$
0 [kt]	1.00	1.00	1.00	1.00	1.00	1.00
1 [kt]	0.82	0.87	0.92	0.94	0.91	0.94
2 [kt]	0.64	0.76	0.84	0.89	0.83	0.87

These results, along with what was found in the literature, lead to the conclusion that the current plays an important role in the difference in thruster performance between shallow and deep water. Further investigations are needed through computational fluid dynamic simulations to represent the flow behaviour in such conditions better.

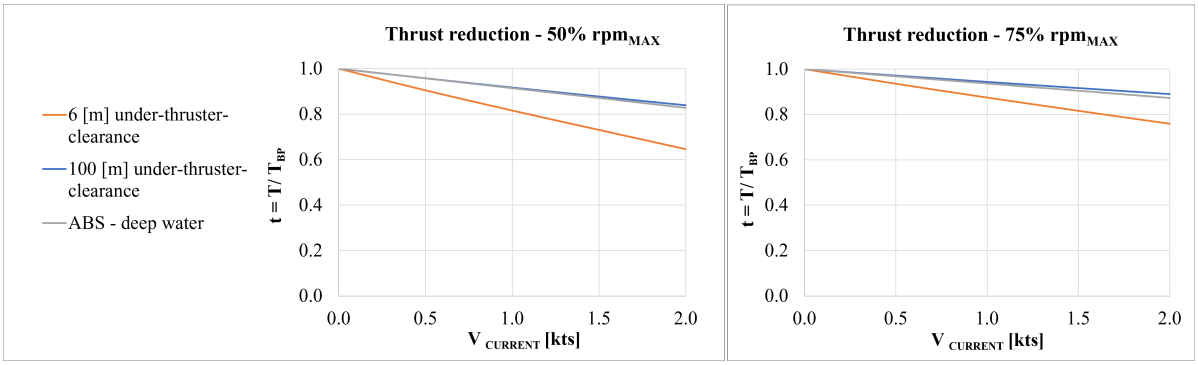

Figure 3.3: Thrust deduction factor ($t = T/T_{BP}$) due to higher inflow velocity in shallow water (6 meters under-thruster-clearance) and deep water under the assumption of 2D flow (Bernoulli equation).

3.3. Estimating effects of Thruster-Hull interactions

The thruster-hull interactions include multiple effects, all of which play a relevant role. Among these are the Coandă effect and blockage as well as frictional losses. The main interest for DP capabilities lies in the first two effects, as knowledge of the shallow-water scenario has not been investigated yet. Therefore, it is relevant to obtain an estimation of the magnitude of the effect in such a condition. It should be mentioned, however, that the quantification of the problem from an analytical point of view is not predictable, mainly due to the Coandă effect on the flow.

A possible estimation of this effect has been derived through a least square analysis of test results by *Nienhuis* [43]. However, the used nozzle differs from the installed one on the vessels of interest. It is also relevant to mention that, as *Nienhuis* [43] stated, the provided formulation is not precise enough due to insufficient data. Furthermore, the velocity profile estimation is not available, as stated previously, leading to an incorrect velocity magnitude estimation at the round bilge position.

For all the previously mentioned reasons, the ABS formulation for the blockage effect of the thrust-hull interaction is considered more reliable than a direct calculation. The estimating formula is provided below.

$$t_p = 0.8 \cdot \frac{L_P}{55} \tag{3.9}$$

t_p represents the thrust deduction factor caused by the blockage effect, while L_P is the downstream centerline between two pontoons in meters. Strictly correlated to the blockage thrust reduction is the Coandă effect, which is accounted for through a thrust deduction factor (t_c) of 0.97.

In dynamic positioning operations (with no forward speed), ABS provides an estimation of the thrust reduction factor due to frictional resistance on the (Figure 3.5). Thrust degradation due to hull friction is related to the length and breadth of the downstream flow along the hull. However, the provided estimation does not specifically cover the case of a semi-submersible vessel with a thruster operating directed towards one of the pontoons. The estimation is based on two parameters of the vessel: the length of the hull (L) and its breadth (B). In the case of interest, the length consists of the pontoon distance downstream of the thruster, resulting in a total length ($L = L_1 + L_2$) of 50 meters. The maximum available breadth for the estimation has been used (B =30 meters). This approach has been chosen because the coefficient depends on the frictional resistance of the hull due to the thruster jet stream. In this particular case, the thruster is oriented towards the downstream pontoon. Hence, the aforementioned lengths have been considered. The obtained t_f is equal to 0.96. (Figure 3.1).

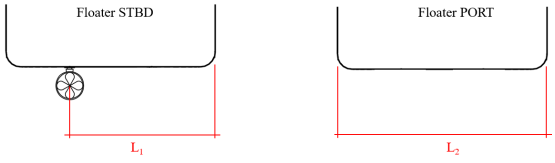

Figure 3.4: Definition of length to be considered for the thrust reduction ratio (t_f) due to frictional resistance on the hull.

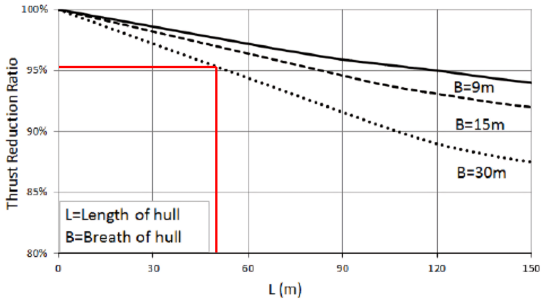

Figure 3.5: Thrust reduction ratio (t_f) due to hull friction as a function of thruster downstream length (L) and breadth (B)

The obtained estimation of all the effects is specified in Table 3.3 for the floater width to floater distance ratio, which will be further used in the numerical simulations. (see Figure 3.1).

Table 3.3: Thrust reduction due to thruster-hull interaction form *ABS*. (t_p: blockage effect, t_c: Coandă effect, t_f: friction, $t_{hull} = t_p \cdot t_c \cdot t_f$

	t_p	t_c	t_f	t_{hull}
$L_p/X_f = 0.7$	0.47	0.97	0.96	0.44

The results indicate that the interaction between the thruster and hull is a significant factor in thruster operations. It is important to note that the ABS guidelines are primarily based on deep water scenarios and do not account for the influence of seabed proximity. Therefore, further investigation into the impact of shallow water on this interaction is necessary to confirm the obtained values and evaluate whether these values are affected by reduced thruster clearance.

3.4. Estimating effects of Thruster-Thruster interactions

Thruster-thruster interaction has been theoretically described in Chapter 2; in this section, the approach consists of a first estimation to gain a general understanding of the magnitude of the effect. Specifically, two thrusters are considered to operate, one behind the other and not under a plate, as the estimation of the flow field velocity downstream of the thruster has only been studied experimentally in open water conditions. Despite some approximations provided by *ABS* [2] based on the results obtained in previous studies, a case-specific estimation has been carried out.

Specifically, the flow developed by the thruster in front has been derived using the velocity profile derived by *Nienhuis* [2], as the nozzle type is the same as in the case study. The formula is provided below.

$$V_s = \frac{0.805}{(x/D)^{0.389}} \cdot u_1 \tag{3.10}$$

where u_1 consists of the propeller-induced velocity. To evaluate the average outflow velocity, an alternative method is applied as described by *Zondervan et al.* [57]. The method consists in fully separating the propeller from the ducted propeller system, which results in the definition of the nozzle-induced velocity (u_n) as the difference between the outflow velocity (u_1) and the propeller-induced velocity (u_p).

$$u_n = u_1 - u_p \tag{3.11}$$

Furthermore, the mentioned velocities can be related to the advance ratio and the thrust coefficient. The proposed formulation also satisfies the requirements that, in the propeller plane, the sum of the propeller and nozzle-induced velocity is in accordance with the induced velocity of the entire system [57]. Combining the two induced velocities and considering the bollard pull condition, it is possible to derive a formulation for the thruster-induced velocity.

$$u_1 = u_n + u_p = \frac{1}{2\tau} nD \sqrt{\frac{8K_{T-Prop}}{\pi}} \tag{3.12}$$

In the previous relations, the ratio τ consists of the ratio between the thruster's total thrust and the propeller's contribution to thrust.

$$\tau = \frac{T_{prop}}{T} \tag{3.13}$$

The proposed technique has been tested and confirmed for the No.19A nozzle type, which applies to the studied case. Therefore, this methodology has been used to evaluate the velocity of the thruster outflow. The authors state that the proposed method demonstrates certain enhancements in estimating the outflow velocity, although it is unsuitable for assessing the induced flow field within the duct due to its high viscosity.

The magnitude of the interaction has been studied using the maximum velocity generated by the thruster upstream as the inflow velocity on the thruster downstream. Therefore, the provided thrust has been derived through the open water diagram. Each of these calculations has been carried out with both thrusters set at the same rotational speed to compare the performance decay of the thruster behind and compare them to the one in front.

In Figure 3.6, a comparison of the obtained results is provided. Specifically, the ABS estimation of thruster-thruster interactions is proposed along with the direct calculation, which relies on the estimated outflow velocity specific to the case of interest. It can be observed that as the distance from the thruster increases, the calculated solution aligns more closely with the ABS estimation. Closer to the thruster, higher interaction (therefore, lower thrust deduction factor) is obtained.

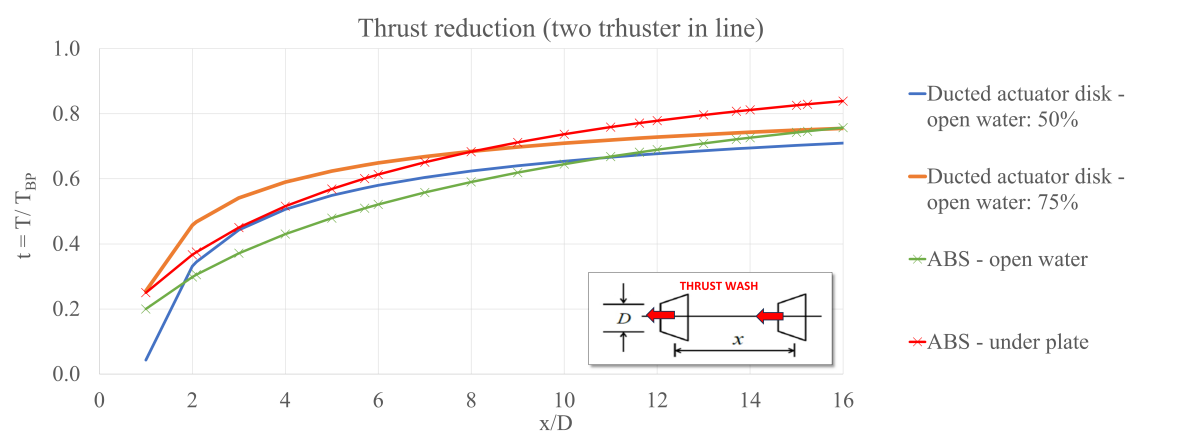

Figure 3.6: Thruster-Thruster interaction evaluation. Numerical calculation for 50% (blue) and 75% of n_{MAX} (orange) compared with *ABS* [2] estimation in open water (green) and under plate (red) scenarios.

The difference obtained could be explained by the different velocity profiles derived for a thruster under a plate. Indeed, as previously explained, the velocity decay could be less impacting than in open water with a constraint on top. Furthermore, a uniform distribution of velocity has been assumed for the calculation; however, it is not the case when looking at the real situation from which the provided calculation is derived. However, as proved by *Zhao et al.* [56], the ABS prediction is not accurate at very low distances from the thruster, where the thruster wash does not impact the bottom of the hull or is not greatly affected by its presence.

Further improvement could be done by evaluating the velocity profile at the nozzle location and deriving mean inflow velocity at the thruster behind, however, this calculation will still not include the modified velocity profile due to the plate.

3.5. Estimating effects of Thruster-Wave interactions

For the thruster-wave interaction, not only the inflow speed is relevant but it is equally relevant to take into account the direction of the inflow. Specifically, the induced orbital motion led to a harmonic inflow behaviour that varies between 0 and π; therefore, positive and negative inflow alternates harmonically. This is particularly true when considering regular waves as this is the case. To consider the mentioned aspects, a typical performance diagram is used (Figure 3.7), as the single-quadrant open water diagram does not cover the negative inflow velocity and positive thrust scenario.

The increase in the thrust coefficient for the Wageningen propeller can be observed in the fourth quadrant region, as highlighted in Figure 3.7. Assuming that the thruster is set at the same rotational speed and with opposite inflow velocity, similar to an airy wave, it can be noted that the resulting thrust with reverse inflow is higher than with the inflow velocity aligned with the thrust direction. Hence, it is important to investigate the loss of thrust in the propeller due to wave orbital velocity under the latter condition.

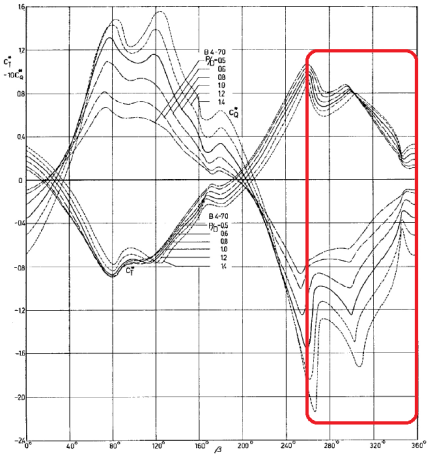

Figure 3.7: Four Quadrant Measurement Results of B4-70 Propellers

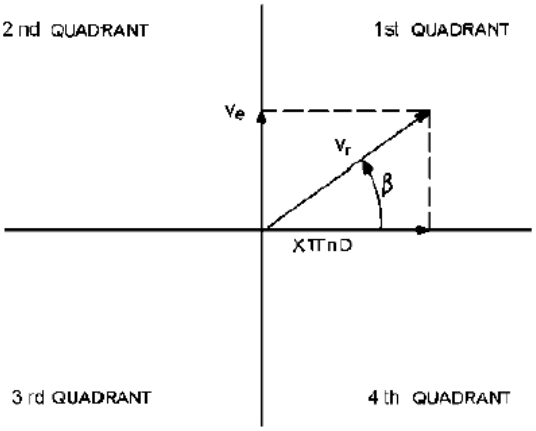

Figure 3.8: Four Quadrant Measurement Results of B4-70 Propellers

Coefficients in Figure 3.8 are defined as follows.

$$\beta = arctan\frac{V_a}{0.7\pi nD} \qquad C_t = \frac{T}{1/2\rho(V_a^2 + (0.7\pi nD)^2)\frac{\pi}{4}D^2} \tag{3.14}$$

where $V_a = -V_e$ is the velocity of the entry (inflow) and V_r is the resulting velocity.

However, this performance information is not available about the actual case. Therefore, it has been assumed that the performance of the thruster is the same with positive and reverse inflow velocity. The procedures remain the same as explained at the beginning of the chapter. The performed calculations demonstrate that the thrust loss is not as significant as in other types of interactions. Its magnitude is lower than 5% in the maximum operational scenario, which involves a significant wave height (H_s) of 2 meters and a peak period (T_p) of 7 seconds.

3.6. Ventilation effects on thrusters

Vertical motions of the vessel, together with wave height, could compromise thruster performance due to ventilation [34]. Specifically, ventilation occurs when part of the thruster emerges. Therefore, this situation stands in place when the thruster is operated in proximity of the thruster.

Therefore, to determine whether this effect should be taken into account in the most relevant type of interactions, some simulations have been done with the help of the company software Liftdyn which provides the SDA (significant double amplitude) of a POI (point of interest) on the vessel. The input provided to the programs is significant wave height (H_s) and the Wave peak period (T_s). Specifically, the wave period has been related to H_s through the following relation, which holds for the North Sea region.

$$\sqrt{13 \cdot H_s} \leq T_s \sqrt{30 \cdot H_s} \tag{3.15}$$

The calculation model employed in this study is founded on the Jonswap sea spectrum and assumes a Rayleigh distribution for wave height. Hence, it is important to highlight that the analysis focuses on determining the worst-case scenario for the Heave SDA at the thruster location by deriving the Most Probable Maximum (MPM). To achieve this, the formulation for the Most Probable Maximum in a Rayleigh Distribution is utilized. This formulation enables the determination of both the most probable wave height and the most probable vertical motion at the thruster location.

$$MPM = SDA\sqrt{\frac{1}{2}ln\left(\frac{T_{duration}}{T_p}\right)} \tag{3.16}$$

It should be mentioned that some approximation has been used in the evaluation of the results since the scope of the calculation consists of providing and estimating the impact of the heave motion on the thruster efficiency. Specifically, the observation period $T_{duration}$ is 3 hours. An average zero-crossing period T_{m02} of 10 [s] is assumed for every peak period T_p, leading to a number of observed waves $N = 1000$. For each value of H_s, 10 periods (T_s) has been considered.
Maximum responses, therefore, the worst-case scenarios, occur for the heading direction (0°) and the longest peak period. Consequently, the value of the MPM of the heave motion of the thruster location is evaluated. It is, therefore, provided the resulting distance between the wave trough and heave peaks, assuming they happen at the same instant.

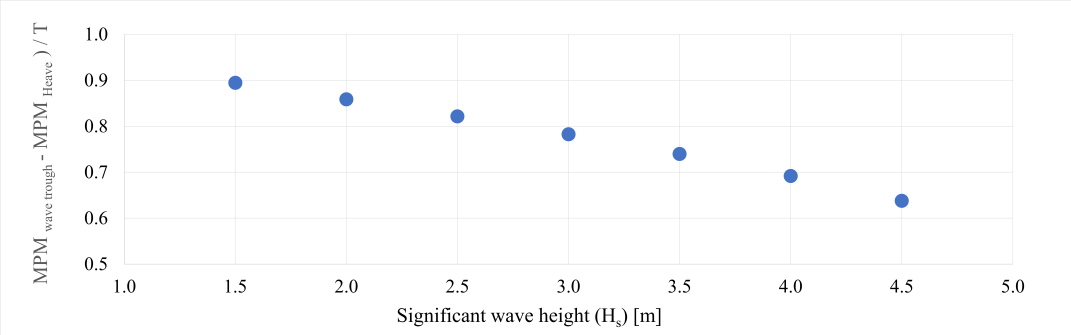

Figure 3.9: Ventilation risk assessment. The distance left between the wave through and the MPM heave elevation is at the thruster location w.r.t vessel draft (T). Always positive values, therefore thruster is not emerging from water

In the above plot (Figure 3.9), the origin of the response system is set at the top thruster location, therefore, at the upper part of the thruster nozzle. This choice allows to take into account that ventilation can occurs starting form the upper part of the thruster, it is therefore not needed that the entire thruster is completely emerged form water.

As illustrated in Figure 3.9, the ratio of the difference between the most probable maximum wave trough ($MPM_{wave\,trough}$) and the most probable maximum vertical position of the thruster (MPM_{Heave}) relative to the floater draft (T) is always less than 1. This indicates that the risk of ventilation due to thruster interactions is minimal for a semi-submersible vessel, even in shallow draft conditions. Additionally, the standard operational limit for wave height is set at $H_s = 2\,meters$. The analysis also includes more extreme sea conditions to ensure that the ventilation risk remains low even under severe scenarios, such as when the vessel might not need to maintain its position.

3.7. Conclusions on interaction effect estimation

Given the explained procedure, along with the associated uncertainties and the obtained calculated results, a comparison among the different types of interactions can be performed to assess which of them represents the most relevant effect that is important to investigate. Along with this aspect, a more practical approach should be taken into account to obtain, as a result, a reasonable number of simulations that allow for capturing the essence of the problem.
All the obtained maximum values of interaction as thrust deduction factors are provided in Table 3.4.

Table 3.4: Thrust deduction factors for each type of interaction

	t
Thruster - current	0.64
Thruster - hull	0.44
Thruster- thruster	0.69
Thruster- wave	0.94
Ventilation	not occurring

To summarize the obtained information and more explicitly define the results for different cases, Figure 3.10 provides the histogram with all the results.

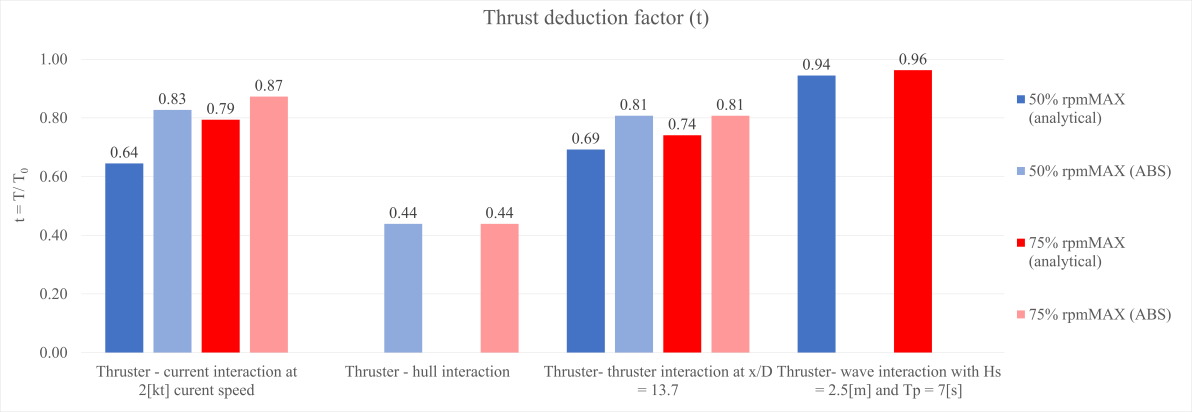

Figure 3.10: Thrust reduction factor for all the estimated thruster interactions at 50% and 75% of n_{MAX}

In Figure 3.10, it is evident that the most significant factor affecting thruster performance is thruster-hull interaction, which is based solely on ABS estimation. The impact of thruster-current and thruster-thruster interactions is comparatively significant. However, the latter depends on the inflow velocity, and conclusions can be drawn by observing the jet developed by the upstream thruster. In contrast, thruster-wave interaction is negligible compared to the other predicted interactions.

The approach will, therefore, focus on developing a methodology and a set of simulations that allow for capturing the effect of current on the delivered thrust and its impact on the thruster-hull interactions. However, obtaining a method that describes the flow field around the hull to estimate the inflow velocity at other thruster locations is also important.

4

Computational Fluid Dynamics (CFD) Methodology

In previous chapters, the simplified approach and the available data used to establish the framework for numerical simulations were described. This chapter delves deeper into the problem through the methodology used to develop the appropriate CFD (Computational Fluid Dynamics) model for the open-source OpenFOAM software. Initially, the theoretical background of the numerical methods used will be presented. This will be followed by the description of selected cases to run the simulations. This description will start with the characteristics of the models, followed by the grid generation method and its convergence study. Furthermore, this chapter aims to provide the pre-processing steps preceding the results visualization and discussion.

4.1. Background theory on CFD simulations

To provide a complete picture of the used methodology, it is firstly useful to illustrate some basic principles and recommendations defined by *ITTC* [26, 25] as guidelines to CFD simulations.

Mesh characteristics

In ship hydrodynamics, an unstructured mesh is often used, with a prism mesh for the hull boundary layer and a tetrahedral mesh elsewhere. This approach significantly reduces meshing time compared to structured meshes. However, the spatial accuracy of unstructured elements like triangles, tetrahedral, and pyramids is typically lower than that of quadrilateral and hexahedral elements.

Hence, the preferred approach followed the traditional method for ship hydrodynamic numerical simulations, involving an unstructured mesh that allows for more flexibility in defining the mesh shapes given the complex geometry that needs to be modelled.

Ship viscous-flow computations typically have three fixed boundaries: the ship surface, the symmetry plane, and the (still) water surface. However, the flow direction impacts the vessel hull from the beam-side, leading to a non-symmetrical hull shape with respect to the flow direction (y-axis). Therefore, in this case, the applied boundaries consist of the still water surface modelled as a symmetry plane and the closed domain of the two hulls.

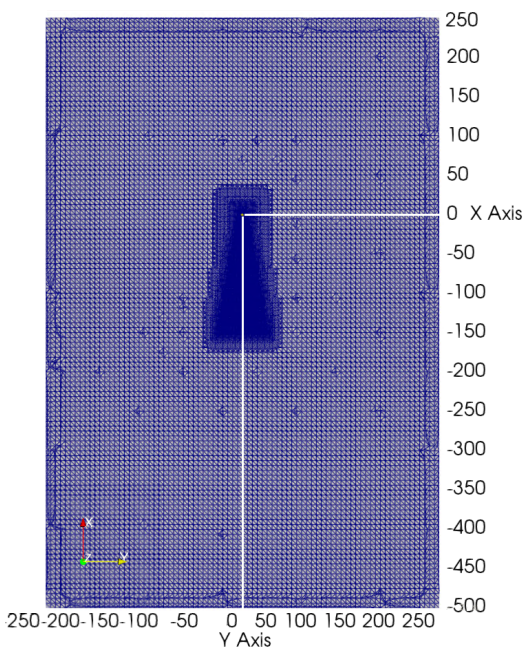

Figure 4.1: Mesh grid top view example to highlight the domain boundaries for the open water test. The thruster position is located at (0,0). (Number of cells: 7.6 million)

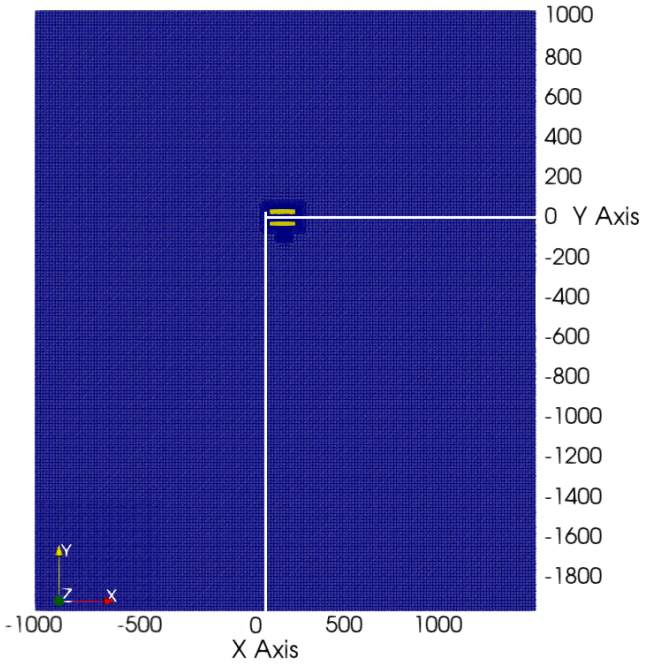

Figure 4.2: Mesh grid top view example to highlight the domain boundaries for the hull + thruster tests. (0,0) position corresponds to the aft centerline of the vessel. (Number of cells: 13.8 million)

Furthermore, three additional boundaries have to be defined to create a closed domain around the ship. These include an inlet, an outlet, and an exterior boundary, where boundary conditions have to be defined. These boundaries have to be placed sufficiently far from the ship to minimize their effect on the solution. For the inlet and exterior boundary, either uniform (undisturbed) flow is usually imposed. In that case, these boundaries should be located 1-2 L_{PP} away from the hull [26]. Further indications within the CFD community provide some qualitative guidelines about the definition of the domains. In particular, it is suggested to have some expectations in advance about how the flow will develop around the hull to better tune the case of interest and allow the flow to properly develop. For the scope of the actual thesis, previous simulations have been carried out with comparable geometries. Therefore, the definition of the boundaries has been guided by the experience of specialists in the numerical simulation field within the company. The defined domain respected the suggestion of having a length of a minimum of 5 times the dimension of the body along the direction of the flow to allow enough space for the flow to be properly developed. The precise characteristics will be provided in Section 4.4. Similarly, it is usually recommended to leave a space of about 2 times the body width on each side to allow for local flow deviation.

Numerical solver

Some background information regarding the solver is also necessary. It is relevant to mention that the scope of the thesis was not to implement a new OpenFOAM code but rather to apply a previously developed code within the company to the case of interest, making necessary modifications.

From the very beginning of the thesis project, given the substantial number of simulations involved and the experience from previous similar tasks, it was decided to carry out steady-state simulations (RANS) and eventually post-process the data to determine if more in-depth analysis and complex simulations were required. In particular, the RANS solver has been preferred to more complex solutions (e.g. unsteady approach URANS) based on previous CFD tests carried out within the company. Furthermore, the number of simulations and the time involved led to the conclusion that the RANS simulation would have been the most efficient trade-off between the available time and the desired results.

A brief description of Reynolds-Averaged Navier-Stokes (RANS) equations is essential to comprehend the physics behind the chosen approach. RANS equations are time-averaged equations of motion for an incompressible fluid (such as water in this case), which can be written as follows for a stationary flow:

$$\rho\bar{u}_j\frac{\partial\bar{u}_i}{\partial x_j} = \rho\bar{f}i + \frac{\partial}{\partial x_j}\left[-\bar{p}\delta ij + \mu\left(\frac{\partial\bar{u}_i}{\partial x_j} + \frac{\partial\bar{u}_j}{\partial x_i}\right) - \rho\overline{u_i'u_j'}\right]. \tag{4.1}$$

The left-hand side represents the change in mean momentum of the fluid, accounting for the unsteadiness in the main flow. This is balanced by the mean body force, the mean pressure field, the viscous stress, and the Reynolds stress ($-\rho\overline{u_i'u_j'}$) which represents the fluctuating velocity field. The Reynolds stress is necessary to solve the turbulence model, which is essential for accurately modelling the physics of turbulence in the flow. For this case, the $k-\omega SST$ model is used. This model is a two-equation model that combines$k-\epsilon$ (in the outer region of and outside of the boundary layer) and $k-\omega$ (in the inner boundary layer).

This choice was also made in accordance with the fact that steady flow modelling using the Reynolds-Averaged Navier-Stokes (RANS) equations is a common practice. The characteristics of the RANS equations consist of a time-averaged description of fluid flow, neglecting unsteadiness. This approach is suitable for problems where the flow field operates in a quasi-steady state and small variations over time.

However, it is important to recognize the limitations of steady-state approach. RANS solutions may not be suitable for modelling scenarios involving strong time-dependent phenomena, such as vortex shedding. This aspect plays a major role in evaluating the obtained results. Indeed, neglecting the unsteadiness in the flow can lead to inaccurate predictions of the vortex shedding frequency and its effects on the surrounding structures.

Moreover, the rotor modelling adopted for the purpose consists in the Moving Reference Fram (MRF) approach (or Frozen Rotor). This method simulates the effect of motion on a stationary mesh. It is used for simulations that are steady in time, making it an assumption on the thruster wake. The equations account for rotation even though the mesh itself does not rotate. This is achieved by defining cell zones with different rotational speeds ω. The Navier-Stokes equations (RANS mehtod) are solved using an absolute formulation, steady-flow approach. It should be taken into account that this approach neglects the time history of the propeller flow, which is intrinsically related to the incoming flow. However, if the incoming flow is uniform, this approach is perfectly correct [39]. The Moving Reference Frame method has the advantage of incorporating propeller blades into the simulation, including their rotation, through a distinct region. This results in a rotating wake behind the thrusters [46]. From the literature research, it has been derived that MRF results are usually a good estimate of the thrusters interaction phenomena [39].

Regarding the number of iterations performed for each case, the maximum has been set to 3000 steps. However, in the post-processing of the data, it was noticed that for some specific cases, a higher number of simulations was required to confirm the convergence of the system. Therefore, for a limited number of cases, the iterations have been extended to 6000. This aspect will be further discussed while presenting the obtained results.

In conclusion, since the measured force is used as the parameter of interest to carry out the post-processing of the data, it is fundamental to provide more information about the followed procedure for this purpose. With reference to Equation 4.1, the two force components of interest can be identified:

- Pressure-induced force: it is the pressure-induced force and acts normally to the hull. It is represented by the pressure gradient term $-\bar{p}\delta_{ij}$. The related force is obtained by integration along the surface.

$$-\bar{F}_{pressure} = \int_S -\bar{p}\bar{n}dA \tag{4.2}$$

- The second component of the total force is represented by the viscous stress term

$$\tau_{j,i} = \mu\left(\frac{\partial\bar{u}_i}{\partial x_j} + \frac{\partial\bar{u}_j}{\partial x_i}\right) \tag{4.3}$$

which represents the viscous forces on the hull due to the fluid's viscosity. The related force is also obtained by integration.

$$-\bar{F}_{viscous} = \int_S \tau_{j,i} dA \tag{4.4}$$

Through the previously calculated force components, the total force acting on the object is therefore obtained by adding each component. The force is obtained for each coordinate component (x, y, z).

$$\bar{F}_{total} = \bar{F}_{pressure} + \bar{F}_{viscous} \tag{4.5}$$

Consecutively, the moment acting on the object can be obtained through the following formulation:

$$\bar{M}_{total} = \int_S \bar{r} \times (\bar{F}_{pressure} + \bar{F}_{viscous}), dA \tag{4.6}$$

where $\bar{r}$ consists of the position vector of each cell with respect to the origin point, as will be presented in the next chapter.

4.2. Definition of simulation scenarios

As a result of the performed estimations and predictions in Chapter 3, some cases have been identified to investigate the problem further. In particular, a combination of 3 different parameters has been identified for the first set of simulations:

- Beamside current at three speeds: 0, 1 and 2 knots. Given the results obtained from these three cases, one more scenario has been introduced, specifically 0.5 knot.
- Thruster rotational speed: the non operating thruster (0%), 50% and 75% of the maximum applicable rotational speed (n_{MAX}) obtained from the reference case;
- Under-thruster-clearance: 6, 10 and 100 meters have been considered to investigate the difference between shallow and deep water.

Overall, this set of simulations involved 34 cases.

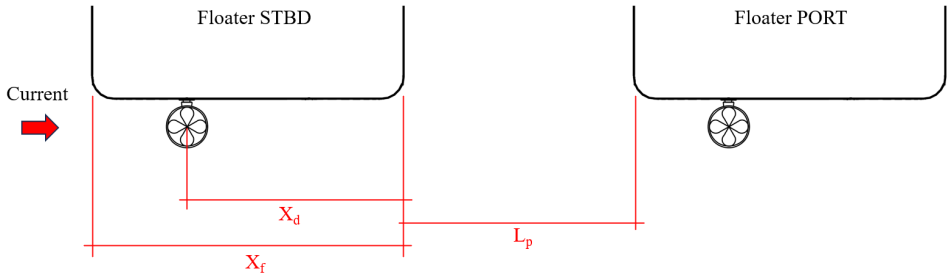

Figure 4.3: Schematic illustrating the model geometry.

The next step consisted of evaluating the effect of different geometries set up, specifically in terms of thruster position and floater distances. The parameter of interest has already been investigated in the literature; however, the add-on in this research included the effect of current combined with variable under-thruster clearance. Therefore, a base case of 2 knots of beam-side current speed and a thruster speed equal to 75% of n_{MAX} have been used for 4 different geometrical variations. Furthermore, the case with no working thruster has been run to obtain the current load on the vessel. A total of 18 more runs were necessary to accomplish the goal.

The following combination of thruster position and floater distance has been investigated. It should be mentioned that the variable parameters are L_p and X_d, while the floater width X_f is constant.

- $L_p/X_f = 1.2$ & $X_d/X_f = 0.7$
- $L_p/X_f = 0.6$ & $X_d/X_f = 0.7$
- $L_p/X_f = 0.6$ & $X_d/X_f = 0.36$
- $L_p/X_f = 1.2$ & $X_d/X_f = 0.36$

The first case consists of the base case for which the initial set of simulations has been used. Figure 4.3 provides the geometrical representation of the aforementioned geometry.

4.3. CFD Simulations of thrusters in Open Water

The first step in the modelling process consisted of defining the thruster geometry and subsequently testing it in open water conditions without the presence of the hull above. Given the high number of simulations to be performed, this step also allows to properly verify the mesh sizes and critically evaluate the following steps.

4.3.1. Thruster geometry

As anticipated before, the position of the thruster and its characteristics play an essential role in the determination of the interactions. Therefore, it is key to introduce how the thruster has been modelled and which configurations will be used.

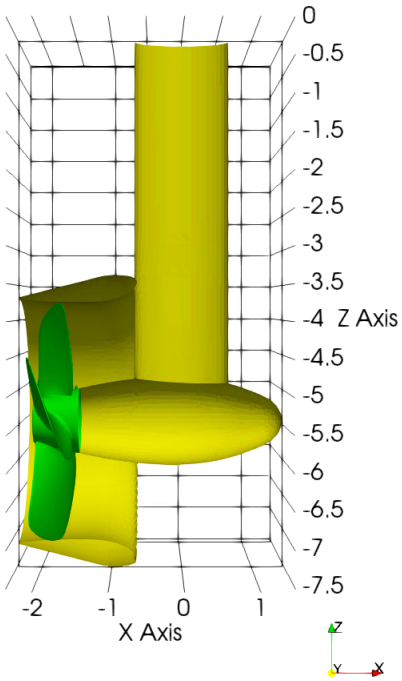

Figure 4.4: Thruster visualization: side view.

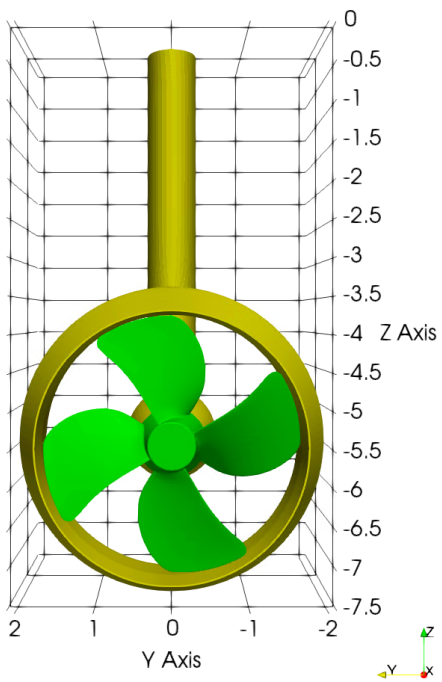

Figure 4.5: Thruster visualization: front view.

The used thruster consists of a 4-blade thruster with $P/D = 0.99$ (pitch/diameter ratio) and nozzle shape based on the Wärtsila underwater mountable thruster design. The thruster shaft drive has been modelled with a general elliptic shape, as shown in Figure 4.4.

A fixed position distance from the hull has been defined. In particular, a hull distance (between the hull and centerline of the gearbox) over diameter ratio of 0.72 has been used. The CFD thruster model representation is provided in Figure 4.5. The provided visualization of the thruster includes a slightly longer thruster pod to ensure that the thruster is placed far enough from the surface and that the physical effects are well captured. This is because the free surface waves have not been modelled within this project.

4.3.2. Open water grid generation

Given the characteristics of the thruster, the following steps consist of defining the characteristics of the meshes that have been developed. This allows to identify which mesh size is more suitable for carrying out the desired set of simulations regarding the best trade-off between precision and requested computational power.

For this purpose, the grid study was carried out based on the open water (referred to as OW) thruster performance, with the propeller rotating at 191 [rpm]. This investigation was performed as the first step before the thruster tuning.

Based on the previous experience and similar tests performed within the company, 4 different meshes have been created. All of them consist of a decomposed case with the same refinement ratio, and the first characteristic parameter consists of the side length of the outer cells (far from the surface of interest, at the boundary of the domain). To obtain this achievement *Cadence Fidelity Automesh* software has been used. Specifically, a volume-to-surface unstructured mesh has been developed, starting from the definition of the boundaries (inlet, outlet, side walls, atmosphere, and seabed) and moving towards the specific geometry of the thruster.

Therefore, four different mesh sizes are generated, and their characteristics are provided below.

- Mesh 1: average cell volume: 13.43 [m^3]
- Mesh 2: average cell volume: 6.45 [m^3]
- Mesh 3: average cell volume: 4.36 [m^3]
- Mesh 4: average cell volume: 3.24 [m^3]

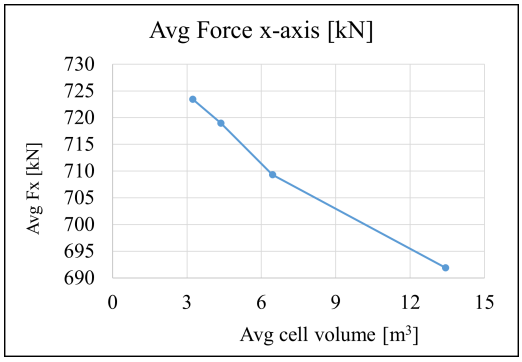

Figure 4.6: Average Forces along x-axis (Thrust) in [N]. The average value of the last 500 iterations.

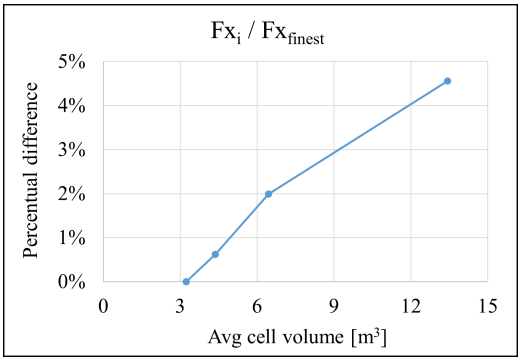

Figure 4.7: Percentage difference in the measured delivered force along the x-axis (Thrust) between the i-grid and the finest grid (16[m]).

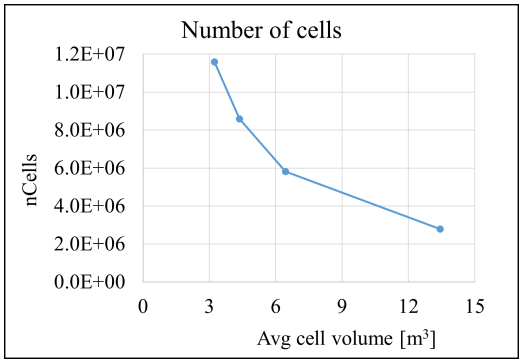

Figure 4.8: Number of cells per mesh size.

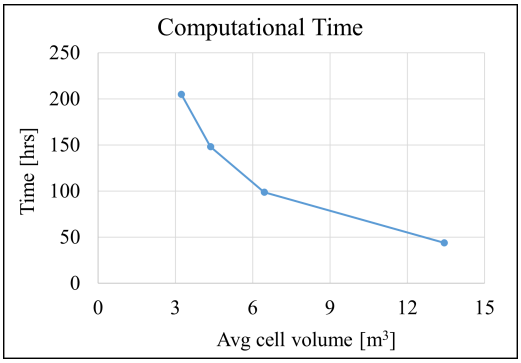

Figure 4.9: Total computing time

Table 4.1: Grid refinement ratio (h_i)

Avg V $[m^3]$	h_i	F_x **[kN]**
13.43	2.50	692
6.45	1.56	709
4.36	1.13	719
3.24	1.00	724

Each of the generated mesh has then been run through the OpenFOAM code with the previously described conditions. Simulation results are then extracted with a specific focus on forces (F) and moments (M) with reference to the 3 axes (x, y, z). The parameter of main interest consists of the forces along the x-direction (F_x) as it consists of the delivered thrust in the direction of the thruster shaft. This parameter has been evaluated taking into account the average value of the last 1500 iterations of a total number of iterations equal to 3000.

All the previous graphs illustrate the characteristics of each of the four created meshes. To choose the best option based on time and cost, it's essential to compare the total time and the number of processors used for each mesh size. The obtained values for the studied case are provided in Figure 4.7 and 4.9.

4.3.3. Grid verification & validation

Provided the description of the test characteristics for conducting a grid study, additional precise calculations are necessary. Specifically, the verification and validation procedure consists of the next steps. However, it is important to notice that the used propeller has never been used. Therefore, the only viable option remains verification of the mesh grid.

The definition of verification is provided by *Eca et al.* [17]:

'Verification is a purely mathematical exercise that intends to show that we are "solving the equations right". [...] This means that verification deals with numerical errors/uncertainties whereas validation is concerned with modelling errors/uncertainties.'

Verification

The first approach for grid verification is based on the iterative parameter convergence provided by *ITTC* [27]. Having tested 4 different mesh sizes and using as a governing parameter the force along the thruster axis direction (F_x) it is possible to define the convergence ratio R. This parameter is obtained using the parameter of interest (ϕ_i) for each grid size, which in this case is the mean value of the force along the x-axis (f_X) over the last 1500 iterations.

$$R = \frac{\phi_1 - \phi_2}{\phi_2 - \phi_3} = 0.29 \ ; \qquad R = \frac{\phi_2 - \phi_3}{\phi_3 - \phi_4} = 0.47 \tag{4.7}$$

Table 4.1 provides the correlation between average cell volume, the grid refinement ratio (h_i) and the obtained F_x.
From Table 4.7, it can be derived that the solutions are monotonically converging as the convergence ratio is $0 < R_i < 1$. Therefore, the evaluation of the discretization error can be carried out starting from the mesh refinement. The proposed approach is based on the methodology illustrated by *Eca et al.* [17].

In particular, the goal of the following procedure consists of assessing the verification of the solution and, therefore, the uncertainty (U) of a given calculation. It is important to mention that uncertainty is defined by *Roche* [49] as the interval that should contain the exact solution. Therefore, with the following steps, it is expected to obtain reduced uncertainty for smaller mesh sizes, allowing the uncertainty for the chosen mesh size to be evaluated.

In principle, CFD solutions have 3 types of numerical error components:

- Round-off error: is a consequence of the finite precision of the computers;
- Iterative error: due to non-linearity of the mathematical equations which always exists given the iterative solution approach;
- Discretization error: due to the made approximations to transform the differential equations into a system of algebraic equations.

According to *Eca et al.* [17], the first two types of errors are negligible when compared to the discretization error. Specifically, when noisy data are given, the least-square error estimation is suggested when dealing with practical problems, as it is in the case of interest. Equation 4.8 provides the definition of the weighted least-square equation that needs to be solved to assess the uncertainty.

$$S_{RE}^{w}(\alpha, \phi_0, p) = \sqrt{\sum_{i=1}^{n_g} (\phi_i - (\phi_0 + \alpha h_i^p))^2} \tag{4.8}$$

where:

- α is a constant to be determined;
- ϕ_0 consists of a function of a local flow quantity, which in this case consists of the force along the x-axis;
- p is the observed order of grid convergence;
- n_g is the number of grids (4 in the actual scenario);
- ϕ_i is the estimate of the exact solution;
- h_i consists of the typical cell size and, therefore, the average cell volume.

The weights (w_i) are calculated based on the grid refinement ratio (h_i), which has been chosen as the edge length of the cell at the domain's boundary.

$$w_i = \frac{\frac{1}{h_i}}{\sum_{i=1}^{n_g} \frac{1}{h_i}} \tag{4.9}$$

The procedure requests that the minimum of the function 4.8 is found in order to asses p, α and ϕ_0. This goal is achieved through a dedicated $MATLAB$ script. The calculation has been performed for both the weighted and not-weighted cases . It results that $0 < p < 0.5$ in both cases. Therefore, the error (δ_{RE}) obtained from S_{RE}^{w} would result in a too conservative error [17].

The suggestion is to perform least square analysis, both for weighted and not weighted approaches with a fixed order of convergence $p = 1$ and $p = 2$, and their combination. Specifically the least square calculations are listed in Equation 4.10, 4.11 and 4.12.

$$S_1(\alpha, \phi_0) = \sqrt{\sum_{i=1}^{n_g} w_i(\phi_i - (\phi_0 + \alpha h_i))^2} \tag{4.10}$$

$$S_2(\alpha, \phi_0) = \sqrt{\sum_{i=1}^{n_g} w_i(\phi_i - (\phi_0 + \alpha h_i^2))^2} \tag{4.11}$$

$$S_{1,2}(\alpha_1, \alpha_2, \phi_0) = \sqrt{\sum_{i=1}^{n_g} w_i(\phi_i - (\phi_0 + \alpha h_i + \alpha h_i^2))^2} \tag{4.12}$$

For each least square analysis, a standard deviation (σ) is obtained and listed in Table 4.2. The procedure indicates that the results related to the lowest standard deviation must be considered before proceeding with the definition of uncertainty.

Table 4.2: Least-squares analysis results

	ϕ_0	α_1	α_2	σ
δ_1	743	-20.4	-	1.81
δ_2	727	-5.65	-	15.7
δ_{12}	758	-39.8	5.46	1.05
δ_{1w}	743	-20.9	-	1.86
δ_{2w}	727	-5.65	-	15.9
δ_{12w}	758	-40.9	5.76	1.06

From Table 4.2, it can be noticed that the lowest standard deviation is measured for the case of δ_{12}. Therefore, the discretization error can be computed as follows.

$$\epsilon_\phi \approx \delta_{12} = \alpha_1 h_i + \alpha_2 h_i^2 \tag{4.13}$$

Calculating the estimated discretization error allows the estimation to be concluded to obtain the uncertainty. Indeed, the last step consist in defining the uncertainty U_ϕ which contains the exact solution with 95% coverage:

$$\phi_i - U_{phi} \leq \phi_{exact} \leq \phi_i - U_{phi} \tag{4.14}$$

To assess the quality of the data fit, a data range parameter is defined (Δ_ϕ).

$$\Delta_\phi = \frac{(\phi_i)_{max} - (\phi_i)_{min}}{n_g - 1} = 10.5[kN] \tag{4.15}$$

In all the analyzed cases $\sigma_{RE} < \Delta_\phi$, therefore, a safety factor 1.25 is introduced in the uncertainty calculation by the Grid Convergence Index (GCI) procedure.

$$U_\phi(\phi_i) = 1.25\epsilon_\phi(\phi_i) + \sigma_{RE} + |\phi_i - \phi_0| \tag{4.16}$$

where ϵ_{phi} is defined as the discretization error and calculated in Equation 4.15.

Table 4.3: Uncertainty estimations solutions

Avg V [m^3]	h_i	**T [kN]**	**U [kN]**
13.43	2.50	692	148
6.45	1.56	709	111
4.36	1.13	719	87
3.24	1.00	724	78
Estimated exact solution (ϕ_0)		758	0

The obtained results are presented in Table 4.3, including the uncertainty estimation. Furthermore, the estimated exact solution (ϕ_0) is presented. A visual representation of the uncertainty is provided in Figure 4.10.

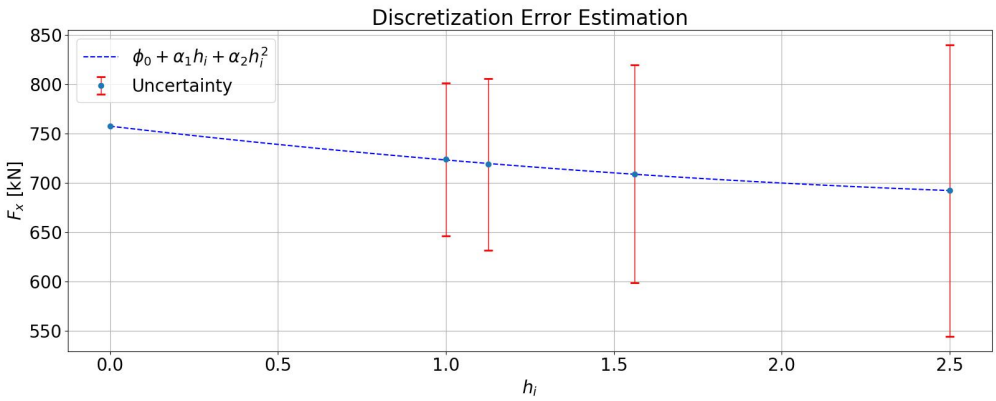

Figure 4.10: Uncertainty assessment on 4 different grid sizes. Mesh size is defined through the average cell volume (x-axis). Thrust along the x-axis is used as the local flow quantity of interests (x-axis).

The next and final step is intended to provide sufficient motivation for the choice to use the grid refinement characterized by the h_i ratio of 1.56 with reference to the finest considered grid size.

Table 4.4: Grids comparisons with reference to uncertainty, requested computing time and number of cells (million) in the mesh.

Avg V $[m^3]$	$\mathbf{h_i}$	$\mathbf{U_{\delta_1}/T[\%]}$	**Processing time [hrs]**	**Number of cells [M]**
13.43	2.50	21.4%	43.8	2.79
6.45	1.56	15.6%	98.8	5.82
4.36	1.13	12.1%	148	8.59
3.24	1.00	10.7%	205	11.6

As can be noticed, the uncertainty for the considered mesh size is 15.6% of the delivered thrust (T), while for the finest grid, the achieved value is 10.7%. However, almost double the precision in the results comes at the cost of almost double the required computing time (2.07 times the computing time for the finest grid).

Furthermore, this grid study is based on the open water case, which has considerably fewer cells than the thruster + hull case. Indeed, the objective of the thesis involves the evaluation of a series of different conditions for which a limited amount of time and cost has to be fulfilled. The best trade-off between results precision and computing time/costs has been identified in the grid size characterized by the h_i ratio of 1.56. This section, therefore, acknowledges the uncertainties present in the examined results.

Validation

Validation is defined as the process of assigning simulation uncertainty U_{SM} through benchmark experimental data. To validate a model, the parameter E is suggested by *ITTC* as the comparison error and is defined through the following formulation:

$$E = D - S = \delta_d - (\delta_{SM} + \delta_{SN}) \tag{4.17}$$

Therefore, the CFD model can be validated at U_v level when $E < U_v$. U_v. However, experimental data is needed to pursue such a procedure, which is unavailable for the present scope. Therefore, no validation procedure has been pursued. Despite the absence of experimental data regarding the modelled thruster, the qualitative comparison is carried out with a similar thruster. Specifically, the comparison is between the open water diagram of the modelled thruster and the K_t curve of two other thrusters, equipping comparable semi-submersible vessels. A comparison will be presented and discussed in the next section, as it is necessary to obtain the open water diagram of the modelled thruster first and then compare it to existing models.

4.3.4. Thruster calibration & Open water curve

All the previous thruster studies have been performed with a propeller rotational speed of 191$[rpm]$, which did not provide the desired thrust value. Therefore a re-calibration of the thruster to asses at which propeller rotational speed (n) the modelled thruster results in providing $T = T_{MAX}$ has been performed. The obtained solution has the propeller rotational speed of 208 rpm: at this rational speed, the modelled thruster provides the desired T_{MAX}. The main goal of this tuning procedure consisted of obtaining the requested rpm to achieve the desired thrust in the bollard pull (BP) condition.

To provide a more detailed characterization of the thruster, two more simulations have been performed where the thruster has been run at the same rotational speed (208 rpm) but in two different flow conditions, specifically 1 knot (0,514 m/s) and 2 knots (1,03 m/s). The current has been aligned with the x-axis of the thruster. These simulations allowed to build the open water curve, specifically the K_t curve as presented in Figure 4.11.

In addition, the provided thrust in bollard pull (and open water) conditions as a function of rpm are included in Figure 4.11. This plot also includes the thrust coefficient of two comparable semi-submersible vessels. It can be noticed that the obtained polynomial fit based on the measured value of K_t for different inflow velocities yields values similar to the existing thruster installed on the same type of vessel. While this comparison does not validate the measured data for the considered thruster, it confirms that the obtained characteristics of the thruster unit are realistic and comparable to existing vessels. In the same plot, the quadratic relation between delivered thrust (T) and propeller rotational speed is plotted, and a good match is reached as the quadratic approximation of delivered thrust coincides with the data point obtained from CFD simulations.

The used formula consists of Equation 4.18, and it is a simplified approach generally used by dynamic position systems to calculate the propeller rotational speed, depending on the requested thrust.

$$T = T_{max} \cdot \left(\frac{rpm}{rpm_{max}} \right)^2 \tag{4.18}$$

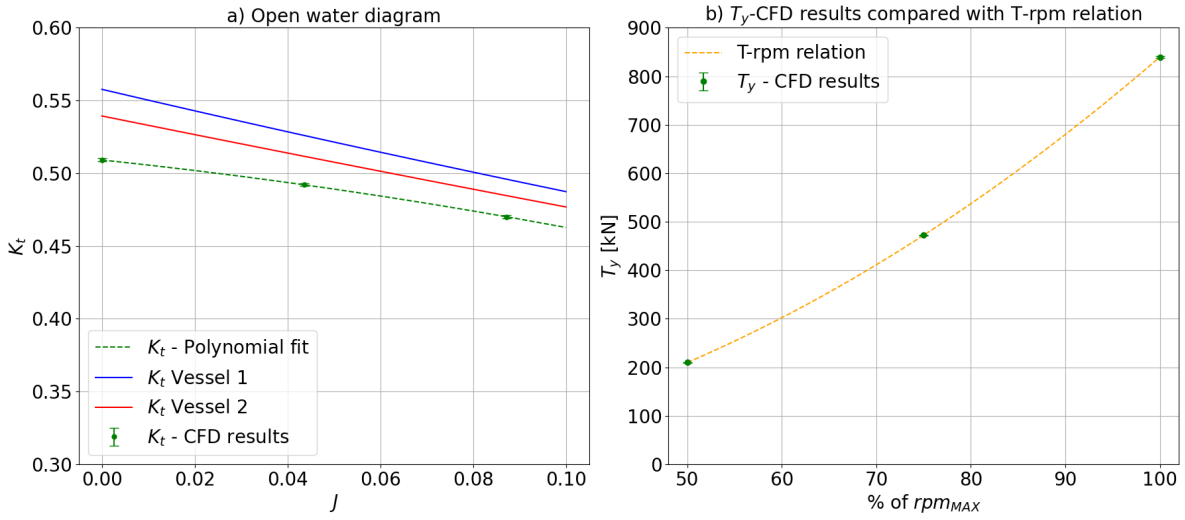

Figure 4.11: Thruster characteristics: a) K_t curve including the standard deviation measured over the last 1500 iterations. 2^{nd} order polynomial fit for the CFD results is shown along with the K_t curve of two other thrusters used in Semi-submersible vessels. b) Delivered thrust in [kN] as functional of maximum propeller [rpm].

4.4. Geometry of vessel hull in CFD Simulations

The second element that needs to be described is the hull modelling in combination with the thruster to investigate the thruster-hull interaction with the working thruster beneath the hull. The used geometry consists of a typical semisubmersible vessel hull with geometrical characteristics illustrated in Figure 4.12 and briefly described in Chapter 1.

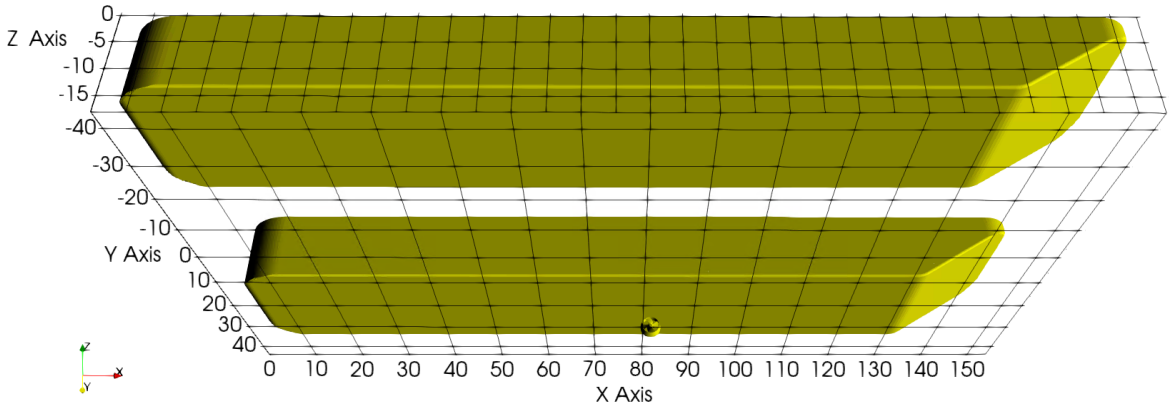

Figure 4.12: Bottom view of the vessel hull model used for the full-scale CFD simulations.

The complete model of the hull also includes the described thruster, which needs to be included in the geometry. The longitudinal thruster positions (x-axis) were chosen based on the expected flow behaviour around the hull. Specifically, the flow is expected to be more turbulent and less predictable in the aft and forward sections of the vessel. This led to the conclusion that using a central position for the thruster would reduce these sections' effects and flow deviations. Given that the flow deviation in the aft and bow regions is not of interest in the present work, it still represents a relevant factor in defining the flow field characteristics, which could lead to additional thrust losses in these regions. Furthermore, as other thrusters could potentially be located in these areas, further investigation would be beneficial to assess the impact of thrusters operating in the aft and forward sections at reduced under-thruster clearance. Therefore, it remains a future task to consider these aspects for further simulations.

Also, an important piece of information concerns the round bilge radius. The round bilge radius has a relatively small influence compared to the position of the thruster and the distance between the pontoons and the thruster's location [43]. To investigate the last two factors, the round bilge radius parameter has been set to 0.5 meters.

The reference system of the vessel located in the aft section at midships is illustrated in Figure 4.13.

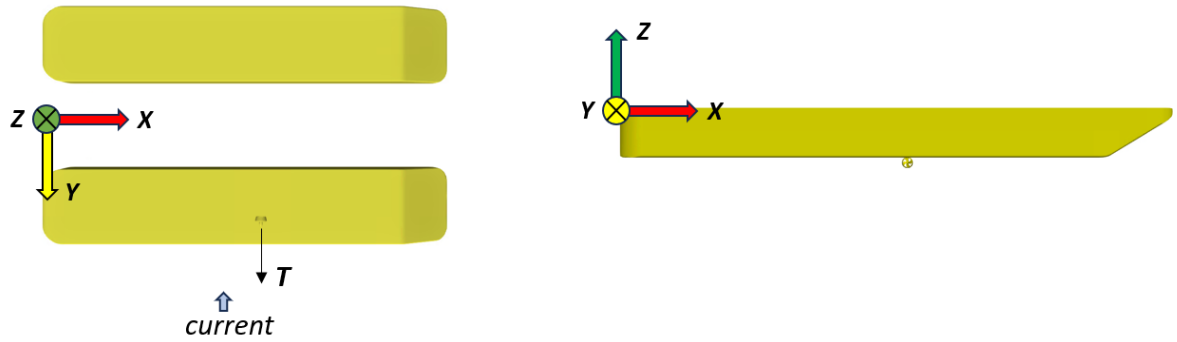

Figure 4.13: Global coordinates for all the developed meshes. Bottom view of the vessel (left); View of the starboard side of the vessel (right)

As introduced in Section 4.1, the boundaries of the domain need to be set properly to avoid any undesired effects. Accordingly, the mesh dimensions have been derived based on the experience developed with previously conducted simulations within a similar scope. Therefore, the simulation domain have been defined as:

- Along the x-axis, the domain is extended for 20 vessel's breadth downstream;
- Along the x-axis, the domain is extended for 10 vessel's breadth upstream;
- Along the y-axis, bow and aft direction the domain is extended for 5 vessel lengths.

The defined domain boundaries are modelled to allow for proper wake development along the y-direction of interest and allow the flow to develop properly upstream and downstream of the vessel. The distance between the vessel edges (aft and forward) and the side walls of the domain has been set to avoid any blockage effect. Indeed, if the side walls of the domain are located too close to the vessel, undesired effects could take place. Specifically, the blockage effect, similar to the model tests basin, could take place inducing modification of the flow field, hence leading to inaccurate results.

Based on the results obtained from the analysis of the open water case, all the created meshes have been developed using a mesh size reference parameter with a cell length of 25[m]. An example of the developed mesh is provided in Figure 4.14. Due to the high number of simulations involved, it is important to mention the amount of cells used for each developed mesh. In particular, with regards to the standard case where under-thruster-clearance is combined with current speed, three main meshes have been developed. Each of them refers to a different water depth, as summarized in the first row of Table 4.5. Conversely, for the geometrical variations of the floaters' distance and thruster position, four meshes need to be created.

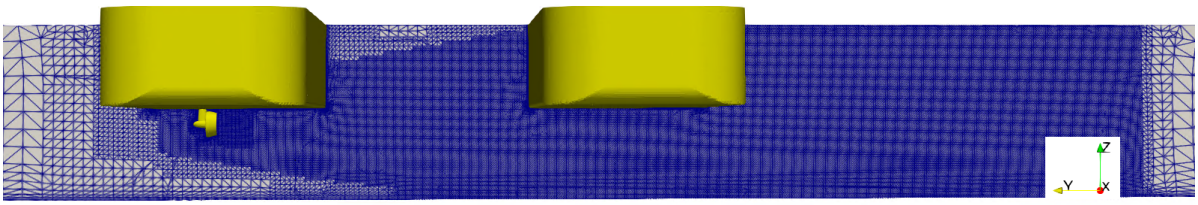

Figure 4.14: Mesh visualization for the case of 100 [m] under-thruster clearance. The detail of a slice of the domain at the thruster's y-axis location is shown, highlighting the grid refinement in the hull region compared to the far field.

It can be noticed that the refinement of the grid increases towards the domain as it gets closer to the hull surface and thruster. Indeed, the higher grade of refinement in correspondence with the vessel hull, the thruster, and the boundary layer on the seabed is visible. This point leads to another consideration which is crucial in understanding how the grid refinements have been developed. Indeed, the computational domain downstream of the thruster underwent further refinements compared to the surrounding region due to the higher turbulence expected in this area. Therefore, two conical sections have been developed in the downstream area of the thruster to ensure better modelling of the thruster (Figure 4.16).

Table 4.5: Number of cells for the base case of $L_p/X_f = 1.2$ & $X_d/X_f = 0.7$ at different water depths.

Under - thruster clearance	Number of Cells [M]
6 [m]	12.6
10 [m]	13.5
100 [m]	13.8

Table 4.6: Refinement level for each component of the mesh.

Surface	Refinement Level
Propeller	6
Nozzle/Gearbox	6
Hull	5
Small Conical Region	7
Large Conical Region	6

To better understand the upcoming section, where the boundary layer will be analysed more in-depth, it's important to illustrate the grid refinement in the round bilge region. This section of the hull, as well as the thruster region, is sensitive to flow variations. The flow in the round bilge areas can either detach or be forced beneath the hull, leading to significant velocity and pressure variations.

Since the solver calculate the solution of the motion equation for each cell, it's important to note that large cells could result in an inappropriate solution due to high parameter variations between adjacent cells. A more detailed discussion of the boundary layer modelling is provided in Section 4.5. Regarding the same issue, the downstream region is located below the thruster. In this area, two conical sections have been used with two different levels of refinement (levels 7 and 6) to create a more detailed solution in terms of pressure and velocity. This approach helps to prevent high gradients between adjacent cells. Figure 4.15 provides visual representation of the conical region.

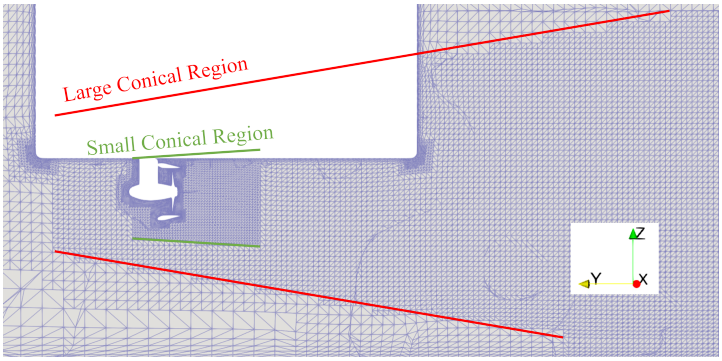

Figure 4.15: Detail of the cones (large and small) mesh refinement region in proximity of the thruster. Thruster mesh of 10[m] under-thruster-clearance

Therefore, different mesh refinements were used for different parts of the hull and thruster to minimise this effect. The mesh modelling utilized an isotropic refinement methodology, subdividing every "parent" cell into four smaller "child" cells. Each reduction in the volume of a cell is referred to as a "level," with higher levels indicating a higher degree of refinement in the cell. For the purposes of this thesis, all generated meshes have been generated with the same levels of refinement as defined in Table 4.6.

4.5. Boundary layer modelling

As discussed in the literature review (Chapter 2), turbulent flow and, therefore, a turbulent boundary layer are present in the area of interest. Particular attention needs to be paid to this phenomenon in the regions near the walls. As previously mentioned, the region near the hull features a more refined grid, with particular attention to the round bilge areas. A successful prediction of wall-bounded turbulent flows requires an accurate representation of the near-wall region. However, similar to grid refinement, computational resources and costs also play a fundamental role in defining the precision of the grid near walls.

Two different approaches are usually proposed to tackle this problem:

- Integrate turbulence to the wall, therefore the viscosity-affected region (the boundary layer) is resolved using a low Reynolds turbulence model. This model works better for the evaluation of the forces on the wall. This method, however, has higher computational costs due to the first cells, which are required to be in the viscous sublayer ($y^+ = 1$).
- The used approach consists in defining the wall function (y^+), which can model the near-wall region. Its aim consists of representing the physics in the boundary layer, bridging the gap between the no-slip condition on the wall surface and the fully developed turbulent region. To achieve this result, empirically derived equations are set in place.

Given the number of simulations to be done and the available computational resources, the chosen approach consisted of the wall function. This allows for a reduction in the mesh size and the computational domain as well.

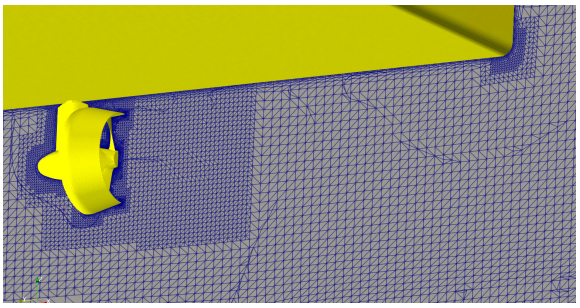

Figure 4.16: Zoom on the mesh region around the thruster and round bilge.

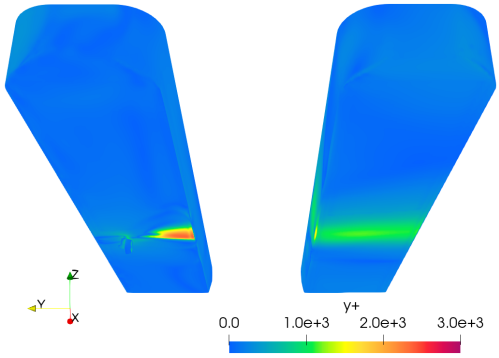

Figure 4.17: Wall function (y^+) around the hull.

Observing the wall function shown in Figure 1, it is evident that higher flow velocities correspond to higher y^+ values. This raises questions about the quality of the mesh used. As previously described, the mesh used is a tradeoff between time and cost considerations, the project's objectives, and the quality of the results obtained. The obtained values are assumed to be sufficiently precise when compared to other studies performed with full-scale simulation ([45]) of a semi-submersible vessel with currents. However, it is noticeable that the y^+ values register a peak in the round bilge of both floaters due to the high velocities in that region. This remains a topic for future work, investigating the effect of using a finer mesh in predicting the flow deviation in this region. Nevertheless, a predominant Coandă effect can already be visualized in the obtained results, as will be discussed in the next chapter (Chapter 5).

4.6. Post-Processing approach for CFD Results

The first part of the data analysis consisted of post-processing the raw data directly obtained from the OpenFoam solver. Although proposing a methodology for post-processing CFD data is not the primary focus of this work, it is valuable to present the methodology applied to the data analysis briefly. This aims to inform the reader of the steps followed, which can later be repeated or improved based on possible further simulations.

The first parameter of interest is the velocity field. The numerical solver calculates velocity for each cell, allowing it to be plotted across the entire domain. Given the interest in investigating the Coandă effect affecting the thruster outflow, it has been considered valuable to identify the flow velocity along the y-axis at a section passing through the thruster location (an example is provided in Figure 4.18). In these plots, it is possible to appreciate the differences between the different water depths and current cases. All data are provided as parameterized velocity therefore, they are non-dimensional.

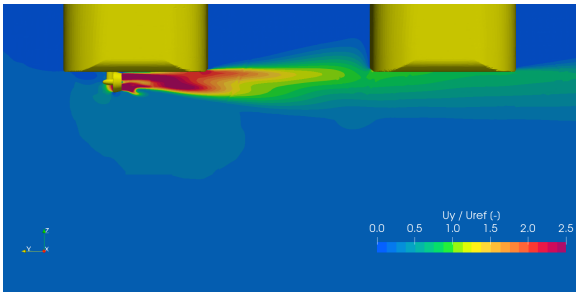

Figure 4.18: y-axis non dimensional velocity (U_y) example plot. U_{ref} = 2.5 [m/s]

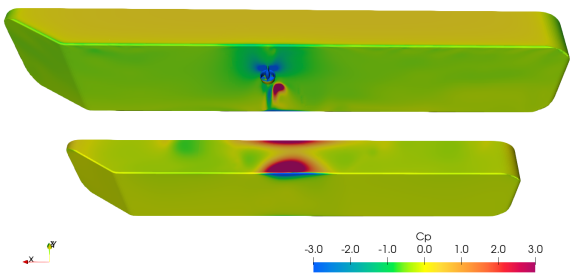

Figure 4.19: Example of pressure coefficient distribution on the hull.

Furthermore, comparing the pressure distribution along the hull is particularly relevant. These parameters provide the necessary insight to better understand how the blockage effects. Through this plot (example in Figure 4.19), it is possible to derive how the thruster outflow impacts the downstream pontoon. The provided results are presented through the pressure coefficient (C_p). Since the coefficient is calculated with reference to the velocity magnitude in the far-field location, it is evident that the pressure coefficient would be infinite in the case of 0 knots. Due to this reason, the reference speed U_{ref} = 1.0 [m/s] is used as suggested by *Ottens et al.* [45].

In conclusion, the data processing will involve evaluating the delivered thrust. In particular, the scope of this last part is to evaluate the propeller's efficiency with respect to open-water performance. The following formulation has been used to achieve this goal.

$$C_{TH} = \frac{F_{y,TH} - F_{y,CURR}}{T_{OW,y}} = \frac{T_{d,y}}{T_{OW,y}} = t \tag{4.19}$$

where:

- C_{TH} is the thruster-hull coefficient as defined by *Ottens et al.* [45].
- $F_{y,TH}$ is the force measured on the vessel with active thruster. Specifically at 75% and 50% of nominal [rpm];
- $F_{y,CURR}$ is the current load. This result is measured considering the thruster not rotating, therefore not producing any thrust but purely resistance. From the difference between $F_{y,TH}$ and $F_{y,CURR}$ the delivered thrust is obtained (T_d);
- $T_{OW,y}$ is the open water thrust calculated from the measured open water performance. Specifically, the open water thrust along the y-axis in the bollard pull condition is used as a reference parameter;
- t is the thrust reduction ratio as defined in the *ABS* [2] (T/T_{OW}).It should be noted that the definition of the thrust reduction factor t differs from the thrust deduction factor typically employed in the definition of propeller efficiency. In that case, the delivered thrust is obtained as $1 - t$.

The provided evaluation of the thruster-hull coefficient (C_{TH}) also includes a crucial intrinsic aspect: the effect of the inflow velocity. Specifically, the velocity profile at the upstream section of the thruster is included in the coefficient's evaluation, potentially representing an additional loss that is principally attributed to thruster-hull interaction. Indeed, the inflow velocity is modified due to the presence of the hull; therefore, this change is part of the thruster-hull efficiency coefficient.

Nevertheless, it is important to investigate the impact of this component further. This aspect is examined by evaluating the forces on the thruster unit, achieved by integrating the pressure on this component and comparing it with the open water performance of the thruster. In this comparison, the open water thrust is considered with reference to the desired thrust direction (along the y-axis).

Equation 4.19 introduces the necessity of defining how the standard deviation has been identified in the process. As explained in the previous chapter, each RANS simulation involved a series of iterations, either 3000 or 6000, to ensure proper system convergence. Extending the simulation by an additional 3000 iterations on top of the standard 3000 was necessary for some specific simulations. This extension was needed to confirm and check if the observed oscillations were indicative of a converging or non-converging simulation or if they were due to the oscillatory behaviour of the measured forces. Nevertheless, some residuals are always present and can be visualized in the oscillation of the iteration trace of each simulation. Since the evaluation of the values of interest has been carried out by considering the mean value of the last 1500 iterations, the respective standard deviation has also been considered to provide a complete picture of the obtained results. It is important to mention that the standard deviation has been evaluated for each simulation and used as a parameter to determine whether the simulation was converged enough and if more in-depth studies are needed to enhance the quality of the prediction.

Figure 4.20 provides an example of a well-converging simulation. The iteration-trace of the force on the y-axis is provided for the case of no current speed, 75% of n_{MAX} and three under-thruster clearances (6, 10, 100 [m]). For all the obtained results, the mean value has been calculated over the last 1500 iterations, correspondingly the standard deviation (σ_y). It is illustrated that the first iteration results have a predominant oscillatory behaviour, concluding that high residuals are still present. With the increasing number of simulations, the solution converges to a stable value with a reduced standard deviation.

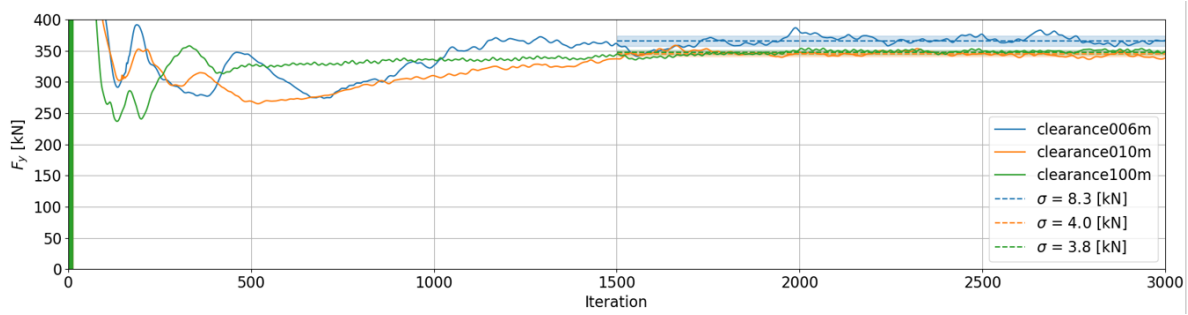

Figure 4.20: Iteration trace example. Current speed: 0 knot, Thruster setting 75% of n_{MAX}

However, in every case, the importance of the standard deviation cannot be neglected (further analysis will be presented in the next chapter), and it is of interest to properly manage it when comparing results from different simulations. Therefore, two different approaches have been used to evaluate the standard deviation, which results from the following operations:

- Regarding the difference between the forces ($F_{y,TH} - F_{y,CURR}$), the obtained standard has been obtained through the following formulation.

$$\sigma_{T_d} = \sqrt{\sigma^2_{F_{y,TH}} + \sigma^2_{F_{y,CURR}}} \tag{4.20}$$

- The standard deviation of the ratio is rather obtained with the propagation of error equation.

$$\sigma_{C_{TH}} = T_d \sqrt{\left(\frac{\sigma_{T_d}}{T_d}\right)^2 + \left(\frac{\sigma_{T_{OW,y}}}{T_{OW,y}}\right)^2} \tag{4.21}$$

The second part of the post-processing involved evaluating the effect of the presence of the hull above the thruster under different current speed conditions. In particular, it is of interest to evaluate how the inflow velocity at the thruster location affects the performance of the thruster. Through the raw data provided in the log file of OpenFOAM, the forces acting on the thruster pod can be obtained and compared to the open water scenario.

The procedure followed is the same as the one introduced above, involving the evaluation of the thruster-hull efficiency coefficient (C_{TH}), specifically modified for the present analysis. In particular, the hull coefficient for the thruster unit ($C_{TH,thruster}$) is evaluated as the ratio between the force acting on the thruster unit when operating beneath the hull compared to its performance in open water conditions. Therefore, the resulting coefficients are expressed in Formula 4.22.

$$C_{TH,unit} = \frac{F_{y,TH}}{T_{OW,y}} \tag{4.22}$$

where:

- $F_{y,TH}$ represents the measured force along the y-axis direction through the direct integration of the pressure field on the thruster unit surface while the thruster operates beneath the hull;
- $T_{OW,y}$ consists of the thrust in open water conditions as described before.

Therefore, the obtained trendlines with variations in current and water depth lead to an estimation of how much the effect of thrust loss can be attributed to positive inflow velocity on the thruster.

In conclusion, post-processing the geometrical variation of the thruster position and floaters' distance was completed using the same approach as for the base case. The comparison term consists again of the comparison of the thruster-hull efficiency coefficient C_{TH}. The objective is to analyze how these changes could benefit or negatively impact the delivered thrust in the desired direction.

To better understand the physical implications of these modifications, the pressure and flow fields upstream and downstream of the thruster will be considered and visually analyzed. A trend in the delivered thrust with respect to the under-thruster clearance will also be identified.

Regarding the definition of the thruster-hull efficiency coefficient, it should be noted that it relates to the case study of a thruster operating beneath the hull, specifically the upstream floater, oriented towards the opposite pontoon and in a beam-on side current condition. Different results would be expected if the thruster position is different. For instance, if the thruster is located beneath the downstream pontoon, no blockage effect is expected due to the impinging jet stream, hence higher coefficient values. Furthermore, the approach used only focuses on evaluating the thrust in the desired direction (y-axis), while considering different azimuth angles would require a more comprehensive definition of the coefficient, combining the thrust along the x-axis and y-axis.

5

CFD Simulations results

This chapter will discuss the results obtained from the CFD simulations. The solutions presented will focus on the impact of low under-thruster clearance from two main perspectives. First, it is important to compare the flow behavior under varying conditions of under-thruster clearance and beamside current intensity. Second, the delivered thrust should be assessed by comparing the open water thruster performance with the active thruster positioned beneath the vessel, providing thrust in the opposite direction to the current.

Specifically, the goals of the current thesis consist of three main areas of interest:

- The characterization of the flow beneath the hull when thrusters operate beneath the hull;
- The effect of the seabed proximity on the thrust-hull interactions, with a particular focus on the effect that this condition has on the flow developments. Special attention has been placed on the investigation of the flow development around the hull at variable thruster settings, under-thruster clearance, and current conditions;
- The assessment of the thruster's efficiency in different working conditions as a combination of the aforementioned parameters (thruster settings, under-thruster clearance, and current speed).

To achieve these goals, numerical data and visualizations of flow fields will be presented based on the data obtained from running CFD simulations. The main sources of inspiration for presenting the results will be the research papers by Maciel et al. [39] and Ottens et al. [46, 45].

Furthermore, the interaction estimations presented in Chapter 3 will be compared with results obtained from numerical simulations with the scope of deriving the precision of the supplied model and the accuracy of the classification society predictions.

5.1. Analysis of simulation results for thruster hull interactions

The first parameters of interest consist of investigating how beam-side current affects the performance of the thrusters while reducing the under-thruster clearance. In particular, as described in Chapter 4, the used parameter to capture these effects consists of the coefficient of thruster-hull efficiency C_{TH}. With this coefficient, it is possible to represent how the interaction between the thruster and the hull affects the effective thrust provided in the desired direction (in this case, beam-side, therefore 90° with reference to vessel heading) with and without current. The obtained results are provided in Figure 5.1

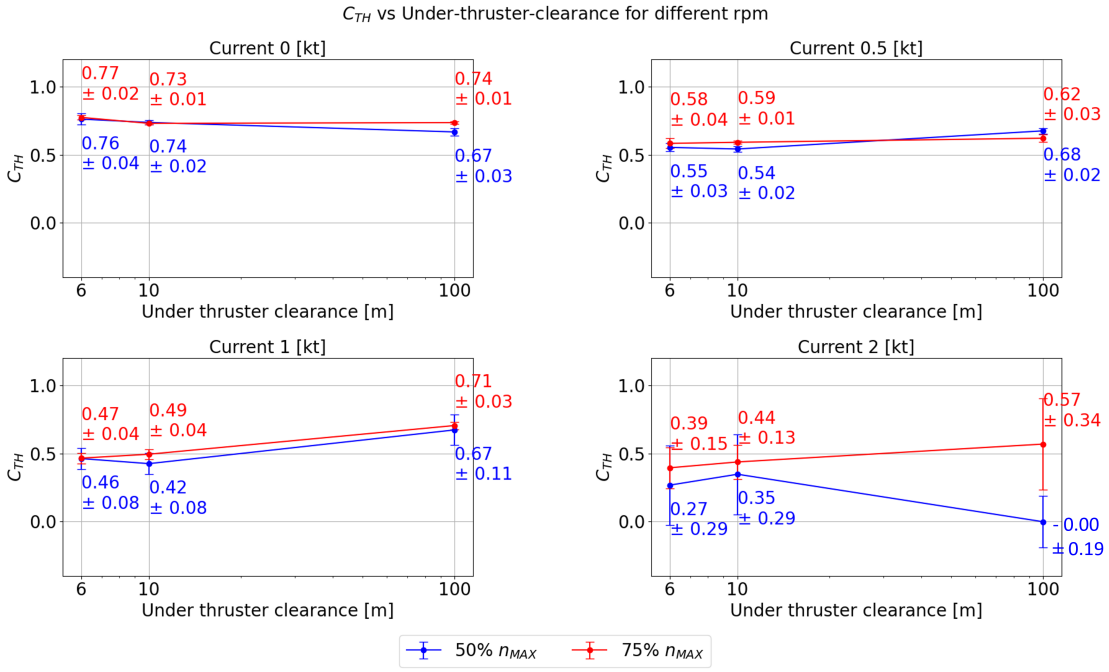

Figure 5.1: Mean thruster-hull efficiency coefficient C_{TH} of the last 1500 iterations as a function of under-thruster clearance at four beam-side current speeds (0, 0.5, 1, 2 knots) with associated standard deviation. An unexpected trend was measured for a 2-knot current due to unsteady phenomena in the flow field.

The impact of water depth and beam-on current on thruster performance can be observed in Figure 5.1. It shows that when there is no free-stream current, the effect of reducing the under-thruster clearance is nearly negligible. This result suggests that the proximity of the seabed does not have a considerable impact on the flow development of the jet created by the thruster. The measured thruster-hull efficiency coefficient does not considerably change at different under-thruster clearances.

Conversely, introducing a beam-side current results in a different trend of the obtained thruster-hull efficiency coefficient (C_{TH}). Specifically, when a current of 0.5 knots and 1 knot is present, there is a noticeable reduction in efficiency when comparing a thruster-seabed distance of 100 meters to a shallow water scenario of 6 meters. Comparing the C_{TH} obtained for 1 knot of current at 6 meters under-thruster clearance, there is a 33% reduction in delivered thrust compared to the deep water case (under-thruster clearance of 100 meters) due to the combination of current interaction and thruster-hull interaction. Furthermore, for this specific case, there is a reduction of 53% compared to the delivered thrust in open water. The thruster-hull efficiency coefficient demonstrates that the presence of a current combined with a reduced under-thruster clearance significantly reduces delivered thrust.

Moreover, it is relevant to further discuss the case with 2 knots of current speed. As shown in Figure 5.1, the obtained trend of the C_{TH} for the thruster setting of 75% of n_{MAX} is similar to the case of 0.5 knots and 1 knot of current, with higher thrust loss as expected due to the higher current. However, unexpected results are obtained for the case of 50% of n_{MAX} where the thruster-hull coefficient is 0 in deep water. Furthermore, in all the measurements of this case, every mean value is related to a comparably high standard deviation with reference to the other current speeds.

This unexpected behaviour has been attributed to two aspects: the development of vortices downstream of the thruster, which will be discussed in Section 5.4, and the magnitude of the obtained forces.

Indeed, the post-processing approach is based on the difference between two mean values:

- the measured force on the vessel when the thruster is not working (0% of n_{MAX});
- the measured force on the vessel when the thruster is providing thrust at 50% or 75% of n_{MAX}.

If the mean values of the two forces of interest show a high standard deviation (as in the case of 2 knots of current), the difference between them will be affected by error propagation, leading to a significant variation in the final results. For the 2 knots current case, the forces F_y at 50% n_{MAX} and 0% n_{MAX} are considerably higher in magnitude compared to results of interest ($T_{d,y}$). With a thruster setting of 75% of n_{MAX}, which aligns more with the results obtained for 0.5 knot and 1 knot of current, the obtained $T_{d,y}$ in deep water accounts for 24% of the total force acting on the vessel. These factors contribute to high uncertainties in these results.

To further discuss and analyze this problem, it is useful to refer to the raw data obtained from the CFD simulations shown in Figure 5.2. Indeed, the definition of the problem from a directly measured data perspective provides more insight into the magnitude of the post-processed forces. Furthermore, the directly measured forces provide a clear picture of the thruster's capability to compensate for the current external load.

Specifically, in Figure 5.2, the plot referring to the current speed of 2 knots shows the reason behind the obtained null value of C_{TH} for the case of 100 meters under thruster clearance. Indeed, the mean value of the force F_y, obtained with and without the operating thruster at 50% of n_{MAX}, are very similar, leading to a difference close to 0 kN.

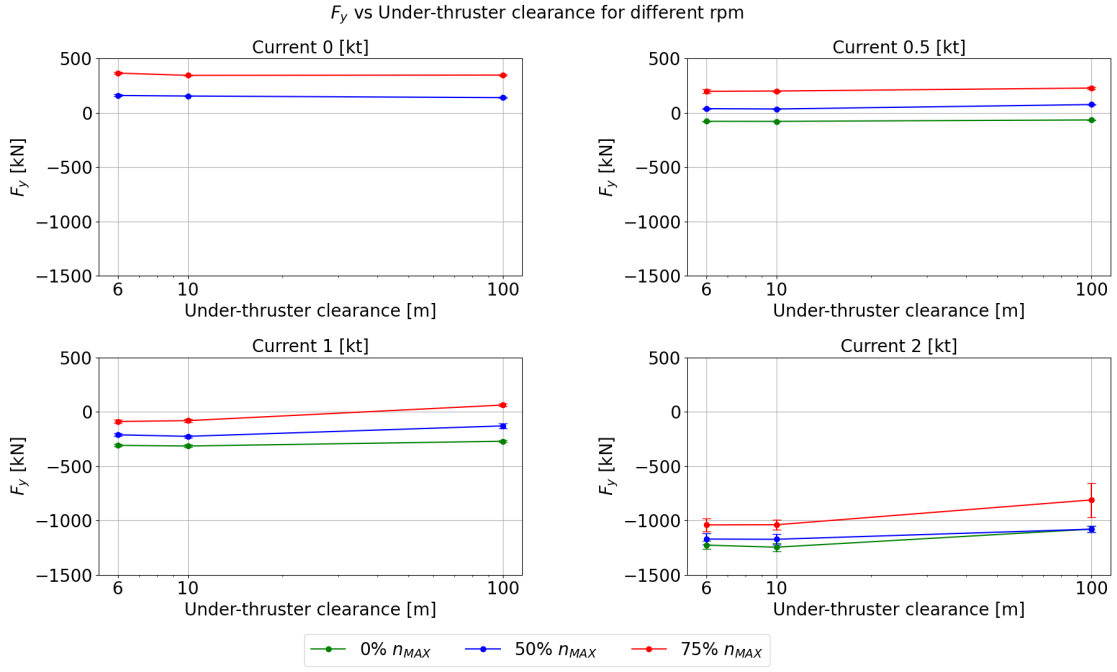

Figure 5.2: Measured force on the vessel in the y-axis direction. Each data point represents the mean value of F_y with the associated standard deviation obtained from the corresponding CFD simulation.

Furthermore, Figure 5.2 shows the scenarios where the effective delivered thrust is sufficient to compensate for the current load. A significant case that highlights the difference between reduced under-thruster clearance and deep-water cases is the 1 knot of current speed.

In shallow water conditions with a current of 1 knot, the provided thrust cannot compensate for the current load, resulting in a negative measured force (F_y). Different results are obtained for the deep water scenario, where 75% n_{MAX} setting is sufficient to compensate for the current load, leading to a positive force on the vessel. In this figure, 0 represents the equilibrium scenario. Hence, the thruster delivers enough thrust to compensate for the current load on the vessel. The scenario described does not reflect realistic operational cases as in normal operational conditions, all thrusters are used at lower rotational speed (n) to maintain position. However, the obtained results show that currents have a more significant impact on the station-keeping performance of the vessel when there is reduced clearance under the thruster.

To better understand the plotted data and the factors discussed in Chapter 2, it is important to relate the obtained values to the measured velocity field in the axial direction near the thruster and hull. This information is presented in Figure 5.3 and Figure 5.6. In this set of figures, it is possible to visualize the effect flow developments along the y-axis by presenting the velocity field in this direction (U_y)

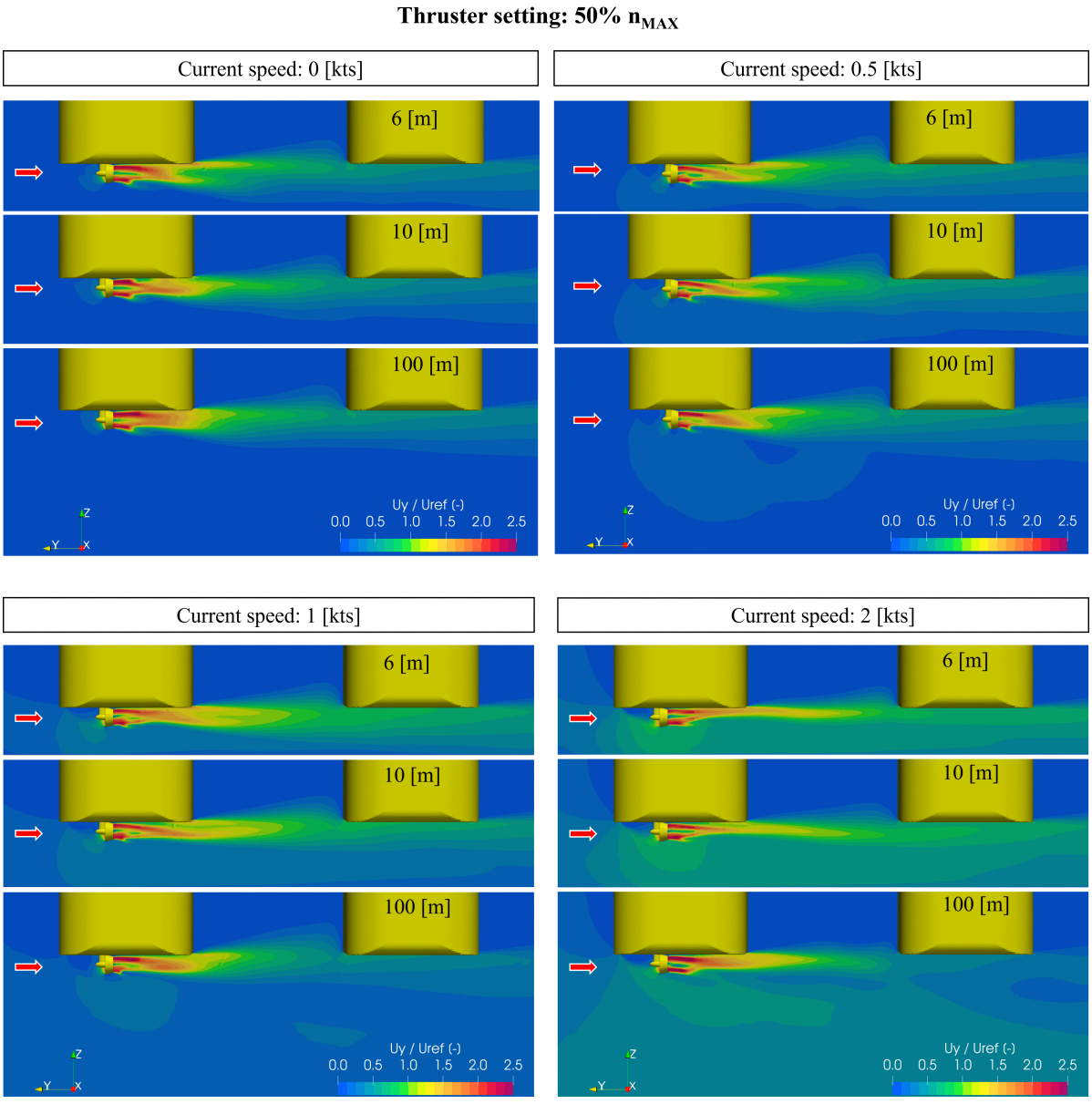

Figure 5.3: y-axis velocity field beneath the hull with 4 different current conditions (0, 0.5, 1, 2 knots) and 3 under-thruster clearance (6, 10, 100 meters) at 50% of the maximum thruster rotational speed (n_{MAX}). Non-dimensional velocity U_y/U_{ref} with U_{ref} = 2.5 [m/s]. The current direction is indicated through a red arrow.

Figure 5.3 depicts the flow field when the thruster is active and operating at 50% of the maximum thruster rotational speed (n_{MAX}). In this case, the impact of the current is highlighted, showing two different effects on the thruster outflow development.

- Firstly, it is clear that a recirculation area is present upstream of the thruster, where the flow velocity is much lower than the velocity in the surrounding region. This aspect is common to all the current scenarios that have been investigated. However, it is evident that with a higher flow rate, the mean inflow velocity increases, reducing the delivered thrust. This aspect is visually highlighted when comparing the case of 0 and 2 knots, where the more marked green colour in the upstream region of the thruster illustrates a higher velocity area.
- The current effect is also visible in the development of the outflow downstream of the thruster. The effect of higher current, at comparable under-thruster clearance, is noticeable and tends to drag the higher velocity further from the thruster, leading to higher velocity beneath the downstream pontoon. This leads to a growing frictional resistance on it at decreasing values of under-thruster clearances.

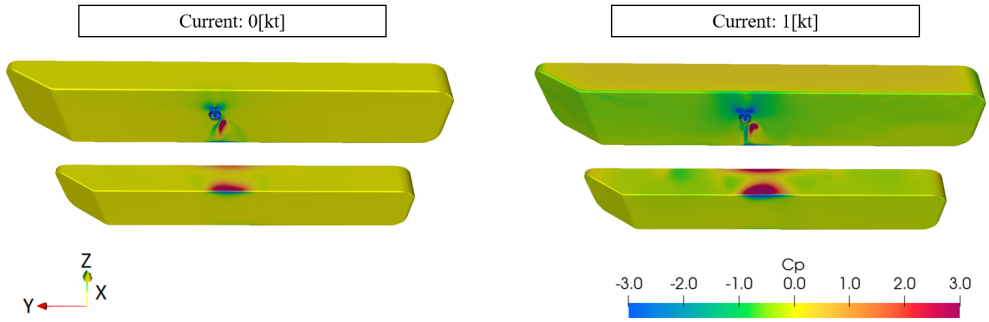

Figure 5.4: Pressure distribution on the downstream pontoon at different current speeds. 6meters under-thruster clearance, 75% n_{MAX}

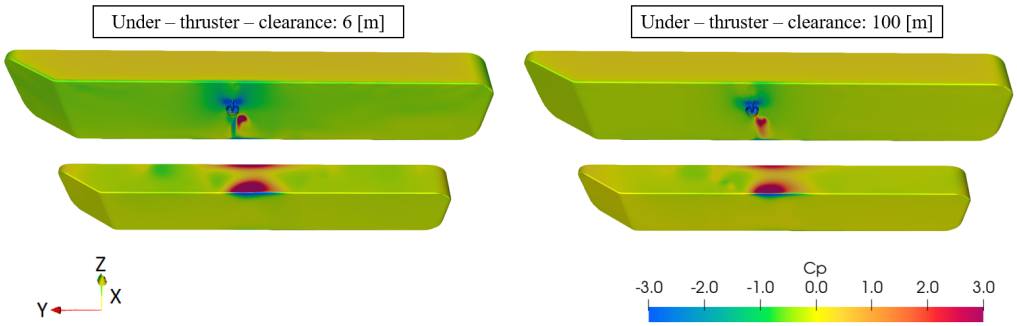

Figure 5.5: Pressure distribution on the downstream pontoon at different under-thruster clearance. 1 knot current speed, 75% n_{MAX}

It is particularly relevant to compare the impact on the flow deviation (Cŏanda effect) at the same under-thruster clearance and different current speeds. A more pronounced flow deviation is observed when current is present, as highlighted by the higher velocity region between the floaters. This effect can also be appreciated in the pressure distribution in Figure 5.4. Similarly, at the same current speed and different under-thruster clearance, the downstream pontoon has a higher pressure region (Figure 5.5) for the minimum under-thruster clearance of 6 meters. This suggests that the Cŏanda effect is enhanced by the free-stream current, leading to the conclusion that the presence of the current results in a more marked deviation of the flow toward the region between the two pontoons and, therefore, a higher force loss due to impingement. Furthermore, from Figure 5.4, it could be noticed that the effect of current impact also the distribution of the pressure on the downstream pontoon. Specifically, the region interested in the impinging effect is more spread out due to the 1 knot current.

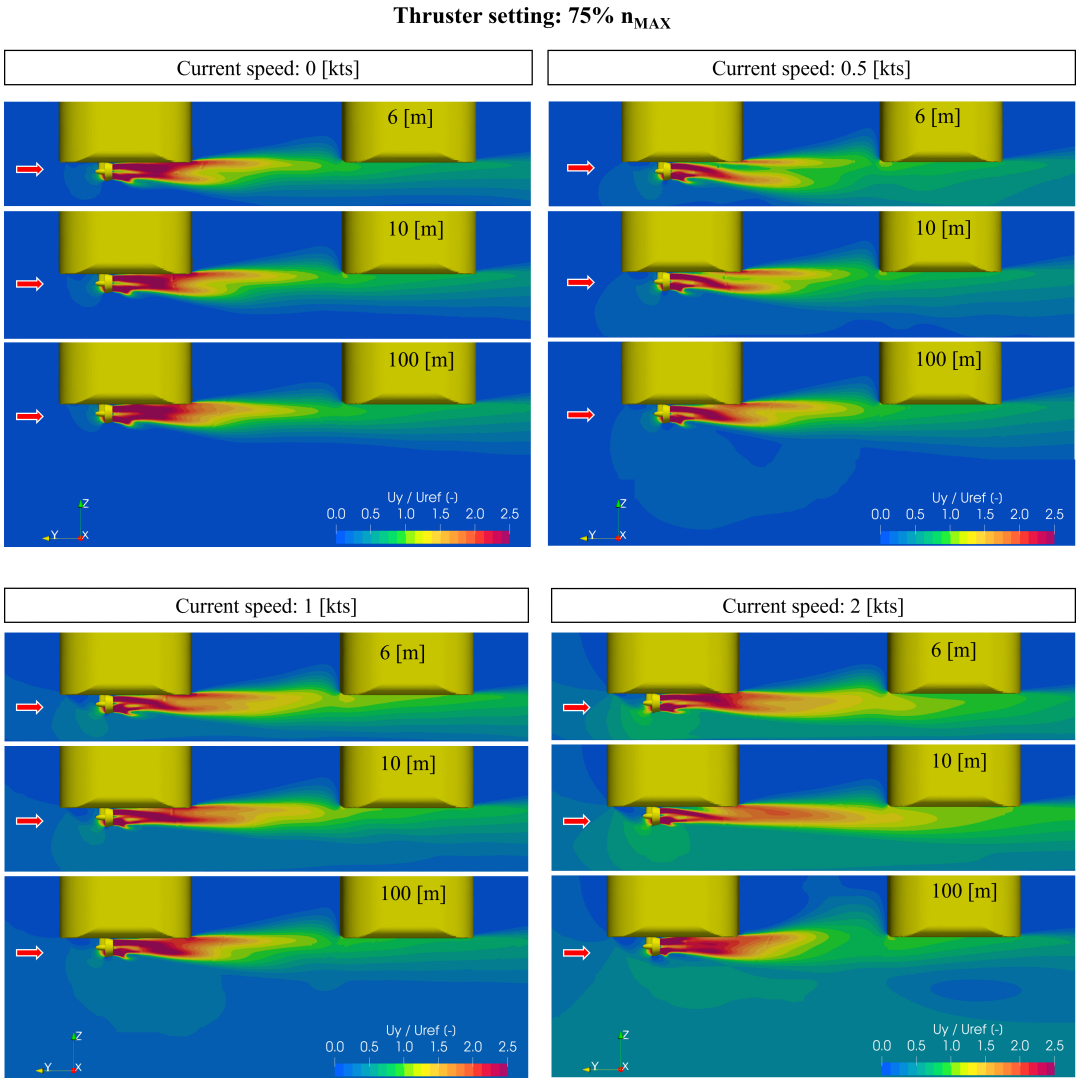

Figure 5.6: y-axis velocity field beneath the hull with 4 different current conditions (0, 0.5, 1, 2 knots) and 3 under-thruster clearance (6, 10, 100 meters) at 75% of the maximum thruster rotational speed (n_{MAX}). Non dimensional velocity U_y. The current direction is indicated through a red arrow.

Similar observations to what has been described for the case at 50% of the maximum thruster rotational speed n_{MAX}, can be made for the 75% of n_{MAX}. The main difference between the two cases is the higher measured velocities due to the higher outflow velocity produced by the thruster at its higher rotational speed. The observed trends presented in Figure 5.1 are also observed in the flow field representation of Figure 5.6.

Nonetheless, the accuracy of the chosen steady-state numerical solver can be identified by the obtained standard deviation of the measured quantities. As seen in Figure 5.1, the standard deviation for each data point increases with higher current speed, reaching values comparable to the mean values when the current speed is equal to 2 knots at 50% of n_{MAX}. Based on the available literature, some hypotheses have been developed about this aspect and will be further explained in Section 5.4.

In conclusion, the main effects of varying under-thruster clearance, combined with variable current speed are:

- Higher flow velocity further from the thruster leads to higher induced frictional resistance.
- Partially increase the flow deviation toward the opposite pontoon, a higher Coandă effect.

In conclusion, the main objective of this investigation confirms that there is a reduction in the effective thrust delivered to the vessel when the thruster is operating in proximity to the seabed. This inefficiency increases with the increasing value of the current speed.

Thruster efficiency VS Current speed

Figure 5.1 shows the obtained thruster-hull coefficient at fixed current speed and variable under-thruster clearance. To further discuss the effect of the current on the thruster interaction, the same results are presented from a different perspective: the thruster-hull efficiency coefficient (C_{TH}) is plotted against the current speed at a constant under-thruster clearance in Figure 5.7.

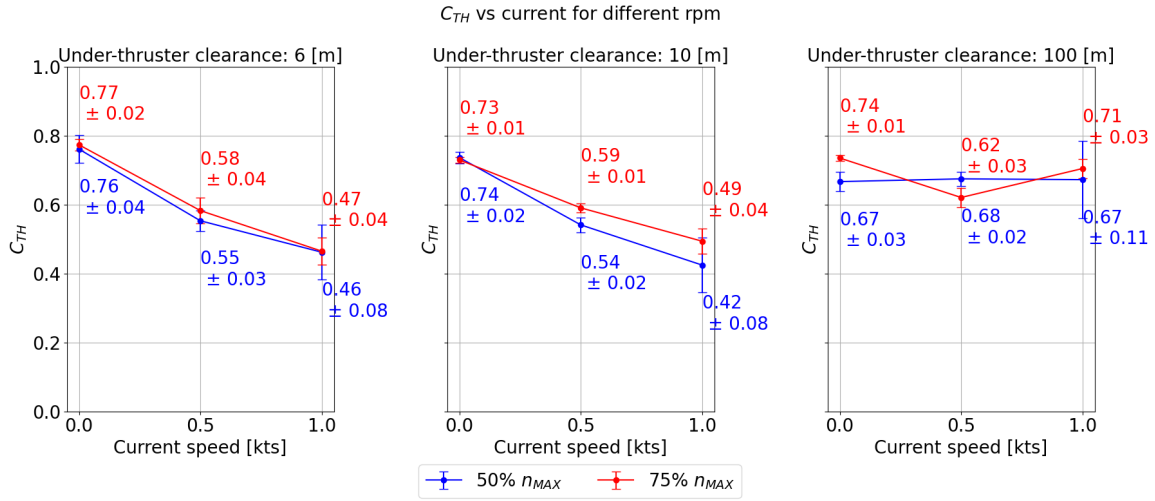

Figure 5.7: thruster-hull efficiency coefficient C_{TH} VS Current speed at 2 different thruster setting conditions (50% and 75% of n_{MAX}) with associated standard deviation.

Only the results characterized by standard deviations much lower than the associated values (up to 1 knot) are presented to ensure a clearer understanding of the captured phenomena. This decision was made due to the high uncertainty observed for the 2-knot current speed case.

It has been observed that the current has a negative effect on the delivered thrust, leading to a reduction in the thruster efficiency, defined as C_{TH}. Figure 5.7 illustrates how an increase in current speed affects the coefficient at a fixed under-thruster-clearance. A similar trend in C_{TH} is observed under shallow water conditions (6 and 10 meters), while a different scenario has been observed in the case of deep water (100 meters). Specifically, for a 6 meters under-thruster-clearance, the percentage difference in C_{TH} between 0 knot and 1 knot of current is 39% for thruster settings of 50% and 75% of n_{MAX}. Conversely, in the case of deep water (100 meters under-thruster-clearance), the measured difference is null for 50% of n_{MAX} and 4% for 75% of n_{MAX}. This observed behaviour suggests that the effect of a free-stream current on a station-keeping vessel reduces the effectively delivered thrust, which is more pronounced when the under-thruster clearance is reduced. Conversely, it is less evident for the deep water scenario.

5.1.1. Inflow velocity impact on thruster performance

The discussion about the thruster-hull efficiency coefficient highlights the relevance of the recirculation zone downstream of the round bilge of the upstream floater, characterized by low-velocity values. This aspect leads to the need for further investigation into the effect of this low-velocity region on the performance of the thruster, as it plays a major role on the provided thrust.

To investigate this aspect of the thruster-hull interaction, the thruster-hull efficiency coefficient C_{TH} has been accordingly modified into $C_{TH,unit}$. In particular, the considered ratio is, in this case, between the measured force ($F_{y,unit}$) on the thruster unit (nozzle, propeller, and gearbox) obtained through pressure integration and the open water thrust (T_{OW}).

$$C_{TH,unit} = \frac{F_{y,unit}}{T_{OW}} \tag{5.1}$$

Only the upstream interaction with the hull is taken into account through the redefinition of the thruster-hull efficiency coefficient. The flow field in this region is modified due to the hull shape, which translates into the variation of the inflow velocity at the thruster location. The measured force consists of the sum of friction force and provided thrust on the thruster unit. Therefore, estimating the eventual loss due to the current induced inflow velocity combined with the effect of reduced under-thruster clearance is possible. Results are presented in Figure 5.8.

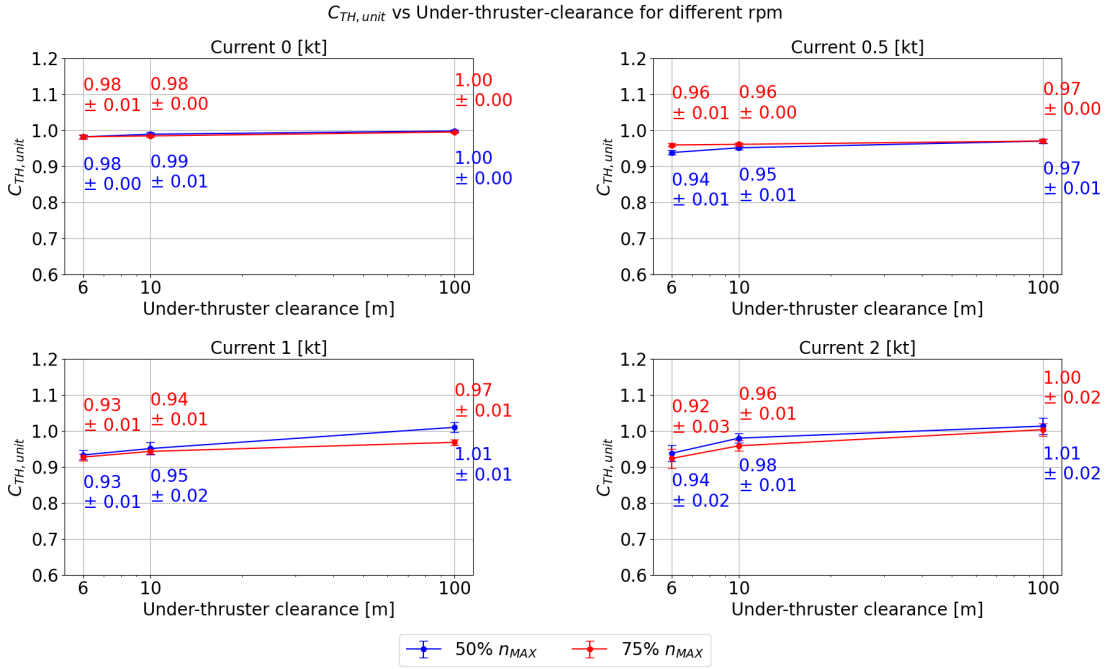

Figure 5.8: Inflow velocity effect investigation. Comparison of thruster-hull efficiency coefficient $C_{TH,unit}$ with respect to the y-axis between Open water and beneath the hull conditions.

Figure 5.8 illustrates how reduced under-thruster clearance impacts up to 7% on the thruster's performance. It shows how the effect of increased inflow velocity due to the current on the thruster is affected by the presence of the hull, which creates a recirculation zone downstream of the round bilge. In the recirculation region, the velocity is lower than the current velocity. As shown in Figure 5.8, the main source of thrust loss due to positive inflow velocity at the thruster location is the reduction of the under-thruster clearance. In the reduced under-thruster clearance scenario, the recirculation area with lower velocity is less vertically developed and more attached to the bottom of the hull. Therefore, the average inflow velocity at the thruster is higher than in the deep water case, wherein the flow is not constrained by both the hull and the seabed, leading to a more expanded low-velocity region. This aspect is visually shown in Figure 5.9.

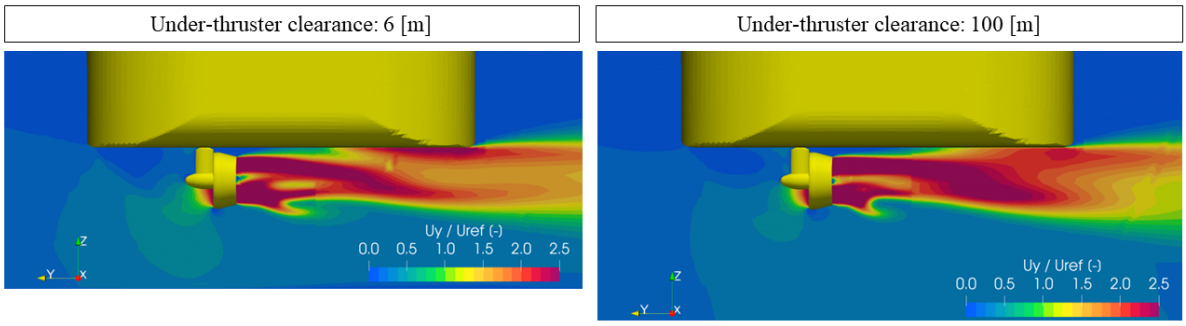

Figure 5.9: Flow velocity details at the thruster: thruster set at 75% of n_{MAX} with a current speed of 1 knot. Focus on the higher inflow velocity to the thruster at 6 meters under the thruster clearance compared to deep water (100 meters).

In the context of the previous results, including the thrust losses due to the entire hull, the obtained results show that the positive inflow velocity only contributes marginally to the overall reduction of thruster performance. The obtained value demonstrates that the low-velocity region below the hull influences the thrust performance, reducing the effective thrust by a maximum of 7%. TThe comparison with the total thruster-hull efficiency coefficient (C_{TH}) where a total thrust reduction of 53% has been measured indicates that the interaction between the outflow jet stream and the hull is more significant compared to the sole effect of the inflow velocity due to the current. It should be noted that a different thruster position could yield different results.

5.2. Comparison with estimated thrust reduction ratio

Following the discussion of the results obtained from the CFD simulations and the conclusions derived from their analysis, it is relevant to compare the results obtained with the estimations carried out before performing the numerical simulations. Indeed, the assessment of the simulation characteristics has been based on the results obtained considering the analytical results and the *ABS Guidelines* [2]. Specifically, the investigated types of interaction consist of the thruster hull and thruster current interactions, as well as their combination.

The reduction ratio obtained in Chapter 3 is defined as:

$$t = \frac{T}{T_{OW}} \tag{5.2}$$

Similarly, the thruster-hull coefficient C_{TH} and $C_{TH,unit}$ are defined as described in Equation 4.19 and 5.1 respectively. The obtained ratio from both cases was reduced to the ratio between the delivered thrust and the open water condition thrust. Therefore, the comparison between the estimated and calculated values is provided below.

As described in Chapter 3, for the case of current interaction due to positive inflow velocity at the thruster, two different approaches has been used to estiamte the thrust reduction ratio: analytical calculations and the predictions as defined by the guidelines from *ABS* [2].

Figure 5.10 compares the results obtained with CFD and the analytical solutions. In particular, the thrust reduction coefficient obtained from CFD refers to the ratio between the measured forces on the thruster unit beneath the hull and the same thruster unit in open-water conditions. Two different rotational speed (n) are used (50% and 75% of n_{MAX}).

Figure 5.10 shows that the approach used of a 2D flow analyzed through the continuity equation overestimated the thrust reduction. Specifically, increasing the current speed led to a larger difference between the data derived from CFD and the estimated results.

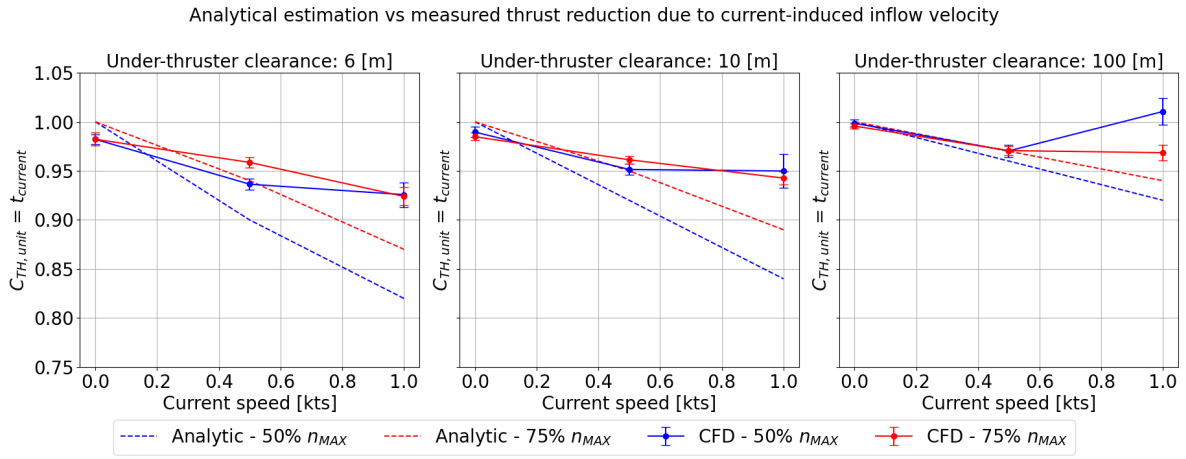

Figure 5.10: Comparison of analytical and simulation results: Thrust reduction ratio due to inflow velocity on the thruster.

In particular, the analytical estimation did not consider the effect of the hull and the recirculation region downstream of the round bilge. This phenomenon plays a fundamental role in defining the inflow velocity at the thruster, which results in a lower mean inflow velocity in the CFD simulation than the one analytically obtained. The maximum registered percentage difference in the thruster-hull efficiency coefficient between the analytical solution and the CFD result is 28.9%, obtained for the lowest under-thruster clearance of 6 meters. Similar results have been obtained for 10 meters, leading to the conclusion that the applied analytical approach provides a remarkable overestimation of the thrust reduction due to positive inflow velocity when the thruster is operating in proximity to the seabed. The detailed percentage differences are provided in AppendixA.1.

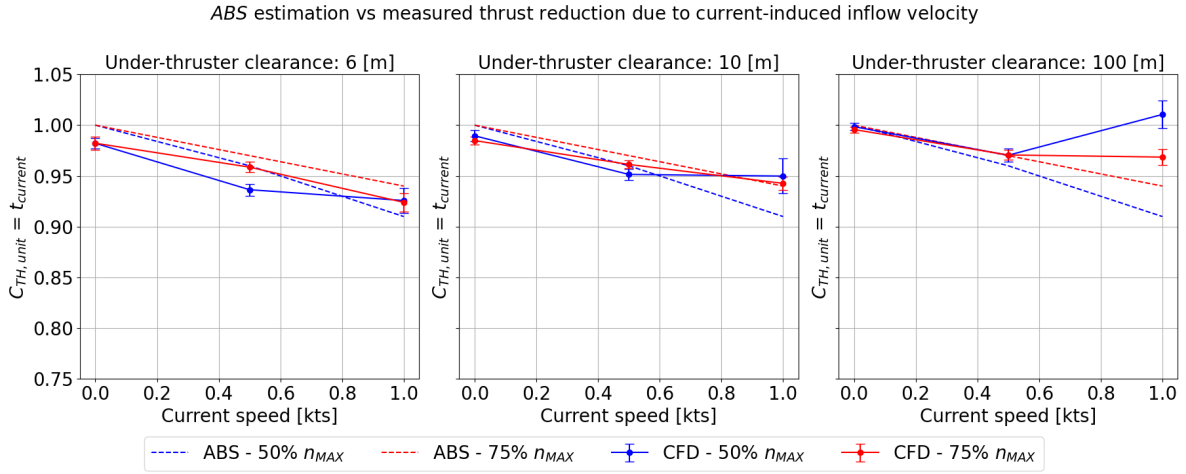

Figure 5.11: Comparison of *ABS* and simulation results: Thrust reduction ratio due to inflow velocity on the thruster.

In Figure 5.11, the effect of inflow velocity on the thrust reduction ratio is shown by comparing the estimation provided by *ABS* [2] to the measured data in the numerical simulations. It's important to note that the *ABS Guideline* [2] doesn't relate the thrust reduction ratio to the under-thruster clearance but only to the propeller-delivered thrust, specifically the disc area load (see Equation 3.8). Therefore, the estimated thrust reduction ratio is constant regardless of the under-thruster clearance. Despite this aspect, the results agree with the thrust reduction ratio obtained from the CFD simulations, even with high current values (1 knot). However, in the case of 100 meters under-thruster clearance, considered deep water, the thruster-current interaction is overestimated at 1 knot of current speed.

This leads to the conclusion that despite being designed for deep water, the *ABS Guidelines* also provides an acceptable estimation for the thruster-current interaction due to the positive inflow velocity in shallow

water scenarios. However, this approach is not conservative, as in the case of 6 meters under-thruster clearance, a minimal overestimation is obtained compared to the CFD data. In contrast, for the case where this relation should be employed, 100 meters under-thruster clearance or deep water, the ABS formulation overestimates by approximately 9.5% the values obtained through numerical simulations. Appendix A.1 provides the detailed percentage differences.

In conclusion, the evaluation of the thrust reduction ratio due to the combination of thruster-hull and thruster-current interaction is obtained as follows.

$$t_{current+hull} = t_{current} \cdot t_{hull} \tag{5.3}$$

Regarding the thruster-hull efficiency coefficient (t_{hull}), it is important to mention that the obtained results only refer to the calculation performed in accordance with *ABS Guidelines* [2], and it is a constant value $t_{hull} = 0.44$. Results presented in Figure 5.12 refer to the thrust reduction ratios obtained following the *ABS Guidelines* both for the estimation of thruster-hull interaction and thruster-current interactions.

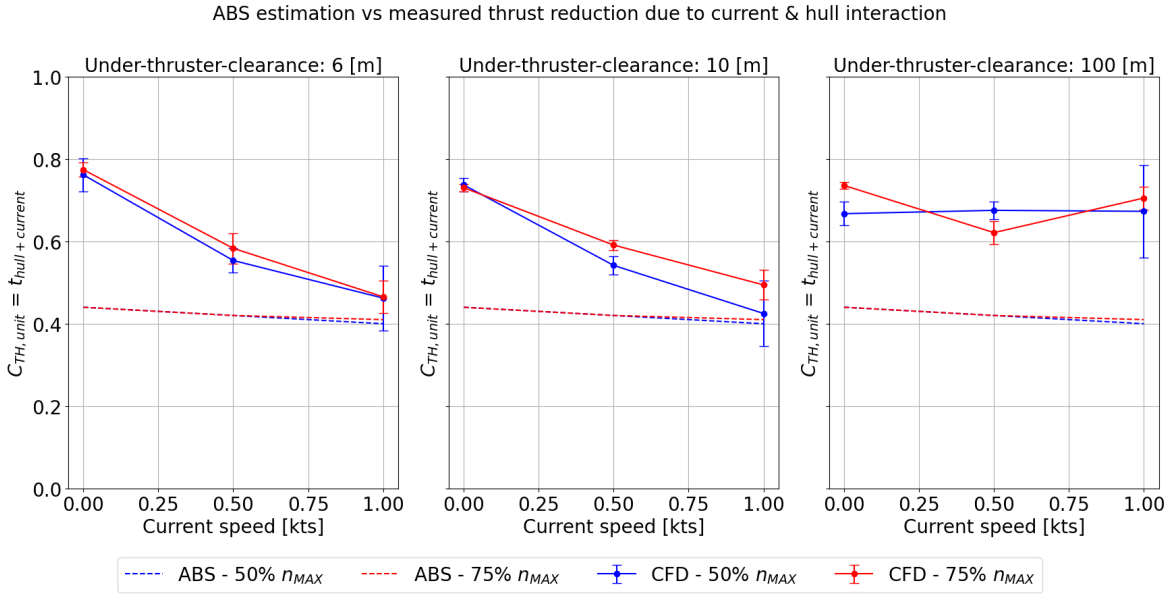

Figure 5.12: Comparison of analytical and simulation results: Thrust reduction ratio of the combined effects of current and hull.

In Figure 5.12, it is shown that the predicted values are overestimated compared to the mean thrust reduction ratios obtained from CFD analysis. The highest overestimation occurs in the deepwater case, for which the prediction formulas were developed. In this case, the highest percentage difference is of 46% when the thruster is set to 75% of n_{MAX}. When the under-thruster clearance is reduced to 6 meters or 10 meters, the trend of the thrust reduction ratio obtained from CFD calculations decreases with the current. In these cases, the prediction provided by *ABS* still results in overprediction of thrust loss, therefore lower t_{c+h}. However, the percentage difference between CFD and *ABS* prediction reduces to 18% when considering the combination of an under-thruster clearance of 6 meters and a current of 1 knot.

The presented results shows that the estimated thruster-hull interaction (t_{hull}) affects the overall thrust reduction ratio ($t_{current+hull}$) the most. The lowest thrust reduction ratio due to current consists of $t_{current} = 0.91$, while the thruster-hull interaction impact for $t_{hull} = 0.44$. Furthermore, among the different components of the thruster-hull interaction reduction ratio, the most impacting is the reduction of the effective thrust due to the blockage effect (t_p) as shown in Table 3.3. Its estimation only depends on the distance between floaters while neglecting the position of the thruster, its delivered thrust, and the hull shape, which all have been proven to be important components in the determination of the thrust loss due to the interaction between the thruster and the hull. Therefore, it can be concluded that the suggested estimation leads to a largely overpredictive value for the thruster-hull interaction effect.

5.3. Impact of geometrical variations on thruster's interactions

The second part of the present project involves the evaluation of the influence of two geometrical parameters (floaters' distance and thruster position beneath the hull) on the flow development, as already explained in Chapter 4. The investigated conditions consist of a fixed thruster speed setting equal to 75% n_{MAX} and a constant beam-side current of 2 knots. Please keep in mind the following text: Figure 5.13 shows the considered geometrical variations. The investigation of scenarios, with a particular focus on the 2 knots of current, has been performed as the last step of this thesis. Therefore, the obtained results are subject to the limitations of using the chosen numerical solution approach in combination with high current values. These limitations have been partially introduced in the previous section and will be further discussed in this section and Section 5.4."

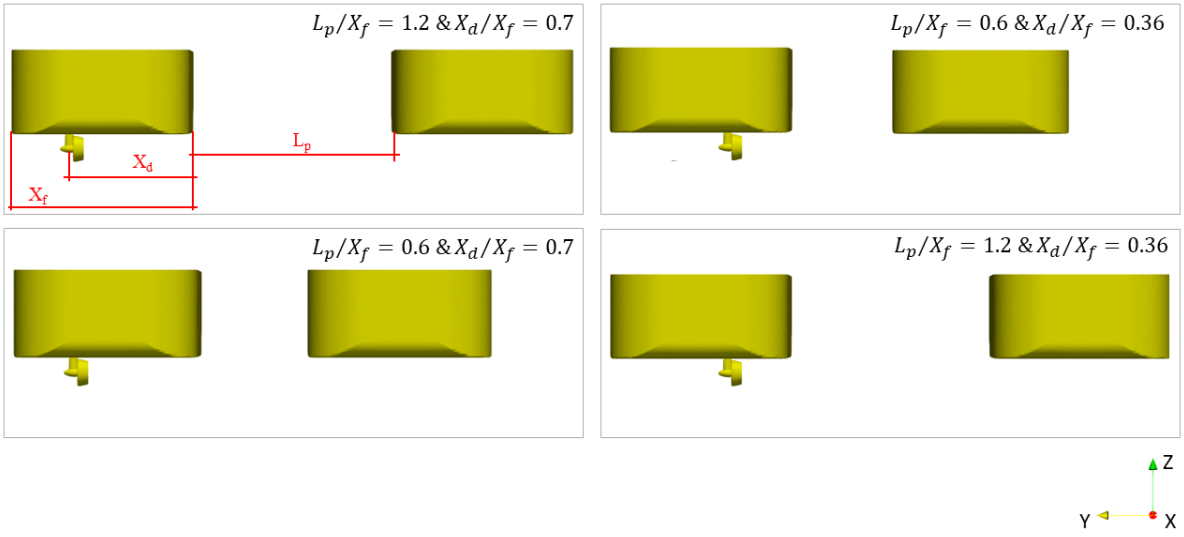

Figure 5.13: Hull and thruster models for studying the variations in thruster-hull interaction with different geometrical configurations.

The obtained results are provided in terms of obtained effective thrust (T_y) and thruster-hull coefficient (C_{TH}) illustrated in Figure 5.14

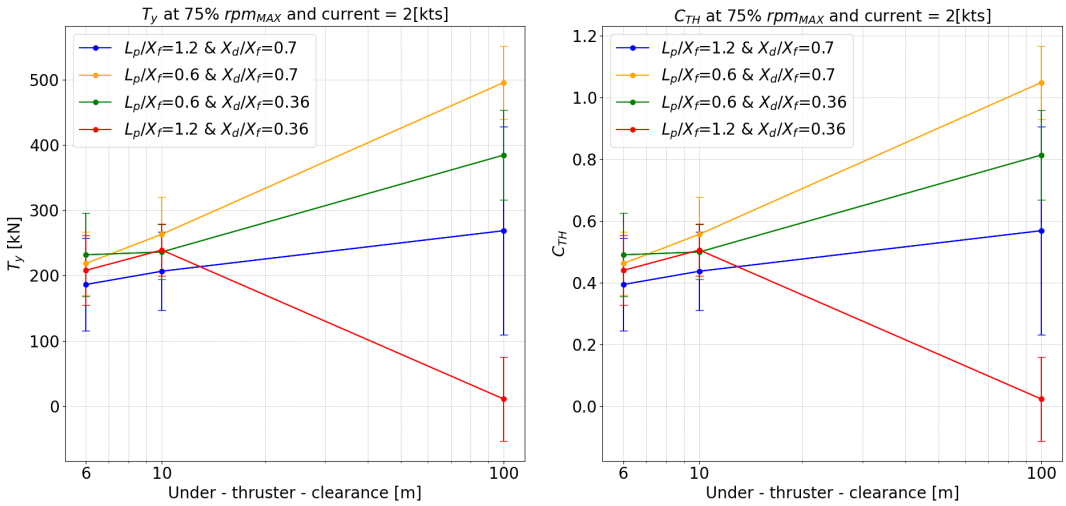

Figure 5.14: Impact of variation in the thruster position beneath the hull and the distance between floaters.

The first plotted in Figure 5.14 shows that closer floaters (orange line) and a thruster position closer to the round bilge of the hull (green line) result in higher performance and a higher thruster-hull efficiency coefficient. However, unexpected behaviour is observed in the case of the thruster position near the

round bilge (red line). Hnces, it is important to analyze the different scenarios from a physical standpoint. Therefore, similar plots to the one proposed in the base case (blue line, $L_P/X_f = 1.2 \quad X_d/X_f = 1.3$) must be analyzed. Figure 5.15, 5.16 and 5.17 presents the flow field directed along the y-axis in correspondence with the section located at the thruster x-coordinate.

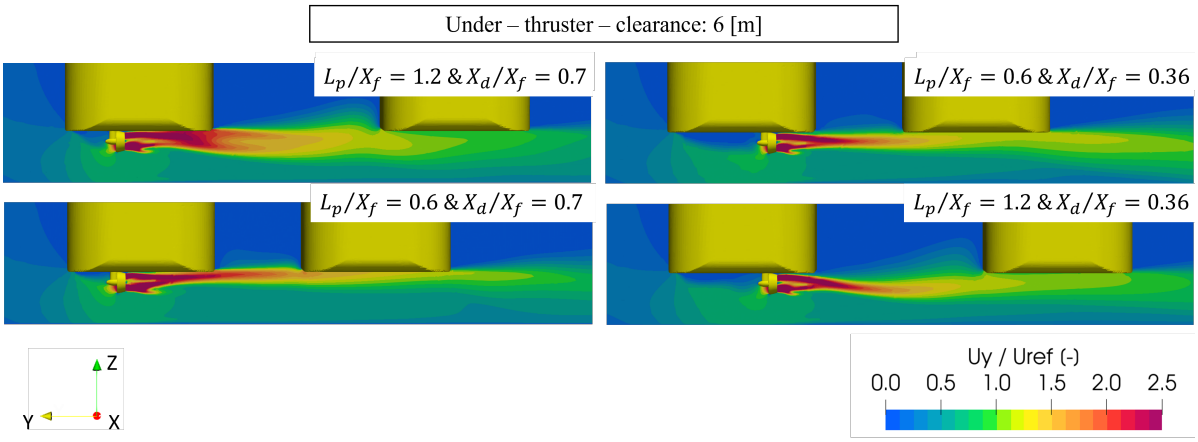

Figure 5.15: Flow field at 6 meters under thruster clearance condition. 2 knots current speed, 75% n_{MAX}

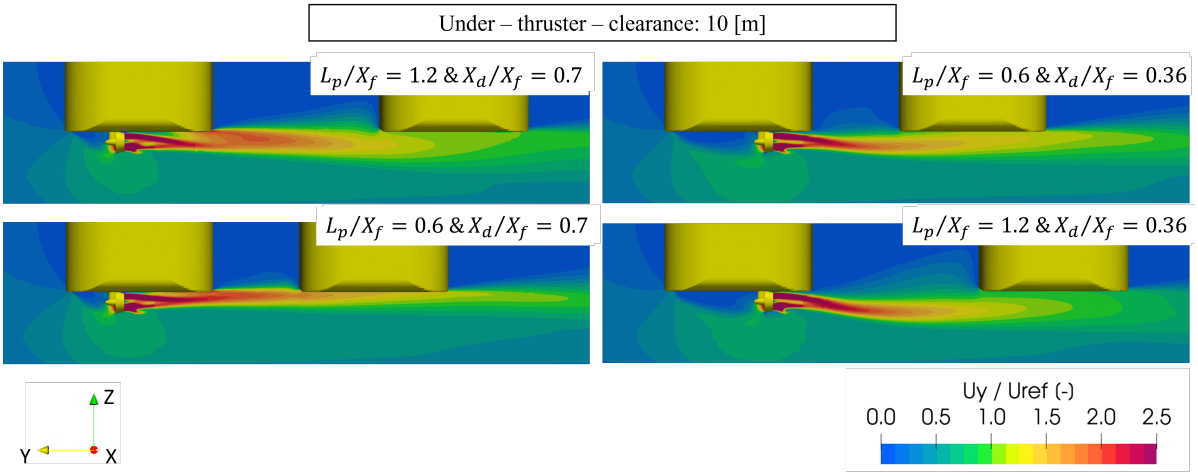

Figure 5.16: Flow field at 10 meters under thruster clearance condition. 2 knots current speed, 75% n_{MAX}

All the illustrated flow fields refer to a case of 2 knots of current and 75% of n_{MAX} thruster setting. The first observation that could be made concerns two cases. specifically, the cases with the thruster position equal to $X_d/X_f = 0.36$, where the thruster position is closer to the round bilge. The obtained flows deviates towards the seabed to a great extent compared to previous results and the expected flow field observed in the literature. This happens for all cases where the thruster is located close to the round bilge, leading to the conclusion that these simulations could be subject to some errors. In particular, a possible explanation for the inconsistent results is that the flow field is not correctly resolved due to the too-coarse definition of the mesh in the round bilge region. When the thruster is located closer to the round bilge, it is expected that in that region, the flow velocity will be higher compared to the case of $X_d/X_f = 0.7$; therefore, the used refinement could be insufficient to solve the motion equation properly, leading to unreliable results confirmed by the flow field visualization.

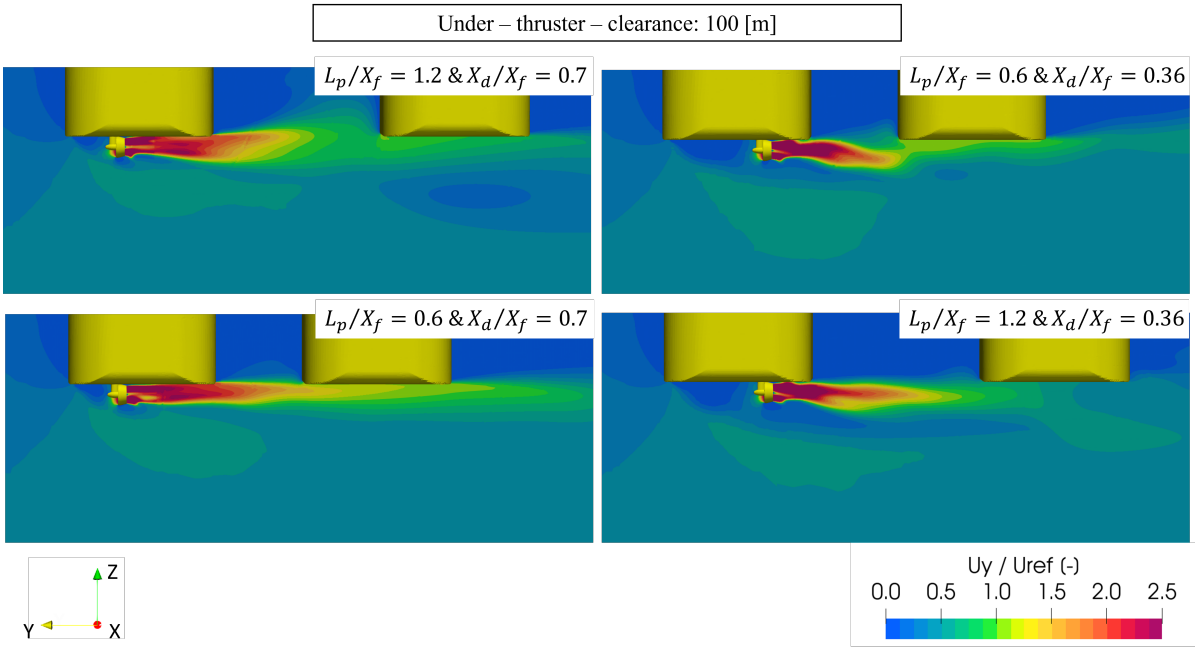

Figure 5.17: Flow field at 100 meters under thruster clearance condition. 2 knots current speed, 75% n_{MAX}

However, focusing on the case with the thruster position equal to $X_d/X_f = 0.7$, the flow field developed as expected, attaching to the hull surface and deviating due to the Cŏanda effect in correspondence with the round bilge. Therefore, comparing these cases, in regards to the difference between the variable distance of the floater, it can be noticed that the flow deviates toward positive z-coordinates in the case of $L_p/X_f = 1.2$ compared with $L_p/X_f = 0.6$. It is possible to appreciate how the distance between floaters predominantly contributes to the thrust reduction due to the impinging jet of the thruster. Nonetheless, when the floaters are located at the farthest distance, it is more evident that the flow deviates towards the downstream pontoon due to the defined phenomena of the Cŏanda effect. Such a difference can also be identified by comparing the pressure distribution as presented in Figure 5.18.

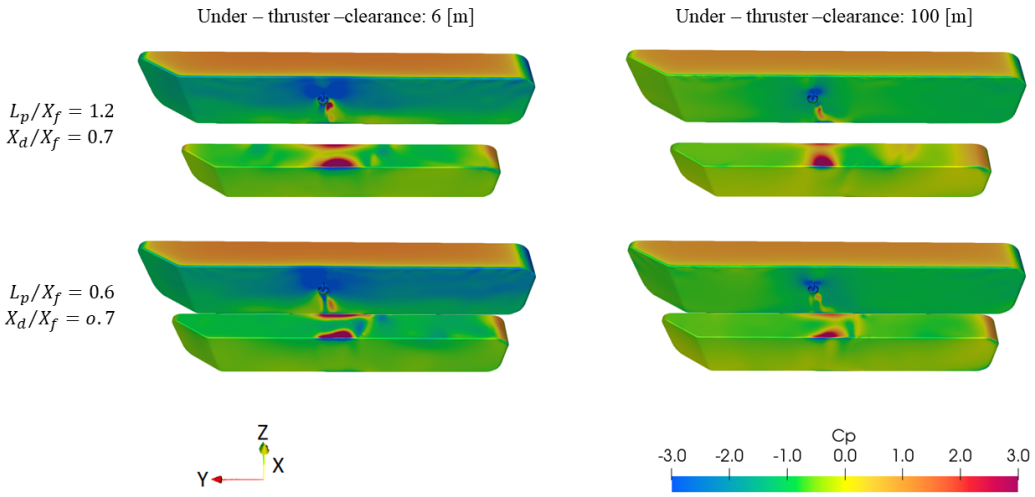

Figure 5.18: Pressure distribution on the hull with the variation of the geometrical characteristics of the thruster position and floaters' distance. Difference between 6 meters and 100 meters under-thruster clearance at 2 knots beam-side current.

The pressure fields in Figure 5.18 confirm the discussed aspect of the position of the downstream floater. It is relevant to highlight the less extended high-pressure area on the downstream pontoon when the floaters are closer to each other ($L_p/X_f = 0.6$). Furthermore, as previously described, it is possible to observe that with reduced under-thruster clearance, the pressure coefficients on the downstream pontoon present higher values than the deep water case. This shows a greater deviation of the thruster jet.

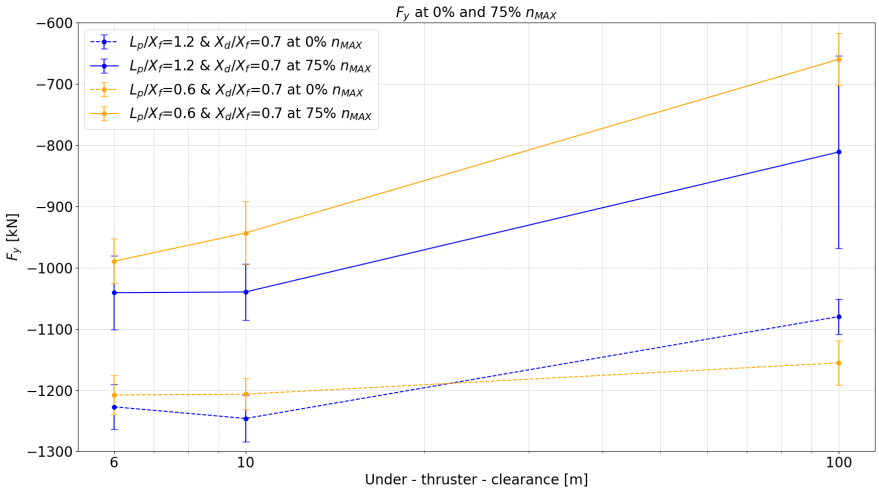

Figure 5.19: Measured force on the hull at 0% and 75% of n_{MAX} for two difference geometrical setup ($L_p/X_f = 0.6$ and $L_p/X_f = 0.7$).

In conclusion, the relevant results obtained from this study focus on the floater distance rather than the thruster position, which requires a finer mesh to model the high velocities in the area of interest. Therefore, it is possible to conclude that the closer floaters present a reduction of thruster-hull interaction. In particular, at 6 meters under-thruster clearance, a measured reduction of 17% in the delivered force when floaters are further ($L_p/X_f = 1.2$ and $L_p/X_f = 0.7$) than the closer position ($L_p/X_f = 0.6$ and $L_p/X_f = 0.7$)

An observation of the obtained results is necessary. A significantly higher increase in difference is observed for the deep water case (100 meters under-thruster clearance). This aspect is visually presented in Figure 5.14. Therefore, a hypothesis could be derived for the possible discrepancy in the obtained value by observing the data plotted in Figure 5.19. The high difference between the two cases, related to different mesh and CFD runs, could be related to the reasons already introduced for the base case at 2 knots of current. Indeed, the magnitude of the obtained force F_y is consistent with the calculated delivered thrust T_y. This emphasizes an important factor when processing data from different simulations: the derived thrust is obtained as a subtraction of two high-number values from a much smaller value, making the derived value more susceptible to uncertainties and errors in each simulation.

Furthermore, the obtained results, specifically in the deep water conditions and thruster setting of 75% n_{MAX}, significant standard deviation is measured, leading to the conclusion that significant oscillations affect the measured force and introduce additional uncertainty to the results. The behaviour will be presented and discussed in the next Section (5.4).

The combination of the previously described aspects does not allow for a clear and reliable conclusion on the thruster's position. In addition, the results obtained regarding the floater's position are not precise enough to give confidence in the obtained values. Therefore, only qualitative conclusions can be made to indicate the expected variations in the delivered forces. It should also be mentioned that the derived conclusions are related to the specific case study, specifically the condition of beam-on current with no forward speed. The beneficial aspect of having a closer thruster cannot be generalized to the entire range of floater distances. The focus of the study was to investigate the impact of reducing thruster clearance at two floater positions instead of focusing on evaluating the thruster-hull efficiency coefficient for a wide range of floater distances.

5.4. Analysis of unsteady behaviours in simulations results

As mentioned in the previous sections, certain simulations displayed a significantly high standard deviation value in the last 1500 iterations. Figure 5.20 illustrates an example of this behaviour, showing the difference in the iteration traces between a case with a low standard deviation and a more oscillating result. This section aims to carry out a more detailed investigation into these phenomena.

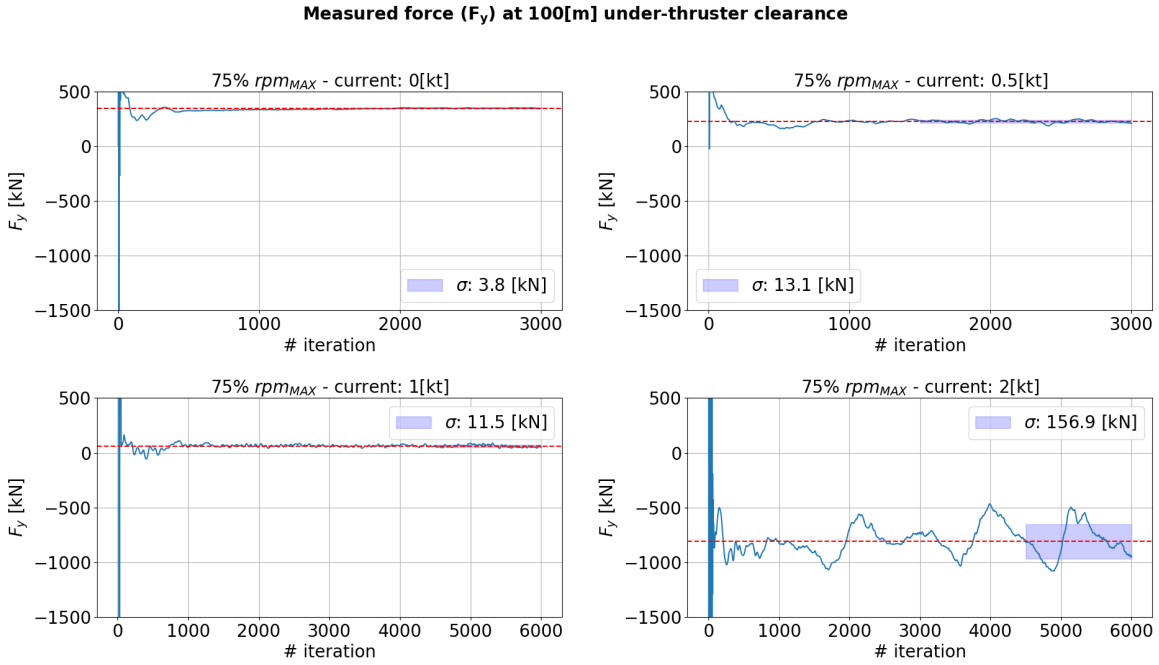

Figure 5.20: Unsteady behaviour of the iteration trace for 100 meters under-thruster clearance scenario and thruster setting at 75% of n_{MAX} with Variable current speed (0,0.5,1,2 knots).

In a CFD simulation, a steady state is considered when all flow characteristics, such as velocity and pressure, are constant. Constant means that the flow characteristics of the current time step do not differ from those of the previous and will not change for any further time. One way to detect transient effects in a steady-state analysis is to check for either transient residuals or transient results of a result control item. For instance, when surface pressure force is not converging to one solution but rather oscillating, it suggests that transient behaviour is occurring. Therefore, the simulation should be checked for a transient solution step [54].

The described scenario can be observed in Figure 5.20, where an increase in current speed leads to oscillating results of the parameter of interest (F_y) around the mean value. This phenomenon can be noted considering the measured standard deviation, which increases with higher current. In particular, the standard deviation (σ) shows a negligible value without current. On the contrary, it presents similar values for the cases of 0.5 and 1 knot of current, highlighting the appearance of a certain instability in the obtained results. This unstable behaviour notably increases in the case of a 2 knots beam-side current. The presented case involves the under-thruster clearance simulation of 100 meters, which is the most representative of flow variation.

Furthermore, it is valuable to introduce the problem from a physical standpoint. As mentioned in the previous line, a steady-state simulation assumes a constant value in the force and, therefore, a constant flow field without velocity and pressure gradients. To better comprehend the phenomena of interest, it is valuable to simplify the case by considering the benchmark case of a backwards-facing step where similar phenomena occur. Specifically, the dynamics of the low-pressure region behind the step, where the flow alternatively separates and reattaches, leads to the generation of vortices. This phenomenon is the so-called vortex shedding and could be defined as follows [15]:

"Vortex shedding refers to the formation of vortices due to vortex flow in the wake region behind the body across which the flow is occurring"

Similar to the backwards-facing step, the case of a semi-submersible vessel involves a bluff body immersed in a constant free-stream current, leading to the generation of downstream vortex shedding and, therefore, oscillation of the forces on the vessel. The occurrence of these factors depends on the flow speed. As shown in Figure 5.20, higher flow speeds result in greater instability. Specifically, higher forces are linked to higher flow speeds, making the oscillations more pronounced in these conditions. Conversely, the oscillations for lower flow speeds are less noticeable in the obtained forces. In the specific case of a bluff body immersed in a free-flow stream (beam-current), an additional aspect to take into account is the ratio between the vessel length and the vessel width. When the ratio is intermediate, as in the case of the considered hull of the vessel (0.23) as stated by *Nakagawa* [42], strong vortices are shaped behind a rectangular prism caused by the interaction between the separating shear layers and the side surface.

In conclusion, the hypothesis about the high standard deviation due to the oscillation of the measured force has been attributed to the approximation made on the steadiness of the flow downstream in the simulation, which is almost totally respected in the case of 0-knot current, while it presents as a dominant factor for the case of 2 knots.

Therefore, when vortex shedding is happening, and vortices are periodically shed from the vessel hull, the flow is inherently unsteady, concluding that the RANS approach may not be precise enough. It is, however, fundamental to conduct an appropriate post-processing study to derive such conclusions. The suggestion for future work lies in the necessity to evaluate the same problem from an unsteady perspective through URANS simulation, for instance, with the scope of evaluating the time trace of the force and further visualizing the impact of vortices.

5.5. Practical implication on the operability of a SSCV

The following practical approach describes the measured changes in the delivered thrust. A comparison between the DP system's thrust reduction value and the values obtained from the numerical simulation is proposed. Since this thesis focuses on the operational aspect, the approach aims to identify the variation in the thrust reduction ratio at a fixd under-thruster clearance and variable current speed. Figure 5.21 shows the thruster-hull efficiency coefficient as a function of the current speed.

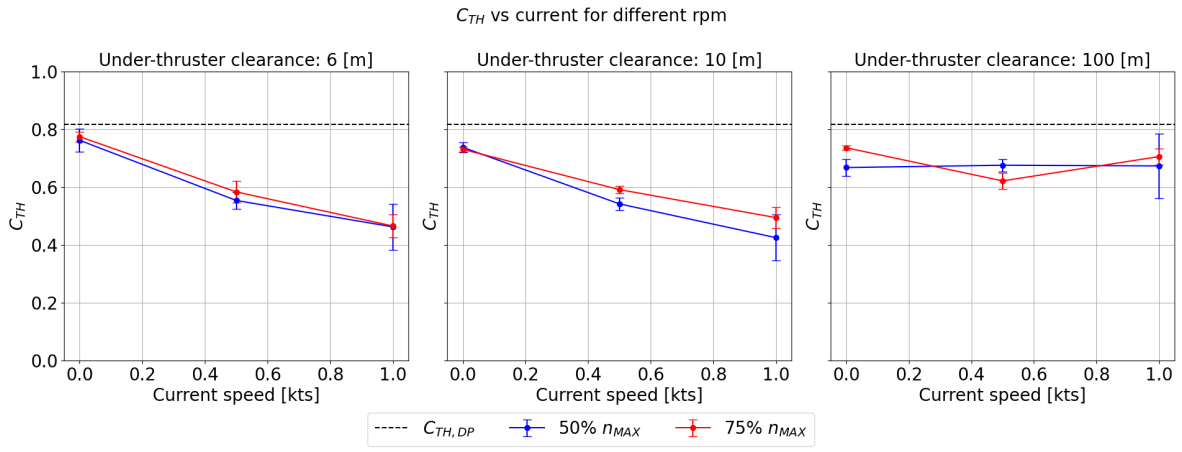

Figure 5.21: Comparison of thruster coefficient in the DP system with the measured reduction with CFD calculation. C_{TH} vs current speed at three under-thruster clearances (6, 10, 100 meters)

The comparison provided in Figure 5.21 assumes that the DP system does not measure the inflow velocity at the thruster. Instead, it relies only on the vessel's velocity, which is null or close to 0 during stationkeeping.

The DP system is set to consider the thruster operating in advance ratio $J = 0$ condition (0 m/s inflow velocity at the thruster) and applies a constant coefficient to the delivered thrust to consider thruster-hull interactions. However, when the current is present, the inflow velocity on the thruster due to the current is not considered and is therefore not accounted for in the DP current. Furthermore, no reductions are applied to account for the reduced under-thruster clearance.

CFD simulation demonstrates that the combination of current and thruster-hull interaction significantly reduces the delivered thrust, resulting in a greater reduction than previously estimated. With a clearance of 6 meters beneath the thruster and a 1-knot beam-side current speed, the measured thrust reduction ratio is 40% lower than the ratio used by the DP system to estimate delivered thrust. Conversely, a minimal difference is measured in no-current conditions. Similar observations can be made with 10 meters of under-thruster clearance. However, in deep water, the estimated thrust reduction coefficient's percentage difference with the DP system's valuer ranges from 10% to 17% and does not show a decreasing trend with varying current speeds. This indicates that in deep water, the thrust reduction ratio remains relatively unaffected by changing current speeds, unlike in shallow water scenarios.

A possible explanation for this difference lies in the definition of the thrust coefficient for the thruster's modelling. The thrust reduction ratio does not vary per thruster. This means that in this model, both upstream and downstream thrusters are taken into account. Based on the literature research conclusions, it could be expected that the upstream thruster experiences a higher reduction in the delivered thrust because of the blockage effect compared to the downstream case, therefore the obtained thrust coefficient presents an average thrust reduction coefficient, while the focus of the case investigated in the present thesis only relies on the upstream thruster.

6

Conclusion and recommendations

The final chapter presents the work's conclusion, provides the findings, answers the research question, and indicates the future direction based on the lessons learned.

Closing remarks
The research question for the present study focused on investigating the effect of reduced under-keel clearance on thrust loss. In particular, it aims to define and develop a trend for predicting this parameter through numerical simulations and comparing them with the characteristics of thruster interactions available in the literature and the prediction provided by the classification society (*ABS*). The study aimed to provide a solid background in which interactions between the thruster and the external factors (geometrical and environmental) cause a reduction in the effective thrust delivered to the vessel during DP operation. Initially, a simplified analytical estimation was used along with the results and formulations provided in the guidelines of the classification society [2]. Later, 53 numerical simulations were conducted to determine the thrust reduction when reducing under-thrust clearance in combination with beam-side current. This was obtained using the definition of an interaction coefficient C_{TH} defined in previous chapters.

The initial finding from the research confirms the observation that there is an increase in thrust losses when the thruster operates in close proximity to the seabed. This was reported by the vessel crew, which served as the case study for the research. It has been confirmed that during operations in shallow water and reduced under-keel clearance: at 6 [m] under-thruster clearance and 1 [kt] on beam current, the delivered thrust toward the desired direction is reduced to 47% of the thrusts delivered in open water. This reduction is obtained from the thruster positioned below the upstream pontoon; a higher delivered thrust is expected for the thruster operating on the downstream pontoon as the blockage effect is not present for that thruster position. Compared with the obtained result for the simulated deep water scenario (100 [m] under-thruster clearance), the effective thrust lies between 67% and 74% of the open water thrust. Therefore, there is a relative difference up to 33% in the thrust reduction ratio between shallow and deep water conditions, given the beam-side current condition of 1 knot. Furthermore, it has been observed that when the vessel is not under the influence of any current, the presence of the seabed has a negligible impact on the delivered thrust compared to deep water. Conversely, the reduction impacts the vessel's performance when the current load exists. To address the issue of thrust loss, a tilted thruster gearbox solution has been developed and proven to reduce thruster-hull interaction, as described in the literature. However, this solution results in scouring of the seabed when operating at reduced thruster clearance. This particular aspect has not been investigated in this thesis, but it represents a relevant and additional potential source of thrust reduction that has not been considered.

Moreover, it has been shown that the interaction coefficient values obtained in deep water conditions align with the estimates given by the American Bureau of Shipping (ABS) for assessing thruster-current interaction, especially regarding the impact of positive inflow velocity on the thruster. However, the predicted thrust reduction ratio resulting from the combination of thruster-hull and thruster current interaction overestimates the actual thrust reduction.

In particular, the evaluation of the blockage effect, the most impactful parameter in the thrust reduction ratio due to thruster-hull interaction, is approximate as it is only provided as a function of the centerline floater distance. However, as acknowledged in the literature and demonstrated in the CFD simulations, the parameters to consider also include the hull shape and the thruster position and direction. It confirms that the estimation of thruster-hull interaction requires detailed and case-specific investigations and cannot be entirely generalized.

The last part of the present thesis focuses on modifying geometry. It has confirmed the hypothesis obtained from the literature: the reduction of the space between floaters is beneficial for the thruster's performance in beam-on current conditions, which experiences a reduced loss of thrust for a better capability of maintaining position for the vessel. This confirms the trend and underscores the importance of accounting for the impact of current combined with under-thrust clearance when addressing thruster performance in DP systems. However, it is relevant to mention that due to the high measured uncertainty, the obtained results do not give full confidence in the obtained values of the results. Furthermore, only two positions have been investigated; therefore, a more comprehensive and extended study is suggested to provide a more precise picture of the impact of the floaters' distance.

Recommendations for future work
The conclusions obtained allow for providing remarks about the work's performance and lessons learned during the process.

Regarding the CFD simulation setup, the first aspect that needs improvements consists of testing a more refined mesh grid, which also involves more computational time and cost. However, it would be beneficial to test these more refined geometries to further investigate the deviation of the flow due to the hull's presence. This deviation has already been noticed in the present work. But as highlighted for the high values of current speed, a more refined grid would allow the reduction of the wall function values for more precise modelling of the boundary layer, especially in the area of most interest, which includes the round bilge of the hull. This is mostly relevant for the case of the thruster located close to the round bilge ratio (e.g. $X_d/X_f = 0.6$) due to the higher velocities involved. Such refinement allows for more precise visualization and improves the precision of the measured pressure distribution, therefore providing a more accurate estimation of the forces.

As a second step, with particular relevance for high current values, investigating transient phenomena such as vortices downstream the flow requires a time-domain solution and, therefore, an unsteady approach (URANS). The obtained oscillatory forces request a more precise representation of the flow around the hull, which could only be obtained with a time domain simulation where the time-dependent fluctuations are properly represented.

Nevertheless, future implementations have been identified throughout the process, in addition to exploring the same developed setup with time-domain simulation. While in the actual work, only one thruster beneath the upstream pontoon has been investigated, it is of interest to provide a clearer and more comprehensive picture of the problem by exploring two more scenarios.

- The investigation of 3 or 4 working thrusters beneath the downstream and the upstream pontoon alternatively, to better capture the differences in terms of loss of thrust. It is important to consider the impact of operating thrusters beneath both hulls to better understand how the combination of current and reduced under-keel clearance affects thruster performance when used in close proximity. These simulations will also enable the investigation of the interaction between thrusters, a type of thruster interaction that has not been explored in the present work;
- Secondly, it is important to capture the behaviour of the flow in such conditions for multiple thruster orientations as well as vessel headings with respect to the current.

Numerous studies have been conducted in the literature to investigate various types of thrust interactions when more than one thruster is operating beneath the hull. However, no information has been found regarding how reducing the under-thruster clearance impacts the jet stream developed by the thruster, depending on the different locations of the thruster and when more thrusters operate simultaneously. Therefore, this aspect constitutes a future implementation for the present work.

Final considerations of the applicability of the obtained thrust reduction coefficients based on comparison with existing DP systems are presented. The obtained coefficients apply to the upstream thruster. However, they could result in overestimating the case for the downstream thruster, as the blockage effects of the downstream pontoon are not present. Furthermore, the thruster azimuth angle has not been investigated, nor has the combination of multiple thrusters (thruster-thruster interaction). These two parameters have been identified as governing parameters in the thruster performance, both for the thruster-thruster interaction and the different thruster jet stream development around the hull, leading to different thrust losses. Moreover, the thruster coefficient has been obtained for a single thruster position beneath the hull, which only partially represents the case of a thruster placed at the ends of the ship (aft and bow) where the flow field is expected to deviate from the scenario investigated in the present work.

In conclusion of the present study, it is interesting to look back at the initial motivation behind investigating the impact of thruster interaction derived from the tests conducted in the North Sea. In light of the obtained results and the limitations of the approach used, some lessons have been learned, and it could be useful to provide some suggestions for future offshore tests. Specifically, it is recommended to replicate the numerically simulated scenario in a confined environment where both shallow and deep water are available (e.g. fjord), in which most of the variables that could cause uncertainty can be minimized. Nonetheless, these tests could be used to validate the results obtained from numerical simulations. They could provide further insight into the need for more sophisticated and time-consuming numerical simulations to investigate different hull shapes and thruster locations. Another possible way to validate the results would be to conduct model tests on the same geometry as the one investigated numerically. However, given the identified limitations of the method used, it is suggested that the same geometry be numerically tested with unsteady flow solutions before being validated with model tests.

References

[1] A. B. Aalbers et al. "Developments in Dynamic Positioning Systems for Offshore Stationkeeping and Offloading". In: *Offshore Mechanics and Arctic Engineering Conference (OMAE)*. Copenhagen: Maritime Research Institute Netherlands, MARIN, June 1995.

[2] American Bureau of Shipping. *Guide for Dynamic Positioning Systems 2021*. Tech. rep. 2021, pp. 96–104.

[3] F Arditti and E F G Van Daalen. "An advanced thrust allocation algorithm for DP applications, taking into account interaction effects and physical limitations". In: *International Conference on Offshore Mechanics and Arctic Engineering (OMAE)*. San Francisco, USA: American Society of Mechanical Engineer (ASME), June 2014, V01AT01A009.

[4] Felipe Arditti and Eduardo Aoun Tannuri. "Experimental analysis of a thrust allocation algorithm for DP systems considering the interference between thrusters and thruster-hull". In: *IFAC Proceedings Volumes*. Vol. 9. PART 1. IFAC Secretariat, 2012, pp. 43–48. ISBN: 9783902823601. DOI: 10.3182/20120919-3-IT-2046.00008.

[5] Paolo Blondeaux and Giovanna Vittori. *Note di Meccanica dei Fluidi*. Genova: Genova University Press, Dec. 2019. ISBN: 978-88-94943-92-4.

[6] D T Brown and L Ekstrom. "Vessel Thruster-Thruster Interactions During Azimuthing Operations". In: *International Conference on Offshore Mechanics and Arctic Engineering (OMAE)*. OMAE2005-67500. Halkidiki, Greece: American Society of Mechanical Engineer (ASME), June 2005, pp. 991–996.

[7] Norbert Bulten and Petra Stoltenkamp. "Full scale thruster-hull interaction improvement revealed with CFD analysis". In: *International Conference on Offshore Mechanics and Arctic Engineering (OMAE)*. Nantes, France: American Society of Mechanical Engineers (ASME), June 2013, V009T12A017. DOI: 10.1115/OMAE2013-10435. URL: https://doi.org/10.1115/OMAE2013-10435.

[8] Hans Cozijn and Rink Hallmann. "PIV Measurements in Thruster-interaction Research". In: *Dynamic Positioning Conference*. Houston, USA: Maritime Research Institute Netherlands (MARIN), Oct. 2014.

[9] Hans Cozijn, Rink Hallmann, and Arjen Koop. "Analysis of the Velocities in the Wake of an Azimuthing Thruster THRUSTERS using PIV Measurements and CFD Calculations". In: *Dynamic Positioning Conference*. DYNAMIC POSITIONING CONFERENCE. Huston, USA: Maritime Research Institute Netherlands (MARIN), Oct. 2010.

[10] Hans Cozijn, Jin Woo Choi DSME Seoul, and Korea Young-Jun You DSME Seoul. "THRUSTER-WAVE INTERACTION DURING DP STATIONKEEPING-MODEL TESTS IN OPEN WATER AND UNDER A SHIP HULL". In: *International Conference on Ocean, Offshore and Arctic Engineering (OMAE)*. Trondheim, Norway: American Society of Mechanical Engineer (ASME), June 2017, V001T01A024. DOI: 10.1115/OMAE2017-62168. URL: https://doi.org/10.1115/OMAE2017-62168.

[11] J L Cozijn and R Hallmann. "The Wake Flow Behind Azimuthing Thrusters: Measurements in Open Water, Under a Plate and Under a Barg". In: *International Conference on Offshore Mechanics and Arctic Engineering (OMAE)*. Rio de Janeiro, Brazil: American Society of Mechanical Engineers (ASME), 2012, pp. 485–494. DOI: 10.1115/OMAE2012-83621. URL: https://doi.org/10.1115/OMAE2012-83621.

[12] J L Cozijn and R Hallmann. "Thruster-interaction effects on a DP semi-submersible and a drill-ship measurement and analysis of the thruster wake flow". In: *International Conference on Offshore Mechanics and Arctic Engineering (OMAE)*. Proceedings of the ASME 2013 32nd International Conference on Ocean, Offshore and Arctic Engineering. Nantes, France: American Society of Mechanical Engineer (ASME), June 2013, V001T01A060. DOI: 10.1115/OMAE2013-11138. URL: https://doi.org/10.1115/OMAE2013-11138.

[13] J. L. Cozijn, B. Buchner, and R. R.T. van Dijk. "Hydrodynamic research topics for DP semi submersibles". In: *Annual Offshore Technology Conference*. Vol. 2. Offshore Technol Conf, 1999. DOI: 10.4043/10955-ms.

[14] J Dang and H Laheij. "Hydrodynamics Aspects of Steerable Thrusters Dynamic Positioning Conference". In: *Dynamic Positioning conference*. Houston, USA: Wärtsilä Propulsion Netherlands BV (WPNL), Sept. 2004.

[15] L Dhar P. *Thermal System Design and Simulation*. Academic publisher, 2016, pp. 583–599.

[16] DNV GL. *Dynamic positioning vessel design philosophy guidelines*. Tech. rep. DNV GL, Oct. 2021.

[17] L. Eça and M. Hoekstra. "A procedure for the estimation of the numerical uncertainty of CFD calculations based on grid refinement studies". In: *Journal of Computational Physics* 262 (Apr. 2014), pp. 104–130. ISSN: 10902716. DOI: 10.1016/j.jcp.2014.01.006.

[18] L Ekstrom and D T Brown. "Interactions Between Thrusters Attached to a Vessel Hull". In: *International Conference on Offshore Mechanics and Artic Engineering (OMAE)*. Oslo, Norway: American Society of Mechanical Engineers (ASME), 2002, pp. 825–834. DOI: 10.1115/OMAE2002-28617. URL: https://doi.org/10.1115/OMAE2002-28617.

[19] Odd Magnus Faltinsen. *Sea Loads on Ships and Offshore Structures*. Trondheim: Cambridge University Press, 1990. ISBN: 521 37285 2.

[20] Henrik Fjørtoft. "Thrust loss on azimuthing thrusters due to Coanda effect". PhD thesis. Trondheim: Norwegian University of Science and Technology (NTNU), June 2010.

[21] Tim Gourlay. "Flow Beneath a Ship at Small Underkeel Clearance". In: *Journal of Ship Research* 50.3 (Sept. 2006), pp. 250–258.

[22] Heerema Marine Contractors. *CFD Scope for Thruster-Hull Interaction based on Model Test*. Tech. rep. 2010.

[23] IMCA. *DP Position Loss Risks in Shallow Water - M121*. Tech. rep. 2016. URL: www.imca-int.com/marine.

[24] ITTC. *Recommended Procedures and Guidelines Dynamic Positioning System Model Test Experiments*. Tech. rep. Quality System Manual, 2014.

[25] ITTC. "Recommended Procedures and Guidelines Practical Guidelines for Ship CFD Applications". 2014.

[26] ITTC. *Ship CFD Applications*. Tech. rep. Quality System Manual, 2021.

[27] ITTC. "Uncertainty Analysis in CFD Verification and Validation Methodology and Procedures". 2021.

[28] Nils Albert Jenssen. "What is the DP Current?" In: *Dynamic Positioning conference*. Dynamic Positioning Conference. Kongsberg Maritime AS, Oct. 2006.

[29] Harold T. Johnston et al. "Influence of a boundary on the development of a propeller wash". In: *Ocean Engineering* 61 (2013), pp. 50–55. ISSN: 00298018. DOI: 10.1016/j.oceaneng.2012.12.033.

[30] Dirk Jürgens et al. "Design of Reliable Steerable Thrusters by Enhanced Numerical Methods and Full Scale Optimization of Thruster-Hull Interaction Using CFD". In: *Dynamic Positioning Conference*. Houston, USA: Voith Turbo Marine, Oct. 2008.

[31] Arjen Koop. "Shallow Water Current Loads on a LNG Carrier Using CFD". In: *International Conference on Offshore Mechanics and Arctic Engineering (OMAE)*. St. John's, Newfoundland, Canada: American Society of Mechanical Engineer (ASME), May 2015, V002T08A037. DOI: 10.1115/OMAE2015-41275. URL: https://doi.org/10.1115/OMAE2015-41275.

[32] Arjen Koop and Alexei Bereznitski. "Model-scale and full-scale CFD calculations for current loads on semi submersible". In: *International Conference on Offshore Mechanics and Arctic Engineering (OMAE)*. Rotterdam: American Society of Mechanical Engineers (ASME), June 2011, pp. 147–157. DOI: 10.1115/OMAE2011-49204. URL: https://doi.org/10.1115/OMAE2011-49204.

[33] Arjen Koop et al. "Determining Thruster-Hull Interaction for a Drill-Ship Using CFD." In: *International Conference on Offshore Mechanics and Arctic Engineering (OMAE)*. Trondheim, Norway: American Society of Mechanical Engineer (ASME), June 2017, V002T08A022. DOI: 10.1115/OMAE2017-61485. URL: https://doi.org/10.1115/OMAE2017-61485.

[34] Kourosh Koushan et al. “Experimental Investigation of the Effect of Waves and Ventilation on Thruster Loadings”. In: *First International Symposium on Marine Propulsors SMP’09*. Trondheim: Norwegian Marine Technology Research Institute (MARINTEK), June 2009.

[35] Erik Lehn. *On the propeller race interaction effects*. Tech. rep. Trondheim: Marintek, Sept. 1985.

[36] Erik Lehn. *Thruster-Hull Interaction Effects*. Tech. rep. The ship research institute of Norway, 1980.

[37] Heng Li et al. “Research on the effect of shallow draft on the performance of Azimuth thruster under bollard conditions.” In: (Nov. 2023). URL: https://papers.ssrn.com/sol3/papers.cfm?abstract_id=4628005.

[38] Ping Lu and Sue Wang. “CFD simulation of propeller and tunnel thruster performance”. In: *International Conference on Offshore Mechanics and Arctic Engineering (OMAE)*. Vol. 2. San Francisco: American Society of Mechanical Engineers (ASME), Oct. 2014. ISBN: 9780791845400. DOI: 10.1115/OMAE2014-23328. URL: https://asmedigitalcollection.asme.org/OMAE/proceedings-pdf/OMAE2014/45400/V002T08A017/4432763/v002t08a017-omae2014-23328.pdf.

[39] P Maciel, A Koop, and G Vaz. “Modelling Thruster-Hull Interaction With CFD”. In: *International Conference on Offshore Mechanics and Arctic Engineering (OMAE)*. Nantes, France: American Society of Mechanical Engineers (ASME), June 2013, V007T08A024. DOI: 10.1115/OMAE2013-10359. URL: https://doi.org/10.1115/OMAE2013-10359.

[40] Francesco Mauro and Radoslav Nabergoj. “Advantages and disadvantages of thruster allocation procedures in preliminary dynamic positioning predictions”. In: *Ocean Engineering* 123 (Sept. 2016), pp. 96–102. ISSN: 00298018. DOI: 10.1016/j.oceaneng.2016.06.045.

[41] Philipp Mucha et al. “An experimental study on the effect of confined water on resistance and propulsion of an inland waterway ship”. In: *Ocean Engineering* 167 (Nov. 2018), pp. 11–22. ISSN: 00298018. DOI: 10.1016/j.oceaneng.2018.08.009.

[42] T Nakagawa. “Vortex Formation Mechanism Behind the Rectangular Prism with Depth to Height Ratio of 0.675”. In: *Experimental Thermal and Fluid Science* (1990), pp. 323–329.

[43] U Nienhuis. “Analysis of thruster effectivity for dynamic positioning and low speed manoeuvring”. PhD thesis. Delft: Delft University of Technology, Oct. 1992.

[44] Harald Ottens, Norbert Bulten, and Radboud van Dijk. “Full Scale CFD Validation on Thruster-Hull Interaction on a Semi-Submersible Crane Vessel in Transit Condition”. In: *International Conference on Offshore Mechanics and Arctic Engineering (OMAE)*. Nantes, France: American Society of Mechanical Engineers (ASME), June 2013, V007T08A022.

[45] Harald Ottens and Radboud van Dijk. “Benchmark Study on Thruster-Hull Interaction in Current on a Semi-Submersible Crane Vessel”. In: *International Conference on Offshore Mechanics and Arctic Engineering (OMAE)*. Proceedings of the ASME 2012 31st International Conference on Ocean, Offshore and Arctic Engineering. Rio de Janeiro: American Society of Mechanical Engineers (ASME), July 2012, pp. 527–538. DOI: 10.1115/OMAE2012-83125. URL: https://doi.org/10.1115/OMAE2012-83125.

[46] Harald Ottens, Radboud van Dijk, and Geert Meskers. “Benchmark Study on Thruster-Hull Interaction on a Semi-Submersible Crane Vessel”. In: *International Conference on Offshore Mechanics and Arctic Engineering (OMAE)*. OMAE2011-49433. Rotterdam, The Netherlands: American Society of Mechanical Engineer (ASME), June 2011, pp. 297–307.

[47] Doug Phillips and Kourosh Koushan. “Dynamics of Propeller Blade and Duct Loading on Ventilated Thrusters in Dynamic Positioning Mode”. In: *Dynamic Positioning conference*. 2007.

[48] Agnieszka Piekło, Anna Witkowska, and Tomasz Zubowicz. “Dynamic Positioning Capability Assessment for Ship Design Purposes”. In: *Lecture Notes in Networks and Systems*. Vol. 545 LNNS. Springer Science and Business Media Deutschland GmbH, 2023, pp. 386–397. ISBN: 9783031161582. DOI: 10.1007/978-3-031-16159-9{_}31.

[49] P.J. Roache. *Fundamentals of verification and validation*. hermosa publ., 2009.

[50] Howard Shatto and Dietmar Deter. “Interaction Between Thrusters, Power Systems, and DP Control Systems”. In: *Dynamic Positioning conference*. Ed. by Shatto Engineering and Nautex Inc. Dynamic positioning conference. Huston, Texas, Oct. 1999.

[51] Manases Tello Ruiz et al. “Propulsion and Steering Behaviour of a Ship Equipped with Two Contra-Rotating Z-drives”. In: *10th International Conference on Hydrodynamics*. St, Petersburg, Oct. 2012.

[52] Radboud R T Van Dijk and Albert B Aalbers. “"What Happens in Water" - The use of Hydrodynamics to Improve DP”. In: *Dynamic Positioning Conference*. Huston, USA: Maritime Research Institute Netherlands (MARIN), Sept. 2001. URL: https://www.marin.nl/en/publications/what-happens-in-water-the-use-of-hydrodynamics-to-improve-dp.

[53] Maoxing Wei, Yee Meng Chiew, and Shih Chun Hsieh. “Plane boundary effects on characteristics of propeller jets”. In: *Experiments in Fluids* 58.10 (Oct. 2017). ISSN: 07234864. DOI: 10.1007/s00348-017-2425-8.

[54] *What Are Steady-State Simulations?* URL: https://www.simscale.com/knowledge-base/transient-behavior-in-steady-state/#:~:text=What%20Are%20Steady%2DState%20Simulations,pressure%2C%20or%20temperature%20are%20constant..

[55] Qin Zhang and Rajeev K. Jaiman. “Numerical analysis on the wake dynamics of a ducted propeller”. In: *Ocean Engineering* 171 (Jan. 2019), pp. 202–224. ISSN: 00298018. DOI: 10.1016/j.oceaneng.2018.10.031.

[56] Bin Zhou and Min Zhao. “Numerical simulation of thruster-thruster interaction for ROV with vector layout propulsion system”. In: *Ocean Engineering* 210 (Aug. 2020). ISSN: 00298018. DOI: 10.1016/j.oceaneng.2020.107542.

[57] Gert-Jan Zondervan, Martin Hoekstra, and Jan Holtrop. “Flow analysis, design, and testing of ducted propellers”. In: *Society of Naval Architects and Marine Engineers Propellers/Shafting 2006 Symposium* (Jan. 2006).

A

Measured thrust

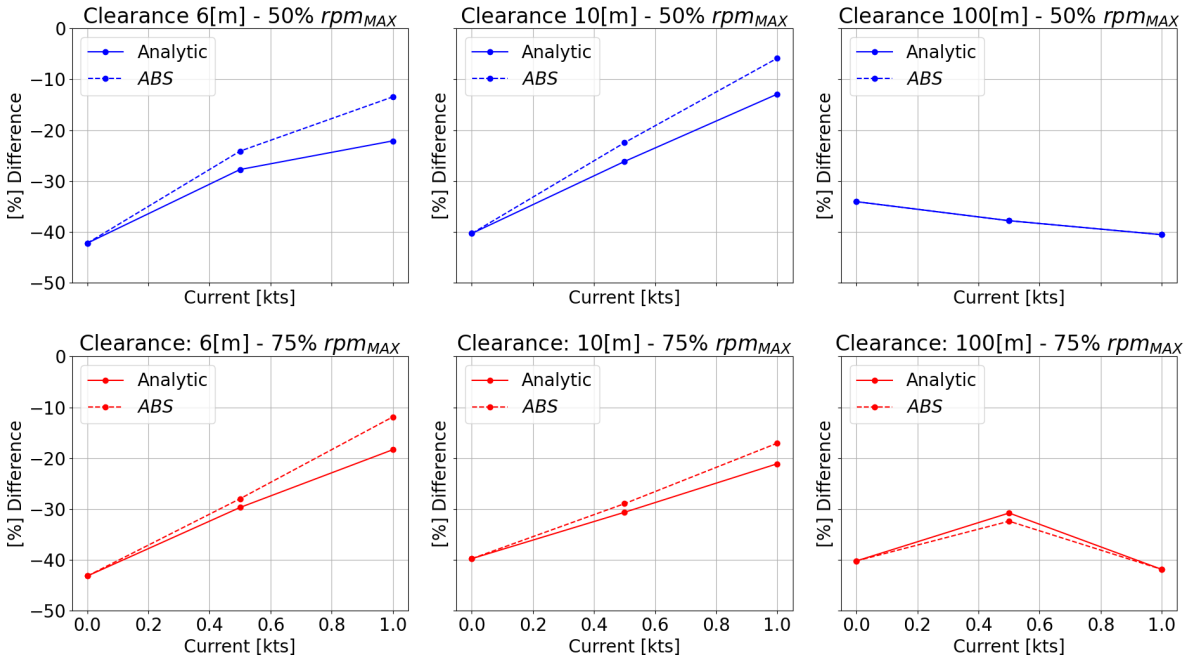

Figure A.1: Percentage difference between estimated (analytically and with *ABS* [2]) thrust reduction ratio and the measured one in CFD simulations.

B

Velocity and pressure distribution

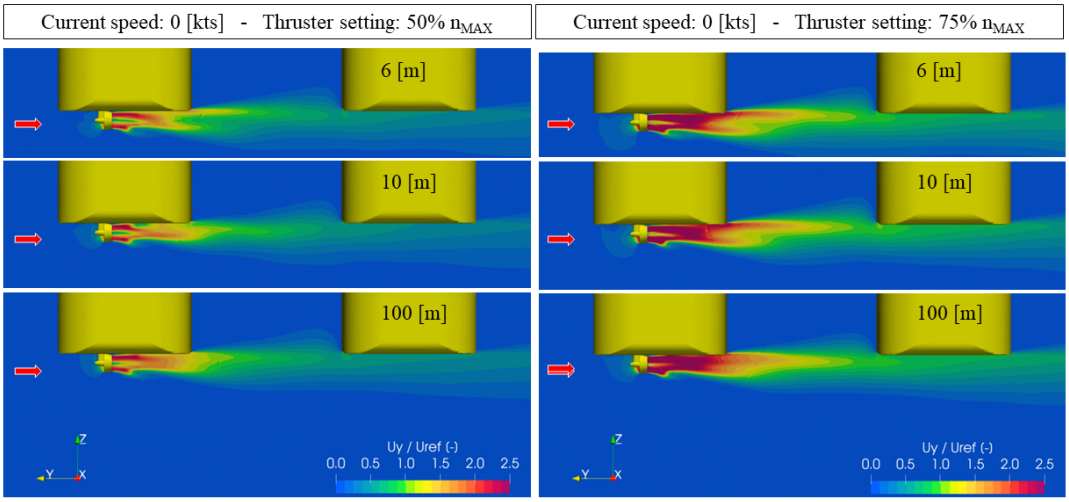

Figure B.1: 0 [kts] beam-side current: velocity field around the hull

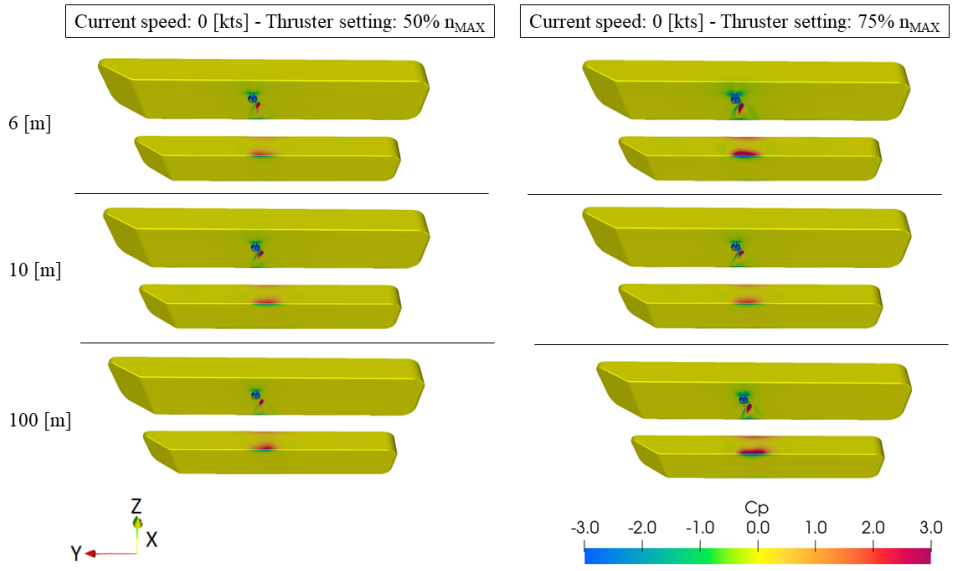

Figure B.2: 0 [kts] beam-side current: pressure distribution around the hull

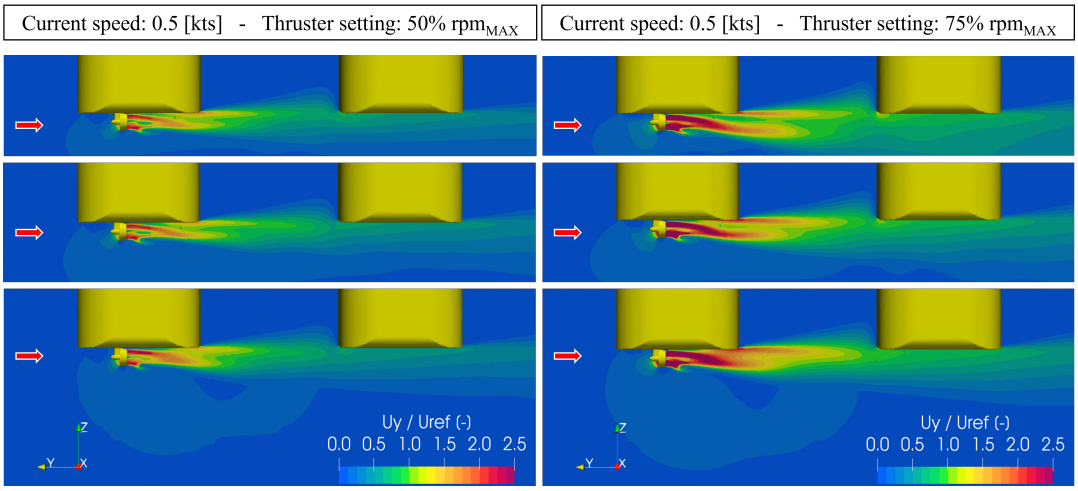

Figure B.3: 0.5 [kts] beam-side current: velocity field around the hull

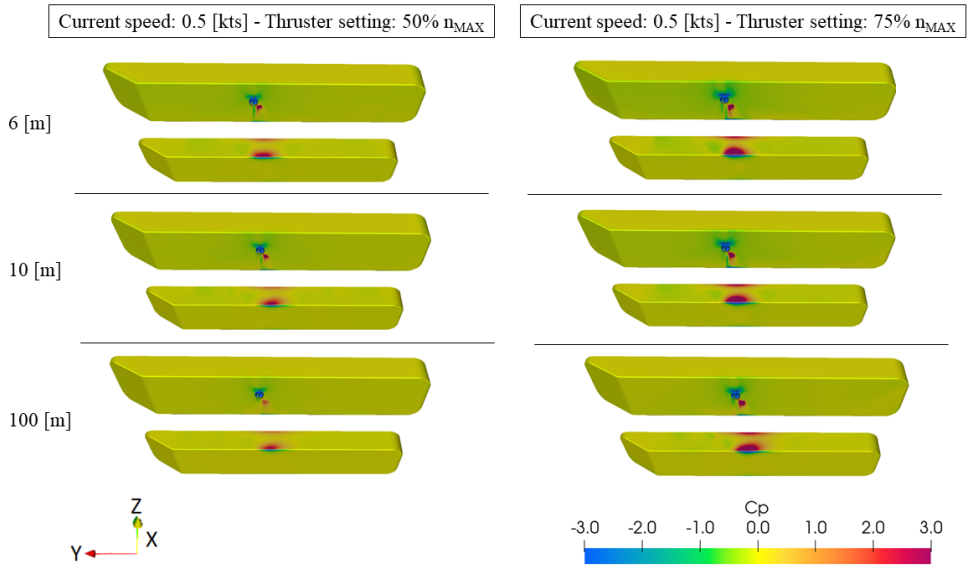

Figure B.4: 0.5 [kts] beam-side current: pressure distribution around the hull

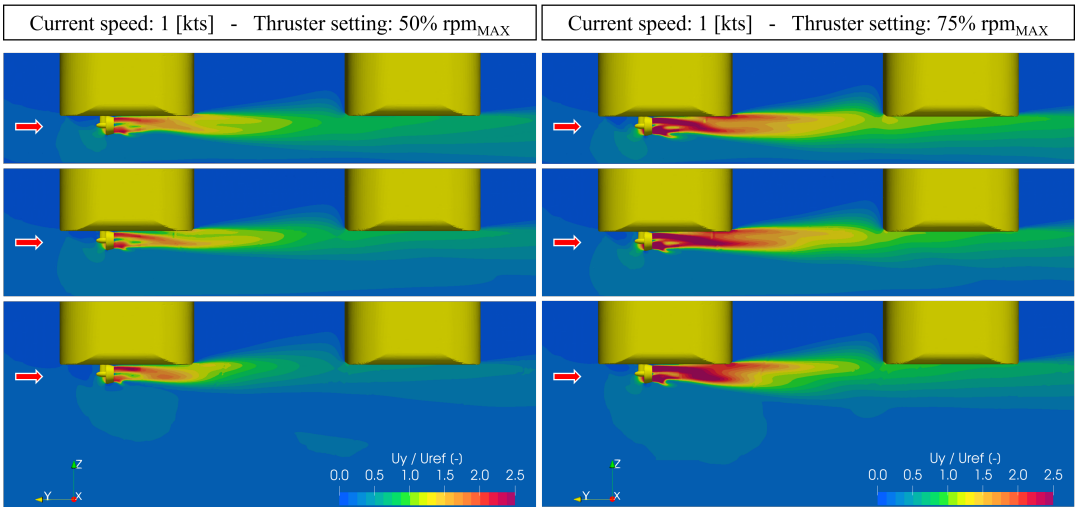

Figure B.5: 1 [kts] beam-side current: velocity field around the hull

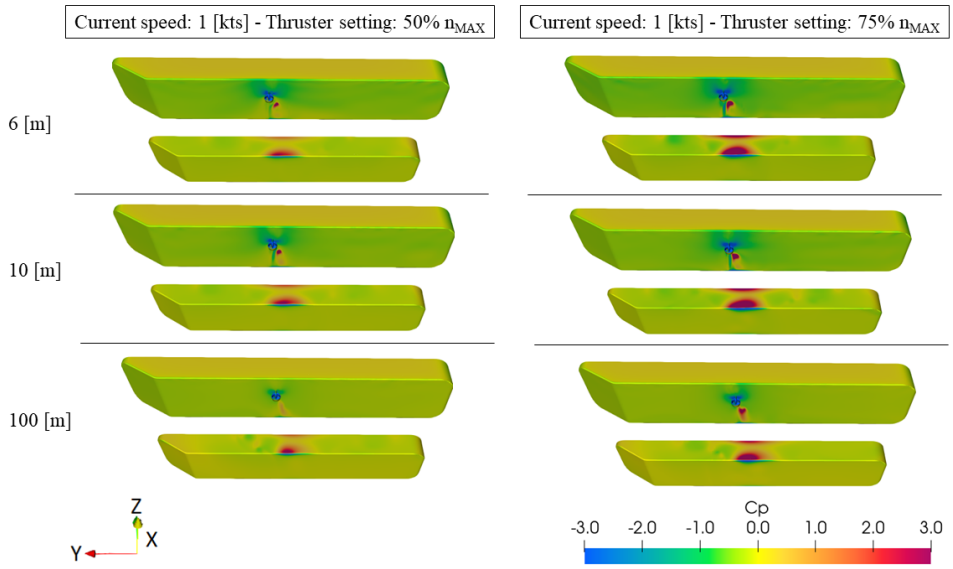

Figure B.6: 1 [kts] beam-side current: pressure distribution around the hull